UNIVERSITÉ DE STRASBOURG

ÉCOLE DOCTORALE DES SCIENCES CHIMIQUES

Institut de Chimie et Procédés pour l'Energie, l'Environnement et la Santé, UMR 7515

THÈSE

présentée par:

ZHANG Yu

soutenue le : 9 décembre **2022**

pour obtenir le grade de : Docteur de l'Université de Strasbourg

Discipline/ Spécialité: Chimie / Chimie Physique

Environmental Friendly Approaches to Optimize ZSM-5 Zeolite for the MTO Reaction

THÈSE dirigée par:

M. LOUIS Benoît — **Directeur de recherche,** CNRS, ICPEES

RAPPORTEURS:

Mme. ESPOSITO Serena — **Professor,** Politecnico di Torino, Turin, Italy

M. PINARD Ludovic — **Professor,** University of Caen Normandy

---

AUTRES MEMBRES DU JURY:

Mme. ROGER Anne-Cécile — **Professor,** University of Strasbourg

M. MUSYOKA Nicholas — **Group Leader** at CSIR, University of Pretoria, South Africa

M. Loic Jierry — **Professor,** University of Strasbourg

Table of Content

Résumé

1. Introduction

Les oléfines légères (éthylène, propylène et butylènes) sont les éléments constitutifs de nombreux produits plastiques modernes et sont produites en grandes quantités. Par exemple, l'éthylène et le propylène sont les principaux produits chimiques organiques produits dans le monde, avec une production annuelle moyenne d'environ 200 millions de tonnes métriques et 100 millions de tonnes métriques, respectivement. Cependant, comme l'hydrogène moléculaire, les oléfines ne se présentent pas comme des ressources naturelles en raison de leur réactivité et doivent donc être synthétisées à partir d'autres matières premières.[1]

Cependant, tout comme l'hydrogène moléculaire, les oléfines ne se présentent pas comme des ressources naturelles en raison de leur réactivité. Ils doivent être synthétisés à partir d'autres matières premières et sont actuellement presque entièrement issus de ressources fossiles. Le vapocraquage est le procédé le plus important pour la production d'oléfines légères. Cependant, des inconvénients tels qu'une consommation d'énergie élevée, un faible rendement en produits de grande valeur et un raccourcissement de la durée de vie de l'appareil en raison de la cokéfaction existaient dans ce procédé. De plus, la rareté (relative) des ressources en pétrole brut dans certains pays a conduit à un approvisionnement insuffisant en matières premières de vapocraquage. Afin d'atténuer les limitations causées par la pénurie de pétrole et de réduire davantage les coûts, la consommation d'énergie et les émissions de CO_2, une variété de nouveaux procédés de production d'oléfines ont été développés.[2]

Au cours de la dernière décennie, le procédé méthanol-oléfines (MTO) a attiré de plus en plus d'attention. Cette dernière est une voie catalytique non pétrolière pour la production d'oléfines. L'ensemble du processus utilise du gaz naturel, du charbon ou d'autres hydrocarbures comme matières premières, qui sont convertis en méthanol par oxydation partielle. Le méthanol est une molécule réactive, facile à stocker, sensible aux transformations catalysées par les acides pour donner des hydrocarbures. De plus, l'utilisation d'un procédé catalytique réduit considérablement la consommation d'énergie, par rapport au vapocraquage.

Actuellement, les zéolithes ZSM-5 et SAPO-34 sont les catalyseurs utilisés commercialement pour la réaction MTO. Ils présentent des performances différentes en raison de leurs propriétés physico-chimiques uniques. La ZSM-5 présente une forte acidité, une activité et une stabilité élevées par rapport à la zéolite SAPO-34. En revanche, SAPO-34 donne une plus grande sélectivité vis-à-vis de l'éthylène, grâce à ses dimensions de pores étroites. Malgré les excellentes propriétés du ZSM-5, les chercheurs travaillent toujours à trouver de nouvelles stratégies de modification pour atteindre des performances encore plus élevées dans la réaction MTO. Parmi eux, le coût, la sélectivité vis-à-vis du propylène et la durée de vie sont trois indicateurs importants pour concevoir et comparer les catalyseurs zéolithiques acides.[3]

Les stratégies de modification couramment utilisées sont : ajuster l'acidité de la zéolithe (dopage des hétéroatomes, ajuster le rapport Si/Al...), augmenter la vitesse de diffusion (tout en élargissant la taille des pores, construire une zéolithe hiérarchisée, mettre en forme...), et utiliser les déchets comme une matière première (cendre volante, cendre de balle de riz et autres minéraux…). La modulation de l'acidité dans la charpente zéolithique peut effectivement modifier la répartition des produits. Des études antérieures ont montré qu'une acidité appropriée peut donner lieu à un rapport P/E plus élevé, réduire le taux de cokéfaction et prolonger la durée de vie du catalyseur. Le dopage des hétéroatomes dans les zéolithes permet d'ajuster efficacement leur acidité. Les hétéroatomes peuvent être des éléments du groupe principal (As, Ga, Sn, Ge, etc.), des éléments non métalliques (B, C, F, etc.) ou des métaux de transition (Ti, Fe, etc.).[4] De plus, la zéolithe hiérarchisée et les zéolithes structurées peuvent effectivement permettre de réduire la résistance au transfert de masse, ce qui non seulement améliore l'efficacité de la réaction mais peut également réduire le taux de cokéfaction. Pour obtenir la zéolithe hiérarchisée, différents gabarits durs (nanosphères de carbone, nanotubes de carbone, noir de carbone, amidon, etc.) ont été utilisés. De plus, du carbure de silicium, des matériaux de verre mésoporeux, des fibres d'acier inoxydable (SS), etc. ont été utilisés comme supports pour obtenir la structuration de la poudre de zéolite. Pour

réduire le coût, cela peut être économisé grâce à l'utilisation de matières premières bon marché et à des conditions de synthèse plus douces, ainsi qu'à l'amélioration des conditions de traitement.[5]

Sur la base des objectifs de modification ci-dessus et attachés au concept de synthèse bon marché et respectueux de l'environnement, nous avons utilisé de manière innovante une variété de matériaux naturels et respectueux de l'environnement (biochar, perlite) pour modifier en profondeur la formulation du catalyseur ZSM-5, notamment: adaptation de l'acidité, construction de les pores hiérarchiques et la structuration des poudres. Les matériaux modifiés sont bon marché et facilement disponibles; le processus de modification est facile à utiliser. De plus, les conditions de synthèse de la zéolithe et les conditions catalytiques de la réaction MTO sont rationnellement optimisées pour assurer des performances catalytiques tout en réduisant la consommation d'énergie.

2. Résultats et discussions

I. Caractérisation et comparaison des performances de la zéolithe ZSM-5 modifiée au biochar

La zéolite ZSM-5 avec une surface externe élevée et d'excellentes performances en utilisant le biochar comme modèle dur a été étudiée dans ce chapitre. Les biochars utilisés dans l'étude provenaient de quatre plantes naturelles : l'herbe, le thé, les algues et la lignine. Ces biochars présentaient des différences significatives dans la morphologie, la taille des particules, la teneur en sel inorganique et les groupes fonctionnels de surface. Et les propriétés physico-chimiques des zéolithes ont été clairement affectées par leur addition.

Par rapport à la Lignine-C, au thé-C, à l'herbe-C et aux algues-C, les échantillons contenaient plus de sels inorganiques (Figure 1 (a)), avec une taille de particules plus petite (Figure 1 (b)), une porosité plus riche et plus contenant de l'oxygène groupes fonctionnels (Figure 1 (c)).

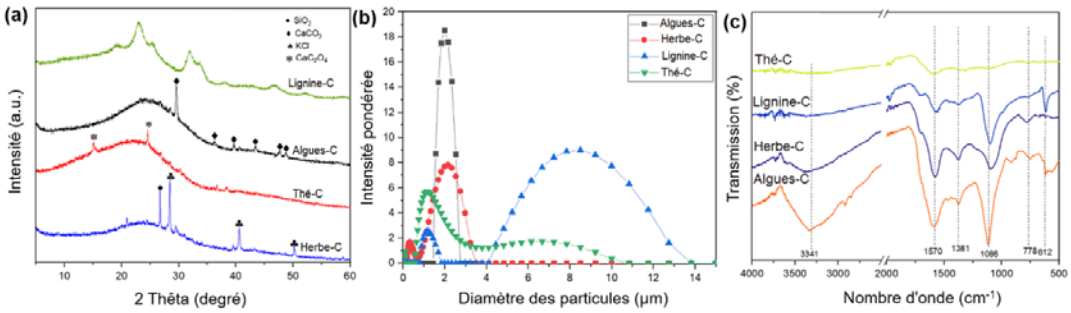

Figure 1. (a) Diffractogramme sur poudre XRD, (b) distribution de taille hydrodynamique dans la mesure DLS (c) spectres FTIR de Algues-C, Herbe-C, Lignine-C et Thé-C.

Les spectres de modèle XRD (Figure 2 (a)) ont montré les cristaux de ZSM-5 synthétisés avec différents biochar (blanc, Herbe-C, Thé-C, Lignine-C et Algues-C). La quantité ajoutée de biochar est la même (400 mg) et les conditions de synthèse hydrothermale sont de 170 oC, 3 d. Tous les échantillons présentaient les motifs de bande fondamentaux confirmant la structure MFI de ZSM-5 et avaient une excellente cristallinité.

Avec une caractérisation plus poussée de la zéolite ZSM-5 modifiée par les biochars, les résultats prouvent que les biochars avec une taille de particules plus petite, plus de groupes fonctionnels contenant de l'oxygène et une surface plus rugueuse, tels que Herbe-C et Algues-C, peuvent former une surface spécifique externe plus élevée pour zéolite. Parce que le biochar avec ces propriétés peut permettre aux cristaux de zéolithe de mieux se développer à sa surface. Pendant ce temps, des changements dans la composition chimique des cristaux de zéolite ont également été observés en raison de l'introduction d'hétéroéléments dans la zéolite.

La surface spécifique et la composition ont un impact direct sur les performances catalytiques de la zéolithe. Comme le montre la Figure 2 (b), la zéolite avec une surface spécifique plus élevée a une durée de vie catalytique plus longue. Dans les conditions catalytiques de 400°C et WHSV=8 h-1, la durée de vie catalytique de l'échantillon H-ZSM-5 sans biochar n'était que de 8 h, tandis que la durée de vie catalytique de la zéolite ZSM-5 modifiée avec Algues-C augmentait à 15 h. De plus, la durée de vie de Herbe-C/ZSM-5 a atteint 9 h.

Cependant, tous les biochars n'ont pas montré d'effet positif sur la réponse MTO de ZSM-5. Par exemple, la zéolite ZSM-5 modifiée par Thé-C n'a pas de changement évident dans les propriétés physiques et chimiques, et la durée de vie catalytique était similaire à celle de H-ZSM-5. Cependant, la durée de vie catalytique de la Lignine-C/ZSM-5 a été considérablement réduite en raison de sa cristallinité relative réduite, ce qui peut être lié à la surface spécifique externe non améliorée et à la cristallinité réduite de la Lignine-C/ZSM-5. Le taux de désactivation est séquencé comme suit:

Lignine-C/ZSM-5 > Thé-C/ZSM-5 > H-ZSM-5 > Herbe-C/ZSM-5 > Algues-C/ZSM-5.

En conclusion, il est possible d'améliorer la durée de vie catalytique de ZSM-5 dans la réaction MTO en ajoutant des types spécifiques de biochar.

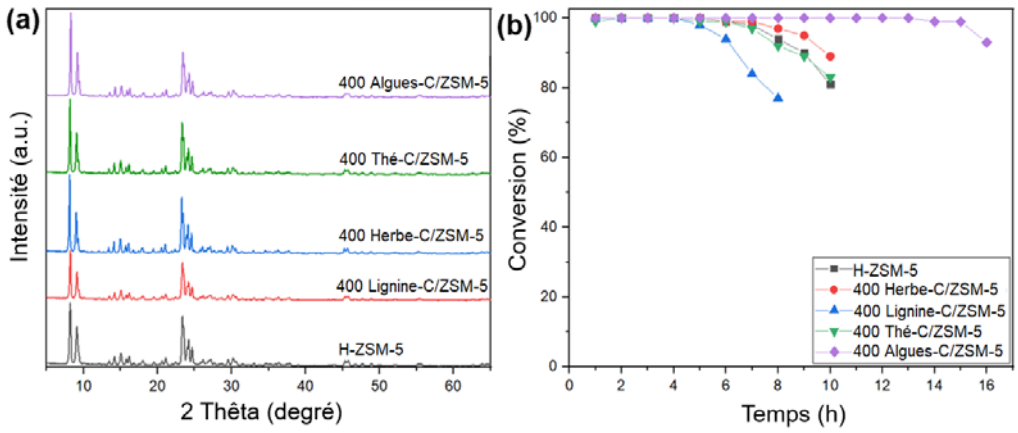

Figure 2.(a) Modèles XRD de biochar/ZSM-5, and (b) conversion du méthanol des produits de 400 mg de biochar/ZSM-5 à 400 °C, WHSV=8 h-1.

II Zéolite ZSM-5 modifiée Algues-C et Herbe-C

Sur la base du résultat de l'expérience de la dernière partie, les Algues-C et Herbe-C ont été sélectionnés comme modèles modifiés pour la zéolite ZSM-5 en raison du meilleur effet. L'influence des paramètres de synthèse sur la zéolithe porte principalement sur: la structure physique, la composition chimique, l'acidité et la cristallinité. Les paramètres du test affectent le taux de cokéfaction de la zéolithe.

Dans cette partie de l'étude, les paramètres de synthèse et de fonctionnement d' Algues-

C/ZSM-5 et Herbe-C/ZSM-5 ont été réajustés, tels que l'ajout de biochar, le temps de synthèse, le Si/Al, la température du test. Les résultats expérimentaux montrent que la durée de vie catalytique de la zéolithe ZSM-5 peut être encore améliorée par l'optimisation des paramètres ci-dessus.

Tout d'abord, l'ajout de biochar peut améliorer la surface externe et de zéolithe. Bien que la surface externe élevée puisse ralentir la formation de cokes dans les réactions MTO, la structure microporeuse de la zéolithe a été détruite avec un biochar excessif entraînant la perte de sites actifs. Les effets néfastes sur les performances de la zéolithe ont été mis en évidence (Figure 3 (a)). Par conséquent, il est très important de choisir une quantité appropriée d'ajout de biochar.

De plus, l'acidité de la zéolithe a montré une tendance à la baisse avec l'ajout de tourbe et de charbon d'algues, et une augmentation de la teneur en hétéroatomes de la zéolithe a été détectée. Une corrélation négative entre la teneur en hétéroéléments et l'acidité de la zéolithe a été confirmée. Les résultats des tests de performance montrent qu'une réduction modérée de l'acidité de la zéolithe est bénéfique pour prolonger la durée de vie catalytique.

La cristallinité de la zéolithe était fortement affectée par le temps de synthèse. Un temps de synthèse trop court n'est pas propice à la formation de cristaux de zéolithe (Figure 3 (b)). La cristallinité a également un effet sur la durée de vie de la zéolithe. Cependant, semble être plus faible que celle de la surface externe et de l'acidité.

Le rapport Si/Al peut affecter de manière significative la sélectivité et l'activité catalytique de la zéolite ZSM-5. Les résultats expérimentaux ont confirmé que la sélectivité de la zéolite vis-à-vis de l'éthylène chute fortement, et inversement la sélectivité vis-à-vis du propylène augmente rapidement. De ce fait, la sélectivité en oléfines légères, notamment éthylène, propylène, butènes, reste stable. Parallèlement, l'acidité de la zéolithe diminue avec la diminution de la teneur en aluminium et conduit à un affaiblissement de l'activité catalytique de la zéolithe.

La température catalytique affecte directement la durée de vie catalytique et la sélectivité du produit de la zéolithe. La sélectivité du catalyseur vis-à-vis des oléfines légères, en particulier l'éthylène, augmente significativement avec l'augmentation de la température. Cependant, la vitesse de cokéfaction est accélérée à des températures de réaction élevées, ce qui entraîne une désactivation rapide du catalyseur, tandis que des températures basses entraînent une activité insuffisante du catalyseur.

Pour l' Algues-C/ZSM-5, les meilleures conditions de synthèse sont la synthèse hydrothermale à 170 ºC pendant 2 d. La température de test appropriée est de 400 ºC. Et, pour la zéolithe Herbe-C/ZSM-5, les meilleures conditions de synthèse sont la synthèse hydrothermale à 170 ºC pendant 3 d. La température de test appropriée est de 350 ºC.

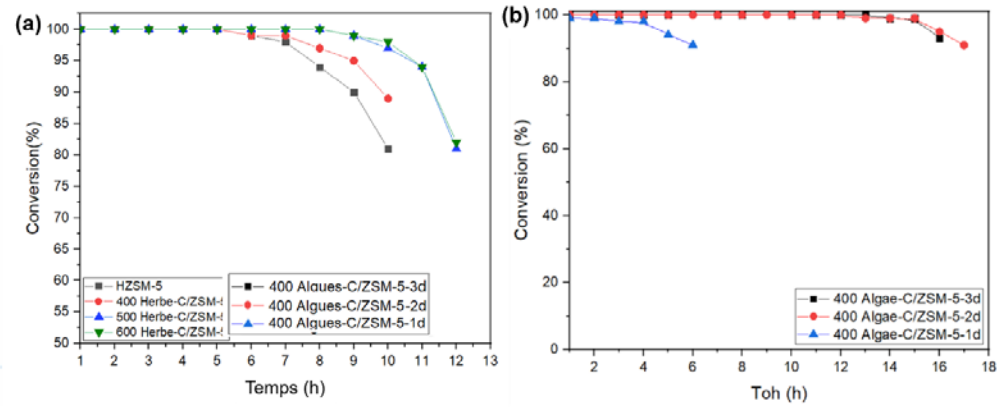

Figure 3. Conversion du méthanol à T=400 °C et WHSV=8,0 h-1 sur des (a) Herbe-C/ZSM-5 avec différents ajouts de Herbe-C (400, 500, 600 mg), (b) 400 Algues-C/ZSM-5 synthétisés avec des temps différents (1d, 2d, 3d).

III. Construction de catalyseurs monolithiques ZSM-5

Les zéolithes ZSM-5 sont des nanocristaux, qui posent des problèmes dans les applications industrielles telles qu'une récupération difficile et une chute de pression élevée, comme le montre la figure 4 (a). De plus, les oléfines légères doivent être rapidement éliminées de la surface du catalyseur pour les empêcher de réagir davantage. Par conséquent, il est nécessaire de construire des catalyseurs zéolithiques monolithiques avec des structures poreuses. La perlite est un minéral poreux principalement composé de silicate d'aluminium

amorphe (Figure 4 (b)). Ce minéral poreux a une excellente résistance thermique et stabilité chimique, et est un excellent matériau de support. De plus, la perlite contient également environ 75 % de SiO_2 et une variété d'éléments métalliques (Al, K, Na…). Les aluminiums occupent environ 11 % de la composition totale. Par conséquent, la perlite peut donc être utilisée comme source d'alumine pour la synthèse de zéolithe.

Le catalyseur composite ZSM-5/Perlite a été obtenu via une synthèse hydrothermale in situ, comme le montre la Figure 4 (c). Dans les expériences de suivi, la taille des particules de perlite et la quantité de perlite ajoutée au catalyseur composite ont été optimisées. Le composite ZSM-5/perlite présente non seulement les avantages d'un taux de récupération et d'une faible chute de pression, mais présente également une excellente activité catalytique. Dans les conditions de réaction couramment utilisées pour les réactions MTO, le composite ZSM-5/Perlite a permis d'atteindre la plus longue durée de vie du catalyseur (14 h) et la plus haute sélectivité en oléfines légères C2-C4 (80 %). Une sélectivité exceptionnelle de 53 % vis-à-vis du propylène a été atteinte, rivalisant avec les meilleures valeurs rapportées à ce jour pour les zéolithes ZSM-5. De manière surprenante, ce catalyseur composite a également démontré d'excellentes performances catalytiques à basse température et à vitesse spatiale élevée. ZSM-5/Perlite a montré une durée de vie allant jusqu'à 30 h à 350 ^{o}C. Pendant ce temps, la sélectivité du propylène atteint 46%. Ces propriétés catalytiques prometteuses bénéficiaient non seulement de la structure du squelette tridimensionnel de la perlite expansée, mais étaient également étroitement liées à la dissolution de l'hétéroélément dans la perlite.

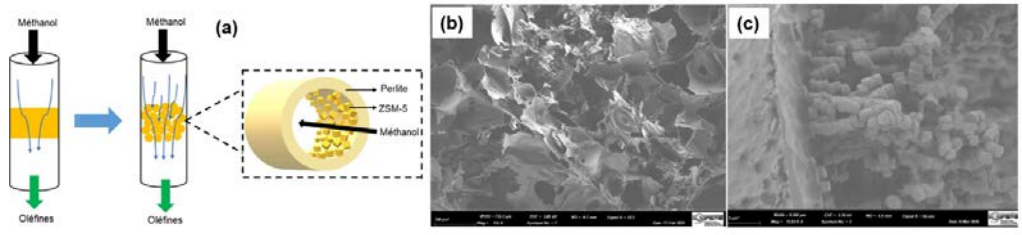

Figure 4. Diagramme schématique de la réaction MTO sur le composite ZSM-5/Perlite (a), Image SEM de (b) perlite et (c) ZSM-5/Perlite.

3. Conclusion générale

Dans cette étude, le ZSM-5 a été modifié en utilisant deux matériaux respectueux de l'environnement (biochar et perlite). Les directions d'optimisation: la construction de pores hiérarchiques, la réduction de l'acidité de la zéolithe et la construction de catalyseurs monolithiques. Les résultats expérimentaux montrent que les hétéroatomes contenus dans les matériaux naturels peuvent se dissoudre et se doper dans les cristaux de zéolithe ZSM-5 lors du processus hydrothermique. Ces hétéroatomes permettent d'ajuster l'acidité de la zéolithe ZSM-5, notamment de réduire significativement l'acidité de Brønsted. De plus, la capacité de formation de pores du biochar en tant que modèle dur dépend fortement de la rugosité de surface et de l'hydrophilie du matériau. Le biochar avec une surface rugueuse, une grande surface spécifique et un groupe hydrophile riche peut apporter une surface spécifique externe plus élevée à la zéolite, ce qui peut prolonger efficacement la durée de vie catalytique de ZSM-5.

De plus, le catalyseur monolithique ZSM-5 a été construit avec succès en utilisant de la perlite bon marché comme support. La poudre de zéolite ZSM-5 a été chargée sur la surface de la perlite par un processus de croissance in situ. Dans le même temps, la perlite riche en élément Al peut être utilisée comme source d'aluminium de la zéolite ZSM-5, ce qui réduit encore le coût de synthèse. Les résultats ont montré que la zéolite structurée obtenue à partir de cette méthode avec une réactivité élevée et une longue durée de vie catalytique dans la réaction MTO. Cette méthode de synthèse fournit une nouvelle idée pour la construction de catalyseurs zéolitiques monolithiques.

General Introduction

1. Goal and scope of the Thesis

Light olefins (ethylene, propylene and butylenes) are the building blocks of numerous modern plastic products and are produced in large quantities. For instance, ethylene and propylene are the top organic chemicals produced globally, with an average annual production of roughly 200 million metric tons and 100 million metric tons, respectively. However, like molecular hydrogen, olefins do not occur as natural resources due to their reactivity and must therefore be synthesized from other feedstocks.

Currently, steam cracking is the main process for the production of ethylene and propylene. The vast majority of steam crackers in the world use a tube cracking furnace. There is no catalyst involved in the steam cracking process, and the products stream contains a mixture of C_1 and C_2, propylene being a by-product. The raw feedstock operated by steam cracking is based on hydrocarbons from petroleum or natural gas. However, steam cracking has some shortcomings, as high reaction temperature, presence of steam, leading to high energy consumption and high yield in low added-value products and short operation due to coking, etc. In addition, the propylene/ethylene output ratio (P/E ratio) is generally is low, being barely regulated due to the occurrence of free radical reaction mechanism. Another crucial issue is the scarcity of crude oil resources in some countries. That led to an insufficient supply of steam cracking feedstocks. In order to alleviate the limitations caused by oil chain supply, to further reduce costs, energy consumption and CO_2 emissions, research and developments of new olefin production processes become mandatory.

For the last decade, the methanol-to-olefins (MTO) process has attracted more and more attention. The latter is a non-petroleum catalytic route for the production of olefins. The entire process uses natural gas, coal or other hydrocarbons as feedstocks, which are converted to methanol through partial oxidation. Methanol is a reactive molecule, easy to store, sensitive to acid-catalyzed transformations to yield hydrocarbons. Moreover, the use of a catalytic process greatly reduces the energy consumption, comparing with steam cracking. At present, ZSM-5

and SAPO-34 zeolites are the commercially used catalysts for the MTO reaction. They exhibit different performances because of their unique physicochemical properties. ZSM-5 shows strong acidity, high activity and stability, compared to SAPO-34 zeolite. In contrast, SAPO-34 yields higher selectivity towards ethylene, thanks to its narrow pore dimensions. Despite the excellent properties of ZSM-5, researchers are still working on finding new modification strategies to reach even higher performance in the MTO reaction. Among them, cost, selectivity towards propylene and lifetime are three important indicators to design and compare acidic zeolite catalysts.

The modification strategies commonly used are: *(a)* adjusting the acidity of the zeolite (heteroatom doping, adjusting Si/Al ratio...), *(b)* increasing diffusion rate (while expanding pore size, *(c)* constructing hierarchical zeolite, shaping...), and *(d)* using waste as a raw material (fly ash, rice husk ash and other minerals…). The modulation of acidity in the zeolite framework can effectively change the distribution of the products. Previous studies have shown that an appropriate acidity can yield to higher P/E ratio, reduce the coking rate and prolong the catalyst life. The doping of heteroatoms in zeolites can effectively adjust their acidity. Heteroatoms can be *(a)* main group elements (As, Ga, Sn, Ge, etc.), *(b)* non-metals elements (B, C, F, etc.) or *(c)* transition metals (Ti, Fe, etc.). Furthermore, the hierarchical zeolite and the structured zeolites can effectively allow reducing the mass transfer resistance, which not only improve the reaction efficiency but may also reduce the coking rate. To obtain the hierarchical zeolite, various hard templates (carbon nanospheres, carbon nanotubes, carbon black, starch, etc.) were used. Furthermore, silicon carbide, mesoporous glass materials, stainless-steel (SS)-fibers, etc. were used as supports to achieve zeolite powder structuring. For reducing the cost, this can be saved through cheap raw materials use and milder synthesis conditions, as well as improvement of process conditions.

Based on the above modification goals, and committed to the cheap and environmentally friendly synthesis concept, we innovatively used a variety of natural and environmentally

friendly materials (biochars, perlite) to comprehensively modify ZSM-5 catalyst formulation, including: *(a)* acidity tailoring, *(b)* construction of hierarchical pores, and *(c)* powder structuring. The modified materials are cheap and readily available; the modification process is easy to operate. In addition, the synthesis conditions of the zeolite and catalytic conditions for the MTO reaction are rationally optimized to ensure catalytic performance while reducing energy consumption.

2. Outline of the Thesis

The thesis consists of **6 Chapters**, starting with a literature review dedicated to the history of zeolite, optimization of the materials and development of MTO process. Then, the types of raw materials, synthesis methods, characterization methods and test conditions used in this study are described in detail. The next three chapters discuss the specific researches done and the results obtained. Finally, the main results of this Thesis are summarized, and the development prospect of this field is aimed. The content of each chapter is outlined below:

Chapter 1 presents an overview of the discovery history of natural zeolite, the development history of synthetic zeolite, and the applications of zeolites. Then the application of zeolite as a catalyst is discussed, including the physicochemical properties of zeolite catalysts, modification methods, etc. Finally, the application of ZSM-5 zeolite in the MTO reaction is reviewed.

Chapter 2 describes the raw materials and methods and modification strategies for the synthesis of ZSM-5 zeolite. The characterization techniques used in this study are described. Besides, the set-up for the MTO reaction and parameter setting and data analysis are also introduced.

Chapter 3 explores the feasibility of biochar as a hard template to design hierarchical ZSM-5 crystals and optimize their performance for MTO. In this chapter, the characterization of four biochars (*(a)* Grass-C, *(b)* Algae-C, *(c)* Lignin-C and *(d)* Tea-C) and modified ZSM-5

zeolite are presented. The effects of biochars on the morphology, composition, and chemical properties of ZSM-5 are investigated. Finally, the biochar modified ZSM-5 zeolites with the best catalytic performance are screened out.

Chapter 4 is a further optimization for the screened zeolites in chapter 3, including the adjustment of synthesis and catalytic conditions, as: the amount of biochar added, the synthesis duration, and the Si/Al ratio, etc. The performance of the catalysts under different test conditions was also explored. In this chapter, the catalytic performance of biochar-modified zeolite is further improved and is much higher than that of un-modified zeolite.

Chapter 5 presents the synthesis concept of an environmentally friendly and inexpensive structed zeolite catalyst. This experiment utilizes natural minerals as a carrier to synthesize a monolithic catalyst through one-step hydrothermal synthesis. In addition, aluminum, present inside the perlite, was used to provide acidity to the zeolite framework. At the same time, the effects of different particle sizes and added amounts of perlite on the performance of this monolithic catalyst were investigated.

Chapter 6 provides a comprehensive overview of the main findings of This thesis. The future application prospects of the MTO reaction and the advantages and limitations of the process are summarized. In addition, the modification direction of ZSM-5 catalyst applied to MTO reaction is discussed. At the same time, application potential of the green synthesis process of zeolite is analyzed.

3. List of scientific contributions

[1] Y. Zhang, Q. Wang, B. Louis, ZSM-5 zeolite coatings on perlite support for MTO application, ***Microporous Mesoporous Mater.*** 323, (2021), 111172.

[2] Y. Zhang, Yanshan Gao, Feng Yu, Qiang Wan, Synthesis of hierarchical Li_4SiO_4 nanoparticles/flakers composite from vermiculite/MCM-41 hybrid with improved CO_2 capture performance under different CO_2 concentrations, ***Chem. Eng.***, 371 (2019) 424.

[3] Y. Zhang, Feng Yu, Benoit Louis, Qiang Wang*, Scalable synthesis of the lithium silicate-based high-temperature CO_2 sorbent from inexpensive raw material vermiculite***, Chem. Eng.***, 349 (2018) 562.

[4] Y. Zhang, Yanshan Gao, Heriberto Pfeiffer, Benoit Louis, Luyi Sun, Dermot O'Hare, Qiang Wang, Recent advances in lithium containing ceramic based sorbents for high-temperature CO_2 capture, ***J. Mater. Chem. A***,7 (2019) 7962.

[5] Y. Zhang, Yanshan Gao, Benoit Louis, Qiang Wang, Weiran Lin, Fabrication of lithium silicates from zeolite for CO_2 capture at high temperatures, ***J. Energy Chem.***, 33 (2019) 81-89.

[6] Y. Zhang, Tuantuan Zhou, Benoit Louis, Feng Yu, Jianming Dan, Qiang Wang, Environmental benign synthesis of lithium silicates and Mg-Al layered double hydroxide from vermiculite mineral for CO_2 capture, ***Catalysts***, 7 (2017) 105**.**

[7] W. Gao, S Liang, R Wang, Q Jiang, **Y. Zhang**, et al. Industrial carbon dioxide capture and utilization: state of the art and future challenges, ***Chem. Soc. Rev.***, 49 (2020) 8584.

[8] G. Lutzweiler, **Y. Zhang**, B. Louis, Marginal strategies of CO_2 use as a reactant for sustainable chemistry and health applications, ***Curr. Opin. Green Sustain. Chem.,*** 37(2022) 100679.

[9] G. Lutzweiler, **Y. Zhang**, F. Gens, A. Echalard, et al. Deciphering the role of faujasite-type zeolites as a cation delivery platform to sustain the functions of MC3T3-E1 pre-osteoblastic cells, ***Mater. Adv.***, (2022).

Chapter 1. Literature Review

ABSTRACT

This chapter provides an overview of the history, modifications, as well as the structured of zeolites. Furthermore, with the advancement of science and technology, artificial zeolites have been successfully synthesized. Thanks to their unique physiochemical properties, zeolites was widely used. Hence, the design of zeolites with better performance has also become a topic to satisfy numerous of needs, as cation exchangers, adsorbents or catalysts. So far, a large palette of modification methods has been developed and led to achieve good results. In addition, a representative type of zeolite catalyst, ZSM-5 zeolite has achieved excellent results in the MTO reaction.

1.1 Zeolites

Zeolite has gone through an extremely long process from discovery, definition to large-scale application, as well as artificial synthesis and design. At first, it was named "zeolite" because of the discovery of a natural aluminosilicate mineral that boils when heated. At that time, the definition of "zeolite" was not clearly, so it confused everyone for years. With further exploration and research, people have a clearer understanding and definition of natural zeolite minerals, and their commercial value has gradually emerged. Later, the concept of "molecular sieve" was proposed, which refers to porous materials that can sieve substances at the molecular level. Although zeolite, as it is now defined, is only one type of molecular sieves, it is the most representative of them. Therefore, the terms "zeolite" and "molecular sieve" are often used interchangeably. With the further development of science and technology, the screening and catalytic ability of zeolite has been revealed. Based on demands of modern industry, the synthesis technology for the artificial products based on natural zeolite have maturated. The types of artificial zeolites have become increasingly abundant, and the classification and definition of them have become more robust. Natural zeolites and artificial zeolites have gained wider application space in different fields.[1]

1.1.1 History of zeolites application of zeolites

The discovery of zeolite was an accident. In 1756, Swedish mineralogist Axel F. Cronstedt discovered a mineral in Swedish Lapland and Iceland with a special property: when the mineral is heated in a flame, they act like boiling. That is why Cronstedt named them "zeolites".[2] In the early days of this ore discovery, progress in their research has been slow because it is rare. With the slow progress of research, the unique properties of natural zeolite are gradually revealed to human beings. In turn, scientists are interested in their potential for

industrial applications.

Initially, it was found to exhibit an ability to adsorb/desorb water without any chemical reaction. This capacity stems from its porous skeleton structure. With the deepening of research, more potential of zeolite in adsorption has been explored, such as large amount of gas: ammonia, carbon dioxide, hydrogen sulfide and alcohol, chloroform and benzene, etc. can be captured by dehydrated zeolite.[3] Further studies have shown that the adsorption of zeolite is selective and has a "sieving" effect.[4] For instance, zeolite can rapid adsorption of linear alkanes (propane, n-butane, n-pentane and n-heptane) on chabazite at temperatures >373 K, whereas branched chain isomers (such as isobutane and iso-octane) are completely excluded. In 1932, J.W McBain, coined the term molecular sieve. Considering the representativeness of zeolite, the two names of “zeolite” and “molecular sieve” are gradually mixed used. Following the discovery of zeolite adsorption property, the ion-exchange property was also revealed. More importantly, in 1930, W.H. Taylor firstly solved the crystalline structure of analcime (ANA) zeolite, followed by natrolite, davynite-cancrinite,[5] and sodalite. Breck further stated "zeolites are crystalline, hydrated aluminosilicates of group I and group II elements*, in particular, Na, K, Mg, Ca, Sr and Ba. (*as formed in nature or synthesized. Higher polyvalent ions, e.g., rare earths, are readily introduced by cation exchange.) Structurally, zeolites are formed with 'framework' of aluminosilicates which are based on an infinitely extending three-dimensional network of AlO_4 and SiO_4 tetrahedra linked to each other by sharing all their oxygens.

However, due to the complexity of the physical properties of zeolites, it is difficult for the above definitions to cover all types of zeolites. Therefore, a broader concept has been proposed. In 1963, J.V. Smith[6] defined zeolite by this way: an aluminosilicate with a framework structure enclosing cavities occupied by large ions and water molecules, both of

which have considerable freedom of movement, permitting ion-exchange and reversible dehydration. However, as more and more zeolite minerals were discovered and a large number of new artificial zeolites have been designed and synthesized, J.V. Smith's definition of zeolite was unable to cover all the characteristics of a zeolite.

In 1993, a sub-committee from the Commission on New Minerals and Mineral Names (CNMNC) of the International Mineralogical Association (IMA) began a long and detailed work to determine a suitable nomenclature for zeolites. In 1997, zeolite had a new definition:

"… a crystalline substance with a structure characterized by a framework of linked tetrahedra, each consisting of four O atoms surrounding a cation. This framework contains open cavities in the form of channels and cages. These are usually occupied by H_2O molecules and extra-framework cations that are commonly exchangeable. The channels are large enough to allow the passage of guest species. In the hydrated phases, dehydration occurs at temperature mostly below 400 °C and is largely reversible. The framework may be interrupted by (OH, F) groups; these occupy a tetrahedron apex that is not shared with adjacent tetrahedra."

Zeolites are characterized by the following properties:

1) High degree of hydration.

2) Low density and large void volume when dehydrated.

3) Stability of the crystal structure of many zeolites when dehydrated.

4) Cation exchange properties.

5) Uniform molecular-sized channels in dehydrated crystals.

6) Various physical properties such as electrical conductivity.

7) Adsorption of gases and vapors.

8) Catalytic properties.

Figure 1.1 Natrolite (Image from the Commission on Natural Zeolites and courtesy of Olaf Medenbach).

Natural zeolite, as shown in Figure 1.1, currently has an extremely wide range of applications, and it is difficult to list them all. For example: In agriculture, they can be used as soil conditioners and as additives to mineral fertilizers.[7] In the construction field, it can be used as building materials and cement additives.[8] In the field of environmental protection, it also can be used for sewage treatment, odor adsorption and hazardous chemical adsorption, etc. [8]

1.1.2 Development of artificial zeolites

From the discovery of natural zeolite, this kind of mineral did not receive much attention in the scientific community for the next two hundred years. Their rarity making them appear useless. With the continuous progress of science, a new type of hydrothermal synthesis method has been designed and developed. Subsequently, Morey and colleagues conducted a review on the development of hydrothermal chemistry from 1845 to 1937.[9, 10] Furthermore, the general evolution of hydrothermal preparation methods from the 19th century to the mid-1980s is summarized by Rabenau.[11] This method has been applied to the synthesis of hydrothermal minerals, zeolite being one of them. It perfectly simulates the synthetic conditions of minerals

in natural state. In 1862, the West Indies-born French chemist Henry Etienne Sainte-Claire Deville claimed to have artificially prepared a zeolite called levynite (levyne). This is the first statement of the existence of synthetic zeolite synthesis. In the early 1940s, R.M. Milton[12] further promoted the development of zeolite synthesis technology, including the synthesis of zeolite mineral mordenite analogs, the discovery of A, X and Y-type zeolites, and important insights into the adsorption properties of zeolites.[13, 14] Beginning in 1951, within 5 years, 12 zeolites were successfully synthesized, some with new structures and others related to known zeolite minerals.[15] Then, synthetic zeolite has ushered its unprecedented attention and development. Barrer and Denny described an amine-related route to zeolites A and X. Kerr and Kokotailo investigated the physicochemical properties of ZK-4 (Si/Al up to 1.7), which is a more siliceous analogue of zeolite LTA.[16, 17] In addition, the successfully synthesized BEA zeolite led to achieve better thermal and acid stability than previous zeolites.[18] In the 1970s, the synthesis of high-silica molecular sieves entered a booming era, such as ZSM-5 molecular sieves, which are still widely used today. With a rapid development of various characterization methods such as spectroscopy and microscopy, the synthesis mechanism of molecular sieves was deeply explored. Novel zeolite formation as aluminum phosphates ($AlPO_4$) and mesoporous zeolites were successfully synthesized.[19] Since the 21st century, computer molecular modeling enables zeolite to be precisely designed according to requirements, which greatly enriches the variety and application potential of zeolite.[20]

In the early days of zeolite discovery, their usefulness did not receive much attention. Until the beginning of the 20th century, the strong adsorption and ion exchange capacity of natural zeolite made it used in the H_2O softening application.[21, 22] In 1925, Weigel and Steinhof demonstrated that dehydrated chabazite can sieve gases according to molecular size, thus opening the door to the application of zeolites in the field of gas adsorption

separation.[23] For example, Union Carbide used Linde type A zeolite to purify argon by adsorbing oxygen in 1953.[24] By the end of 1954, Union Carbide began commercializing synthetic zeolites as a new type of industrial adsorbent for separation and purification. In 1959, the first zeolite-based catalyst was used in hydrocarbon-conversion catalysts. Subsequently, around the 1960s, the acid catalytic properties of zeolites received attention in the cracking and refining of crude oil for the production of transportation fuels and subsequently in the production of value-added chemicals through shape-selective catalysis.[12] Zeolites have revolutionized the petroleum industry due to their excellent activity and selectivity as acid catalysts, for example it has been used in petroleum refining processes for the production of fuels, petrochemicals processing for aromatics production and derivatives, disproportionation of toluene and transalkylation of toluene and trimethylbenzenes and other fields.[24, 25]

Driven by market and economic benefits, the effects of various physicochemical properties of zeolites on their adsorption and catalytic functions have been deeply explored. With the richness of organic template machines and the rapid development of synthetic methods, the artificial zeolites show the explosive growth.[26] Until now, a total of 255 skeleton structure, and the number is still rising.

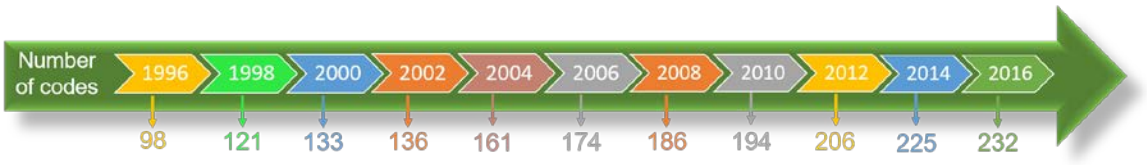

Figure 1.2 The Database of Zeolite Structures (1996-2016).

In modern times, thanks to the rise of computer technology and environmental awareness, the design of new framework structures according to needs,[27] the exploration of microscopic mechanisms[28, 29] and the development of green synthesis routes[30, 31] of zeolite attracted

more attention, as shown in Figure 1.2.

1.1.3 Synthesis methods of zeolites

With the maturity of science and technology, the types of synthesis strategies of zeolite have drastically emerged. Today, many different methods for the synthesis of zeolites are known. The most important ones could be mentioned as follows: hydrothermal synthesis[32], molten salt method[33], alkali activation[34], microwave-assisted synthesis[35], synthesis by dialysis[36]. Among these methods, hydrothermal synthesis is commonly used since the 1950s.[32] This method simulates the formation environment of a given zeolite under natural conditions.

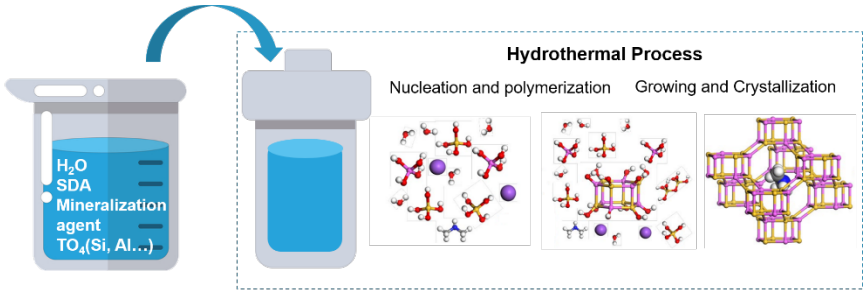

Figure 1.3 The synthesis procedure of zeolites under hydrothermal conditions.[37]

The main synthesis process can be described as Figure 1.3: addition of silicon and aluminum source in alkaline solution (pH > 10) under temperatures ranging between (80-250 ^{o}C) and pressure conditions, and maintain the temperature and pressure for several hours or days until the silica-alumina source completes the processes of dissolution, condensation, gelation, crystallization, and finally forms zeolite crystals. In order to achieve better synthesis effect or obtain zeolite products with specific physical and chemical properties, the synthesis parameters can be adjusted.

1.1.3.1 Hydrothermal method

The hydrothermal method refers to a method of preparing materials by dissolving and recrystallizing powder in a sealed pressure vessel, using water as a solvent.[38] Since Barrer introduced the hydrothermal synthesis process in 1948, it has become the basic route for zeolite synthesis. Several advantages are reflected in this approach, including high reactivity of the reactants, low energy consumption, low air pollution, ease of solution control, formation of metastable phases, and unique condensed phases.[39] This method is considered to be the main synthetic route for many zeolites and zeotypes.[40]

Under hydrothermal conditions, crystal growth mainly undertakes the following steps: First, the reactants are dissolved in the hydrothermal medium in the form of ions or molecules to form a solution. Secondly, due to the temperature difference between the top and bottom of the reactor, ions or molecules are transported to the low temperature zone, where a supersaturated solution rich in seed crystals is formed. Then, the latter species are adsorbed, decomposed, and desorbed at the growth interface. The adsorbed material moves at the interface. Finally, the dissolved matter crystallizes. The morphology of the crystals under hydrothermal conditions is closely related to the growth conditions. The same crystal may exhibit different morphologies under different hydrothermal conditions.[41]

1.1.3.2 Parameters of hydrothermal synthesis

The formation and growth of zeolite crystals in a hydrothermal environment is an extremely complex process. In the whole process of zeolite crystal formation, various parameters will have a direct impact on the morphology, structure, physicochemical properties of the product, and even determine the success or failure of the synthesis.[42] The main influencing parameters are: component source (silica and aluminum source and structure

directing agent), ratio between the different components (SDA/Si, OH/Si, Si/Al, H_2O/SiO_2), time and temperature (crystallization time and temperature, ageing time and temperature).[43]

I. Component Source:

Si and Al elements make up the framework structure of zeolite, so both will have a direct effect on the formation of zeolite. The type of silicon source and aluminum source directly affects the grain size of the zeolite.[44] Furthermore, because the formation process of zeolite crystals is largely dependent on the silicate intermediates liberated at the silicon source in the hydrothermal system, they act as the basic unit of zeolite crystals and have a significant impact on the nucleation and crystallization rates of the crystals. Therefore, the silica precursor has a much effects on the chemical properties and morphology of the zeolite.[45]

Inorganic or organic molecules that are used to direct crystallization into a specific zeolite structure are called the SDA. The application of organic structure directing agents (SDAs) is one of the key factors for the formation of porous zeolite networks and the crystallization process of zeolites. In addition to the pore-forming effect, the addition of different species of SDA can have different effects on the crystal evolution, crystal size, and chemical composition of the zeolite.[46]

II. Ratio of the Different Components:

The ratios of SDA/Si and OH/Si play an important role in regulating the basicity of the initial crystallization solution. The alkalinity means the concentration of R^+, which is an SDA and also a cation balance in the anionic framework of the zeolite, and OH^-, which determines the nucleation and polymerization of silicates and aluminate species by affecting the dissolution and transportation of them in the initial gel. High SDA/SiO_2 and OH/SiO_2 usually lead to highly crystalline nano-ZSM-5 with small crystals, but too high ratios may result in reduced crystallinity and larger crystals.[46]

Water content or H_2O/SiO_2 ratio can affect particle size. The increase in water content results in a decrease in SDA concentration, thus to reduce the solubility of Si and Al sources in the precursor solution. Hence, it leads to an increase in particle size as it lowers the initial solution supersaturation, thus reducing nucleation efficiency. However, if the water content is too low, zeolite synthesis will fail. The ratio of Si/Al plays an important role in the modification of the final particle size and surface properties of the zeolite. For example, changes in the Si/Al ratio can alter the surface charge, protonic and Lewis acid sites of the zeolite.[47]

III. Time and temperature during synthesis process:

Crystallization time is an important factor in zeolite synthesis. Both crystallinity and crystal size are strongly dependent on crystallization time. However, the crystallization time depends on the crystallization temperature. Because, the kinetics of crystal growth is strongly temperature-dependent, temperature has a greater effect on the regulation of crystal size than synthesis time. When the temperature is high enough, the effect of synthesis time becomes negligible, because at these temperatures equilibrium of crystal growth can be reached in a very short time. Increasing the synthesis temperature also accelerates the dissolution of nutrients in the precursor solution, and therefore, faster nuclei growth. At lower temperatures, synthesis time may have an impact on final product particle size. Increasing the crystallization time results in higher crystallinity and larger crystal size. But too long synthesis time can also lead to the decrease of crystallinity and the change of product phase. In the process of hydrothermal synthesis, it is necessary to dynamically adjust the synthesis time and temperature in order to obtain the product with the best performance.[46]

1.1.4 Applications of zeolites

Due to the regular pore structure, uniform pore size and exchangeable framework elements in synthetic zeolite, the latter material has found widespread applications in numerous fields. Moreover, with the continuous advancement of synthesis technology, more and more artificial zeolites are obtained. The structure and physical and chemical properties of zeolites can be designed according to the needs, making them widely used in various fields. There are three main uses for zeolites in industry: gas separation, ion exchange and catalysis.

1.1.4.1 Gas Separation and purification

The different size, shape and structure of the zeolite pores and cavities may lead to favor the diffusion and the interactions between reagents and the surface within the structure. Therefore, some components present in the gas mixture (or in liquid medium) will not be able to enter the zeolite pores, while other components can diffuse within pores and adsorb onto active sites. The purpose of separating and purifying multi-component gas is achieved.[3]

In addition, the physicochemical properties of zeolites can also affect its adsorption and sieving capacity, such as: cationic charge density, cationic concentration, polarizability, and permanent polarity of guest adsorbate molecules. They directly affect the thermodynamic and kinetic selectivity of the zeolite towards reactants. When molecules enter the pores, some are preferentially adsorbed, over others, due to these differences in physicochemical properties.

Thanks to the presence abundant channels with uniform pore size, zeolites can be used for:

1. Removal of impurities (even traces) from a gas: gas drying, desulfurization and removal of toxic, corrosive and heavier organic compounds from polluting gases are areas where zeolites are commonly used. In addition, it is also common to use the adsorption capacity of zeolite to treat impurities in industrial gases.

2. Separation of bulk gas mixtures: the trend is to increase the product purity and recovery and to increase the scale of application while lowering the overall energy requirement and cost for the separation. Figure 1.4.

3. Gas analysis: gas chromatography is extensively used as an analytical tool for research and process control.

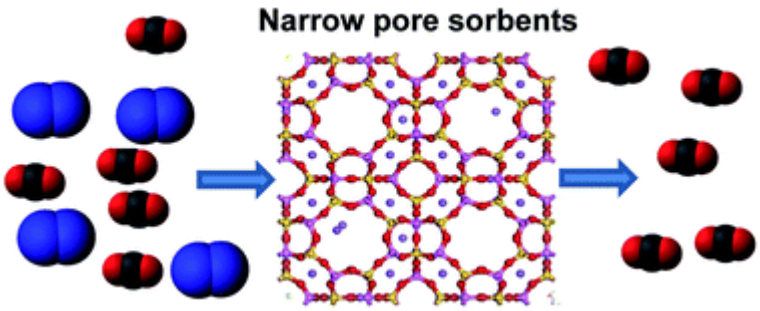

Figure 1.4 Zeolites with narrow pores for CO_2 separation from flue gas.[48]

1.1.4.2 Adsorption and ion exchange

The cations in the zeolite framework are exchangeable. The hydrated cations which bound loosely to the zeolite framework can readily exchange with other actions in aqueous media and their exchange capacity is high.[49] As a water softener, zeolite has the advantages of excellent exchange performance, long-term operation, safety and regeneration. The chemical reaction that occurs in the water softening process is shown in the following equations:

$$Na_2Ze + Ca(HCO_3)_2 \rightarrow 2NaHCO_3 + CaZe$$

$$Na_2Ze + Mg(HCO_3)_2 \rightarrow 2NaHCO_3 + MgZe$$

$$Na_2Ze + Ca(HCO_3)_2 \rightarrow 2NaSO_4 + CaZe$$

$$Na_2Ze + Mg(HCO_3)_2 \rightarrow 2NaSO_4 + MgZe$$

In addition, zeolite can also be used as sewage treatment materials. The wastewater from metallurgical industry generally contains heavy metal ions. Zeolite with strong acid resistance and high ion exchange capacity make it is more suitable for the treatment of acidic wastewater containing heavy metal ions.[50] Furthermore, nitrogen and phosphorus are the two main elements of water eutrophication. Using zeolite to remove nitrogen from sewage, and expired zeolite can be used as soil conditioner to increase the nitrogen source of soil.[51] As shown in Figure 1.5, the issue of removing radioactive substances in water by adding zeolite is also being studied. [52]

The acidity of zeolite also comes from the exchangeability of its framework elements. This feature makes it one of the best solid acid catalysts in the industry today. This will be explained in detail in the next part.

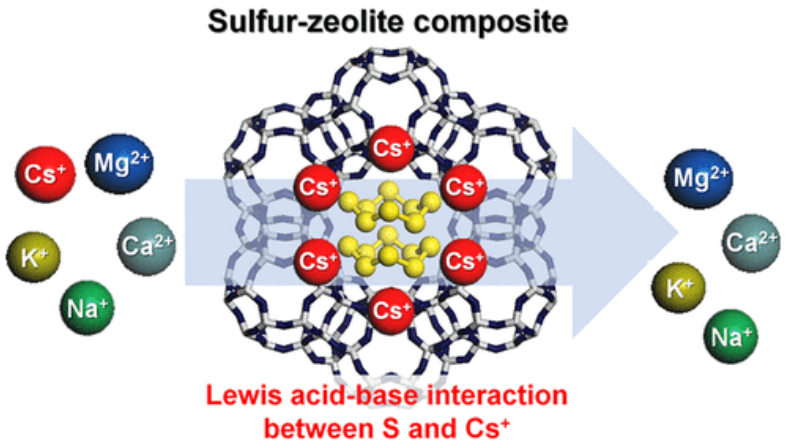

Figure 1.5 Zeolite Framework for Ion-Exchange Selectivity to Radioactive Cesium.[53]

1.1.4.3 Catalysis

At early stages, the commercial use of zeolites had been in adsorption, ions exchange and separation applications such as the removal of water from natural gas, refrigerants, and of hydrocarbon streams. These were non-catalytic applications; however, the commercial use of

solid acid catalysts, based for example, on amorphous silica/alumina, was widely applied since the mid-1950s.[15] When the unique catalytic properties of molecular sieves were discovered in 1960, the field of catalysis ushered in a new revolution. Different from traditional solid acid catalysts, zeolite possesses abundant acid sites, and its uniform and stable pore structure and crystal framework confer unique selectivity and ion exchange. These characteristics make zeolite have better catalytic performance in industrial applications, such as hydrocracking of heavy petroleum distillates, which require high hydrogen pressure. Most zeolites may also operate as bi-functional catalysts-containing both Brønsted acid sites and a component which activates hydrogen (such as a noble metal like palladium or platinum). Such zeolites are applicable in industrial processes such as the isomerization of paraffins to yield a high octane number gasoline fraction.[54]

1.2 Zeolite as catalyst

Broadly speaking, about 20 % of the total zeolite market belong to the catalytic applications, with the remainder was used as detergents (70 %) and adsorbents (10 %). However, in terms of market value, the catalytic application of zeolites is by far the largest, especially in the refining industry.[55] Because the value of zeolite depends not only on the application scale, but also on the value of the final product. The importance of zeolites in the field of heterogeneous catalysis not only on their shape selectivity and acidic catalytic activity, but also on the tunable chemical composition and pore structure making them with wide optimization and design space. Today, zeolites as acid catalysts are closely linked to the development of petrochemicals. However, with the increasing demand for petrochemical products, the catalytic performance of zeolite needs to be further improved. At present, there are many modification techniques for zeolite, which mostly focuses on acid sites, pore size,

particle size, structure, and economic cost, etc.

1.2.1 Characteristics of zeolite catalysts

Abundant acid sites

There are two types of acid site are identified in zeolite: Brønsted acid sites and Lewis acid sites. In the IUPAC Gold book, a Brønsted acid is defined as “a molecular entity capable of donating a hydron (proton) to a base (i.e., an acid is a “hydron donor”) or the corresponding chemical species”.[56] Lewis acid is “a molecular entity, and the corresponding chemical species, that is an electron-pair acceptor and therefore able to react with a Lewis base to form a Lewis adduct, by sharing the electron pair furnished by the Lewis base.” In catalysis by Brønsted acids, the protonation is the crucial step, where the activation energy barrier is reduced. In Lewis acid catalysis, the activation energy is lowered by polarising molecules, thus making them more reactive.

However, pure silicalite has an electrically neutral framework and its surface is not acidic. The acidity of zeolite originates from the isomorphic substitution of Si^{4+} by the introduced trivalent cations such as Al^{3+} changing the framework charge to a negative charge, which is then compensated by the presence of protons, which form the Brønsted acid sites on the oxygen atom of a hydroxyl group bonded to a metal atom (as shown Figure 1.6). Therefore, there are many methods to introduce the Brønsted and Lewis acid sites into zeolite. For example: *(a)* direct proton exchange of charge-compensating metal cations; *(b)* ammonium exchange of the same compensating metal cations followed by calcination to decompose the ammonium cations, leaving a surface proton; *(c)* exchange with multivalent cations that can generate protons through partial hydrolysis of water molecules; *(d)* exchange with metal cations, which can be reduced to lower valence states by hydrogen, again generating protons

on the surface. The Lewis acid site is usually considered to be the non-framework aluminum species produced by the dealumination of the zeolite framework or the tri-coordinated aluminum species with unsaturated coordination on the framework. Moreover, other metal species such as Zn, Ga, Mo, Ag, Sn, etc. are introduced into zeolite can also be used as Lewis acid.

In the catalytic reaction, the acidity of the zeolites largely determines the catalytic performance, including: the conversion rate, yield, selectivity, catalyst life, coking sensitivity and regeneration potential. The acidity usually depends on the chemical composition and framework structure of the zeolite and it is complex. For the factor of chemical composition is generally including the amounts of substitution and types of trivalent cations (Al, Ga, Fe, In, B, etc.). The higher the number of substituted Si^{4+} with trivalent cations, the higher the acidity of the zeolite. For different trivalent cations, the electronegativity of the them is affecting the zeolite acid strength and it is decreasing in series, the order of their acidity in the zeolite framework is as follows: Al (OH)Si > Ga (OH)Si > Fe (OH)Si > In (OH)Si > B (OH)Si. In addition, When the spatial environment of the T atom is different, it will show different acid strengths. For example, an increase in the T-O-T bond angle results in higher acidity of acid site because less energy is required for deprotonation of the bridging OH group. Another framework-related effect is that the strength of each proton site decreases with increasing Al content. Hence, the proton attached to isolated Al with no close Al neighbor is the stronger acid site. This is the effect of the framework structure of zeolite on the acidity.[56]

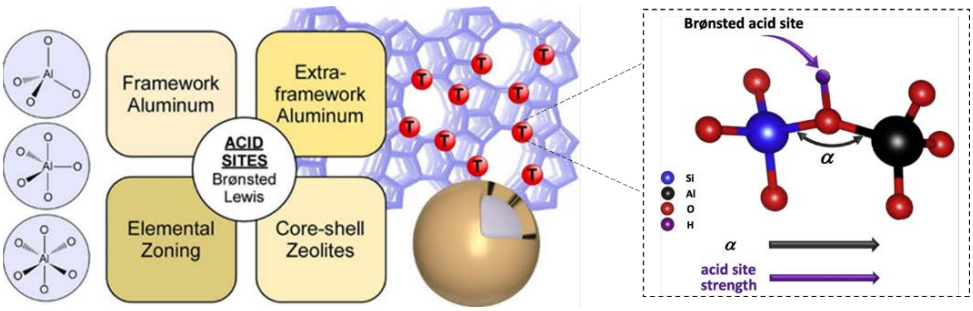

Figure 1.6 Zeolite Brønsted acid sites strength as a function of the T single bond O single bond T bond angle.[56]

Shape selection

Shape selective reactions have been categorized into three types according to their mechanism of action (Figure 1.7). The first is reactant selectivity: some reactant molecules are too bulky to enter the zeolite pores cannot reach active site in the cage of zeolite to perform the reaction. Therefore, the less bulky molecules will react preferentially with respect to larger reactants which are hindered in the zeolite channels.[57]

The second is transition-state selectivity: the reaction products will be restricted diffusing through the zeolite pores due to incompatibilities caused by their size and/or shape when they are formed within the pores. The end result is that the products which are sterically less hindered are able to diffuse out of the zeolite microporous framework. But the bulky products are hindered from moving throughout the zeolite's cavities, and may be converted to less bulky molecules (through equilibration) or ultimately accumulate and block all the zeolite's pores, leading to poisoning and ultimate deactivation of the catalyst.[58]

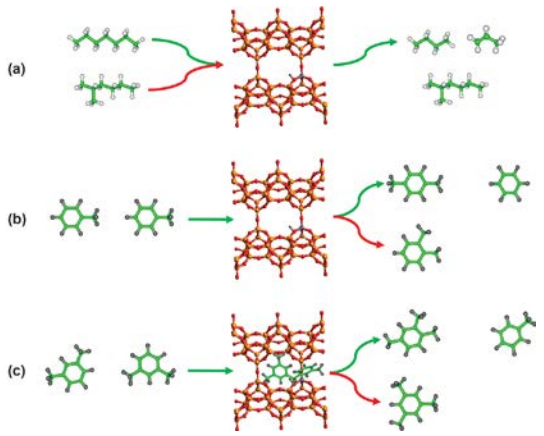

Figure 1.7 Classical concepts of reactant (a), product (b), and transition state shape selectivity (c).[23]

The third is product selectivity. This category occurs when certain reactions are prevented due to the hindrance of the formation of certain reaction intermediates and/or transition states in the reaction pathway, due to a limitation in the shape and/or size of the microporous lattice.[58]

Ion Exchangeable

The ion exchange ability also plays an outstanding role for the zeolite applications as catalyst. For many catalytic applications, a Brønsted acid form of a zeolite is required. Brønsted acid sites in zeolites can be readily generated by introducing ammonium ions followed by a heat treatment or by introducing multivalent metal cations, again followed by heat treatment. In processes which work under hydrogen pressure, such as hydrocracking of heavy petroleum distillates or the isomerization of light gasoline, bifunctional catalysis are needed which contain both Brønsted acid sites and a component which activates hydrogen, typically a noble metal like palladium or platinum. These noble metals can be easily introduced into the zeolite pores by ion exchange, such as $[Pd(NH_3)_4]^{2+}$ or $[Pt(NH_3)_4]^{2+}$, followed by thermal removal of the ammine ligands. More recently, the use of metal-containing zeolite

catalysts for the selective reduction of NO_x with light hydrocarbons, e.g., in exhaust gases from diesel has become a topic of worldwide research.

1.2.2 Modification methods of zeolite catalysts

1.2.2.1 Hierarchical zeolite

Although many excellent results have been obtained using zeolites in a wide range of reactions, there are limitations such as inability to perform reactions involving larger molecules which cannot diffuse inside or outside the zeolite microporous structure. Therefore, in reactions involving large substrates, the efficiency and selectivity are usually lower. These limitations have stimulated research into fractionated zeolites that contain secondary pores (meso- or macropores) larger than 2 nm in size.[59] The term “hierarchical zeolites” arose, as shown in Figure 1.8.

The term “hierarchical zeolites”[60] is usually refers to zeolitic materials having a hierarchical porosity with at least two levels of pore sizes. It means that hierarchical zeolites possess, in addition to their typical and uniform micropores, a secondary porosity. The latter may consist in pores with different sizes extending from supermicropores, to mesopores or even macropores. According to the different pore sizes, hierarchical zeolite can be divided into micro-mesoporous zeolite, micro-large pore zeolite and micro-meso-large pore zeolite.[61]

In most cases, hierarchical zeolites exhibit improved catalytic properties compared with conventional ones.[61] This behavior is especially remarkable in the case of reactions that take place with the participation of large substrates. This can be really considered as the overall consequence of a number of effects derived from the presence of this secondary porosity.

Advantages of hierarchical zeolites

(1) Reduction of the steric limitations toward bulky molecules.

There are at least two active sites present on the zeolite. The first one consists of those sites located in the outer part of the crystalline framework. These sites are quite free of steric limitations for interacting with molecules. The second is the internal site of the crystal, including the site at the entrance of the pore. The steric limitations and shape-selectivity effects will appear in these internal sites when interacting with large compounds.

(2) Increase in the rate of intracrystalline diffusion

It is well known that diffusion of molecules through the zeolite micropores is a slow process, especially when the molecular size of the diffusing species approaches the dimensions of the zeolite channels. As a consequence, the intracrystalline transport becomes the rate-controlling step in many adsorption and catalytic processes over zeolites. These limitations can be greatly overcome with hierarchical zeolites, as the diffusion through the secondary porosity (usually mesoporosity) is quite faster, taking place by mechanisms closer to the classical Knudsen diffusion.

(3) Variation of the selectivity towards the target products

Since the presence of stratified porosity implies a change in the length of the diffusion path, the residence time of the product inside the catalyst changes accordingly. Given the complex reaction pathways of most catalytic reactions, product selectivity may also be seriously impacted.

(4) Decrease in the deactivating effect of coke.

It is well known that zeolite deactivation by coke formation may occur through different mechanisms: site coverage, micropore blockage and deposition over the external surface of the zeolite crystals. The deactivating effect of the coke deposits increasing in the latter order. Thus, the catalytic lifetime extension can be explained by the facile diffusion of coke precursors from the micropores to the outer surface due to the larger outer surface area and shorter diffusion

path length.[62, 63]

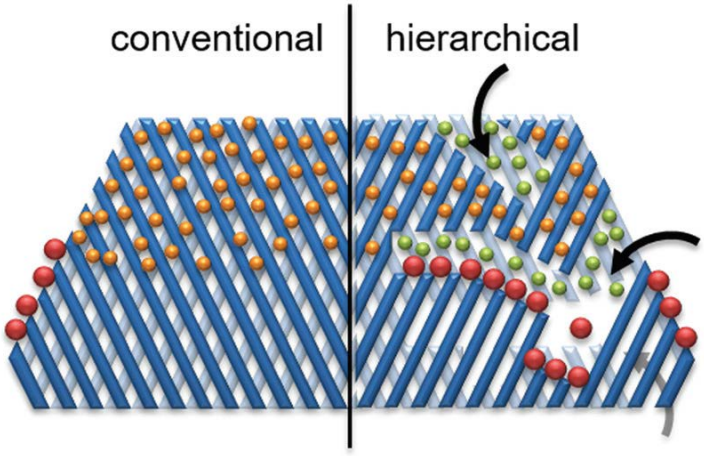

Figure 1.8 Schematic representation of advantages of hierarchical zeolites towards active sites accessibility and transport/diffusion of reactants/products.[64]

Synthesis of hierarchical zeolite

Over the past 20 years, many strategies for preparing hierarchical zeolites have been developed, which are divided into top-down and bottom-up methodologies, as shown in Figure 1.9.[65]

Top-down method usually involves conventional microporous zeolite as pristine material, treating it with reagents with etching properties such as acids, bases, steam, etc., to realize the removal of silicon or aluminum from the zeolite framework.[66]

The bottom-up method is a kind of constructive approach based on the fact that the hierarchical zeolite is directly created during the synthesis process.[65] This method usually uses organic molecules or inorganic materials as pore-forming templates. Therefore, it is also called the template method. Commonly used templating agents can be divided into hard templates and soft templates. For example, surfactants, silylated polymers and organosilanes are soft templates, while carbon materials, biomaterials and polymers are considered as hard

templates.[67]

Carbon materials are commonly used as hard templating agents. It has a wide range of sources, stable properties, and easy removal. The confined space method using carbon blacks as hard templates was adapted for the preparation of hierarchical zeolites with different structures. Christensen et al. using mesoporous ZSM-5 prepared by the confined space method, demonstrated the beneficial effects of introducing mesopores on the mass transport properties of the zeolite. Koo et al.[68] synthesized mesoporous ZSM-5 by mixing the zeolite gel precursor with carbon black nanoparticles and subsequent hydrothermal treatment using microwave heating. Likewise, Kustova et al. corroborated that the use of different carbon sources enables the possibility of tailoring the porosity and crystal size of the final zeolite.[69] Carbon nanotubes or nanofibers have also been employed as templates for the generation of mesopores within zeolites.[70-72] Carbon nanofibers allow cylindrical mesopores with lower tortuosity to be obtained compared to the mesopores templated by carbon black particles.[73] Ordered mesoporous carbons have also been applied as templates for the synthesis of hierarchical zeolites. These carbons are characterized by highly ordered pore structures. Consequently, zeolites obtained exhibit more regular mesoporous structures with smaller and narrower sizes than those templated with traditional carbon materials. One drawback of using ordered mesoporous carbon templates is that their preparation involves costly and/or time-consuming synthesis procedures.

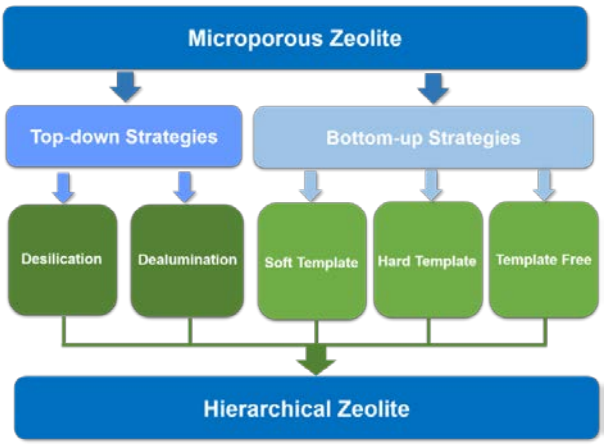

Figure 1.9 Preparation technology of hierarchical zeolite.

1.2.2.2 Adjustment of zeolite acidity

The introduction of zeolite acidity has been mentioned before.[56] Generally speaking, a catalyst with strong Brønsted acidity usually leads to higher catalytic activity, but also to accelerated coke formation. Therefore, the zeolite acidity needs to be adjusted in line with the catalytic process needs to reach the higher economic benefits. The most commonly used methods to adjust acidity are *(a)* changing the Si/Al ratio,[74] *(b)* hydrothermal treatment (dealumination),[75] *(c)* and adding various promoters, including various metallic or non-metallic elements.[76] These three methods are essentially the adjustment of the Al content in the zeolite, because it determines the acidity of the zeolite. However, different adjustment methods will also affect other physical and chemical properties of the zeolite, as discussed below[77]:

Changing the Si/Al Ratio

It is a simple and effective pre-synthesis approach, allowing to adjust the acidity by directly changing the amount of aluminum source in the gel.[78] However, the modification effect of this method is limited, and sometimes it cannot meet the needs of catalysis. Therefore,

it is generally used as a basic step in the modification of zeolite catalysts.

Dealumination Techniques

These are classified into two categories, extraction of framework Al by chemical agents, such as acids[79], and hydrothermal dealumination of the zeolite framework.[80] These two dealumination methods can not only dealuminate the zeolite framework, reduce the number of Brønsted acids and form Lewis acids, but also affect the framework structure of zeolite, such as enlargement of pore size. It should be noted that excessive dealumination will also reduce the stability of the zeolite framework and negatively affect its catalytic performance.

Adding Promoters

In the past few years, introducing heteroatoms into the zeolite framework has become an important strategy to improve its catalytic and adsorption performance. Heteroatom-containing zeolites exhibit different properties than conventional aluminosilicate zeolites in terms of surface acidity, pore structure, particle size, etc.[80, 81] In general, heteroatom zeolites can be synthesized by two strategies, i.e., the direct synthesis and post-synthesis modification. The direct synthesis method uses metal organic compounds or metal salt solutions as metal precursors to introduce heteroatoms into zeolites.[82] The method can also be divided into hydrothermal doping and dry-gel conversion method doping according to the zeolite synthesis method. ENI company successfully synthesized TS-1 by hydrothermal method, which added metal heteroatom solution into silica-alumina sol to generate silica-alumina and heteroatom acid salt sol, ensuring the uniform dispersion of Ti inside the framework.[83] In addition, direct hydrothermal synthesis has a large operating space, and the crystal structure and zeolite morphology can be optimized by controlling the synthesis conditions. However, the direct synthetic route has the disadvantages of long crystallization process, high cost of organic templates, and low content of framework heteroatoms.

Recently, heteroatoms successfully introduced in the zeolite framework can be divided into three categories: main group atoms: (As, Ga, Sn, Ge, etc.), non-metals (B, C, F, etc.) transition metals (Ti, Fe, etc.), non-metals (P), and semi-metals (B). This method is considered as an attractive route to improve catalytic efficiency and adsorption selectivity.[84]

1.2.2.3 Structured zeolites

Powdered materials typically generate issues such as mass/heat transfer differences, high pressure drop, irregular flow patterns, etc. in fixed bed reactors. That inevitably leads to selectivity and activity loss of zeolite catalyst. As a consequence, the structured zeolites were proposed as a viable alternative to design promising catalysts.[85] Figure 1.10 summarizes the synthesis strategies to produce structured zeolites, grouped in two main families: *in situ* crystallization coatings and composite zeolite coatings. Among of them, *in situ* crystallization and sol-gel coating are the most commonly used. [86]

Hydrothermal in situ Crystallization Method

This process can allow to prepare the structured zeolite component by crystallites grown onto a macro-shaped support surface.[87] The main advantage of *in situ* synthesis compared to other coating techniques is that the support is used as a nucleating material and chemical bonds are formed between the zeolite crystals and the outer support layer, which results in a high affinity between the support and the zeolite layer. Therefore, the zeolite/support composite has high thermal, chemical and mechanical stability.[88]

Ionothermal in situ Crystallization Method

Ionothermal synthesis is the use of ionic liquids simultaneously as both the solvent and the potential template for the formation of solids.[89] The main advantage of this technique is that the zeolite crystallization process can be carried out at atmospheric pressure (low vapor

pressure of ionic liquids), avoiding the high pressure autoclave step required in hydrothermal synthesis.[90]

Dry-Gel Conversion Method

Although the dry-gel conversion process also consists of several stages of hydrothermal reactions, the crystallization of zeolite starts from a xerogel precursor in a steam environment, and the whole process does not involve a liquid precursor. Therefore, the crystallization process is simple, the waste is less, and the quantity of template involved remains low.[88]

Sol-Gel Coatings Method

The technology is based on a dip-coating deposition procedure. The basic process including: the carrier is immersed in a binder-zeolite solution. Then, the binder completes the cross-linking reaction and ensures cure of the zeolite coating. However, the use of binder may increase the diffusion resistance, thus to reduce the accessible porosity.[86]

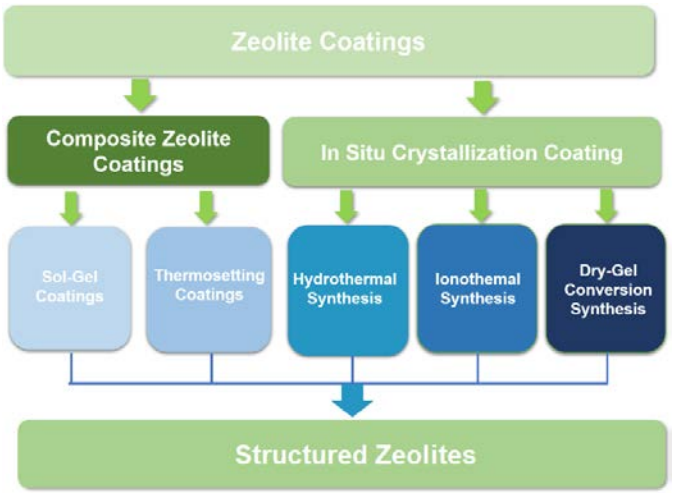

Figure 1.10 Synthetic scheme of the structured zeolite.

1.3 MTO technology

1.3.1 Global market for light olefins

Light olefins (ethylene, propylene and butylenes) are an important cornerstone of the development of modern industry.[91] They are widely used in petrochemistry, bulk chemicals and other fields; in addition their demand is still growing, as shown in Figure 1.11.

Ethylene is one of the largest-volume petrochemical produced worldwide, used in the production of highly important intermediate chemicals in industry such as ethylbenzene, ethylene oxide and dichloroethane.[92] Propylene is a versatile petrochemical which has even more derivatives than ethylene.[93] Consumption of polypropylene has continued to grow over the past 15 years. In 2010, more than 55% of propylene consumption was dedicated to the production of polypropylene in the Western European countries. Approximately 13% of the propylene was used in the production of propylene oxide, which is a chemical precursor for the synthesis of propylene glycol and polyols. Butylenes consist of four isomers with different application values, respectively. In a refinery, butylenes can be used as feedstock to synthesize a high-octane gasoline component. In addition, butylenes are also used to get methyl tert-butyl ether (MTBE) and isooctene, which are both high-quality gasoline blends. Ethylene and propylene are the top organic chemicals produced globally, with an average annual production of roughly 200 million metric tons and 100 million metric tons, respectively. [94]

However, just like molecular hydrogen, olefins are not occurring as natural resources due to their reactivity. They have to be synthesized starting from other feedstocks and are currently almost entirely derived from fossil resources.[95] Steam cracking is the most important process for the production of light olefins.[96] However, the shortcomings such as high energy consumption, low yield of high-value products and shortening of service life of the device due

to coking existed in this process.[97, 98] In addition, the (relative) scarcity of crude oil resources in some countries has led to an insufficient supply of steam cracking raw materials. In order to alleviate the limitations caused by the shortage of oil, and further reduce costs, energy consumption and CO_2 emissions, a variety of new olefin production processes have been developed. [94]

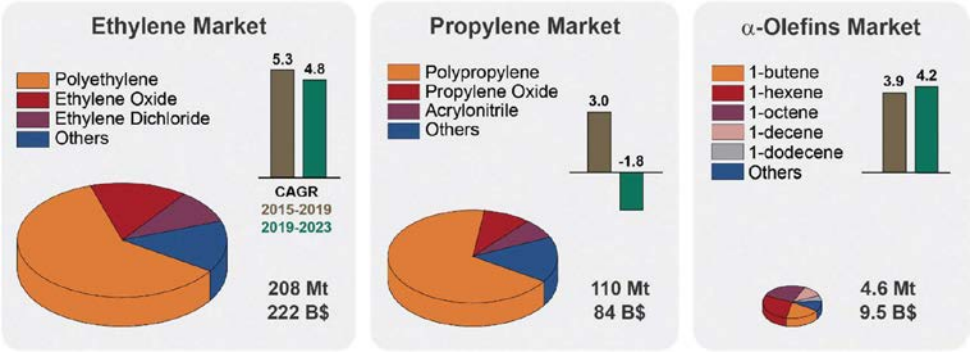

Figure 1.11 the main applications of light olefins together with their market size, trends and predicted growth. Compound Annual Growth Rates (CAGR) over the years 2015-2019 (brown) and the projected CAGR for 2019-2023 (green) are reported as bars.[95]

1.3.2 MTO technology development

Methanol-to-olefins (MTO) reaction has become a successful process for light olefins production via a non-petrochemical route. This process uses methanol, which can be prepared based on coal or natural gas resources, as feedstock over zeolite-based and zeolite-like catalysts.[99] In 1970s, Chang et al., from Mobil Company, first disclosed the MTO process catalyzed by ZSM-5 zeolite.[100] In 1984, the Union Carbide Corporation (UCC) developed a new series of silicoaluminophosphate (SAPO) zeolites, which greatly enhanced the selectivity in light olefins to 90%. However, SAPO zeolites exhibit shorter catalytic lifetime than ZSM-5 zeolite. At present, new catalysts are continuously developed for the MTO reaction, such as ZSM-22[101], SSZ-13[102], and so on. But in general, ZSM-5 and SAPO-34 remain the top-

two catalysts for the MTO reaction based on their excellent activity and selectivity.[103] Many research institutions and companies also have put great effort to decipher the reaction mechanism,[104] catalyst synthesis[105] and process research and development. [106, 107]

1.3.2.1 Mechanism of MTO reaction

Due to the high reactivity of methanol, being quite sensitive to catalysts, essentially acidic zeolites are used to convert it to form hydrocarbons. The reaction process is rather complex, as shown in Figure 1.12.[108, 109] So far, 20 direct reaction mechanisms have been proposed to explain the first C-C bond formation, but all of them were proved either incomplete, or wrong. Currently, it is well accepted that ethene and propene are formed via a direct mechanism in the initial methanol conversion stage; after a transition period, olefins are mainly produced via a hydrocarbon pool (HCP) mechanism in the steady-state stage.[110] The hydrocarbon pool mechanism has been first proposed by Kolboe and colleagues based on MTO conversion experiments over SAPO-34.[111] These compounds, named the “hydrocarbon pool species", are formed and trapped within the channels/cages of the zeolite. They interact with the inorganic framework and serve as a scaffold or an assembly unit for building olefinic products (as well as alkanes and aromatics). [101, 110] The results acquired from industrial MTO plants have also confirmed the rationality of this hydrocarbon pool mechanism over SAPO-34 catalyst.[112] However, the hydrocarbon pool mechanism may not be sole involved in the MTO reaction. In fact, the reaction of methanol on ZSM-5 catalyst is by far more complicated than the MTO reaction over SAPO-34, including a series of parallel and sequential reaction steps between methanol and hydrocarbons. Svelle and Bjorgen [113, 114] have found that the reaction proceeded through a dual reaction cycle. On one side, the aromatics-cycle mechanism occurs besides an-olefin cycle mechanism. The dual cycle mechanism confirms that the active

sites involved in the aromatic pool mechanism and the olefin pool mechanism are different. Indeed, ethylene is supposed to be mainly generated through the cycle of aromatic hydrocarbons, whereas propylene and larger olefins are generated through the methylation-cracking mechanism.[115]

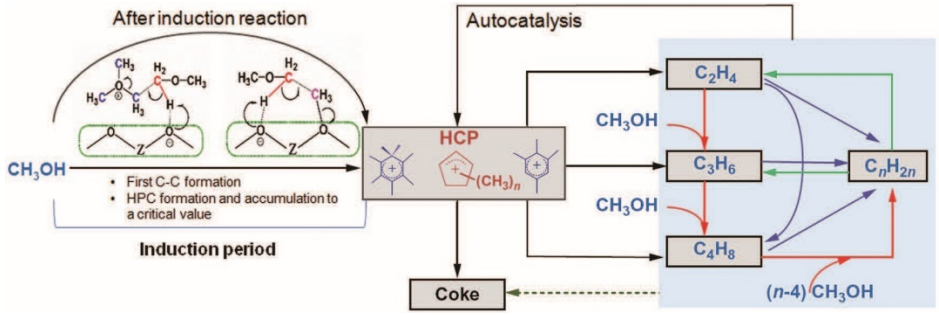

Figure 1.12 Proposed reaction network of the MTO process. Reproduced with permission.[109]

1.3.2.2 Deactivation mechanism in MTO reaction

The deactivation path of an acidic zeolite in the MTO can be summarized as the formation of heavier compounds (called coke) within the pores or on the surface of the zeolite, which are covering the active sites. In fact, the formation of carbon deposits is extremely complex. For instance, SAPO-34 and ZSM-5 exhibit different deactivation modes in the course of methanol conversion (as shown in Figure 1.13). The deactivation of SAPO-34 is mainly due to the conversion of restricted intermediates (such as polyalkyltoluenes) into bulky polyaromatics which are occluded in the CHA zeolite cavity, rendering the active site of the catalyst inaccessible to the methanol.[116] The structure of ZSM-5 excludes the presence of bulky coke species in the 10-membered ring channel. The deactivation of H-ZSM-5 is not related to pore plugging by coke formation, but rather by coke deposition on the external surface as well as acid site poisoning.[110] Therefore, under identical operating conditions, the methanol conversion over SAPO-34 encounters quicker deactivation than H-ZSM-5.[109]

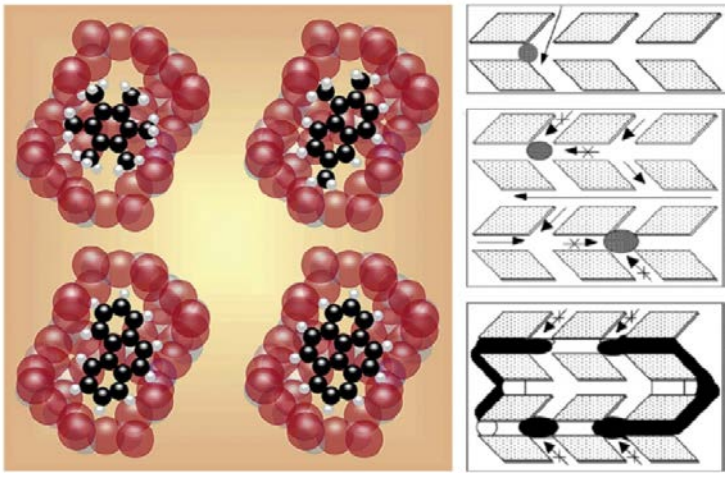

Figure 1.13 Deactivation phenomena involved during the MTO reaction over SAPO-34 (left)[117] and H-ZSM-5 (right).[118]

In addition to the differences in zeolite structures, the types of reactants and products, reaction conditions, the number/strength and location of acid sites in the catalyst can all affect the coking process.[119] For example, in acid-catalyzed reactions, several molecules act as coke precursors such as: olefins and aromatics, which are highly reactive and easily adsorbed on catalyst surfaces.[120]

The reaction temperature also presents a significant effect on the composition of coke and it is usual to classify coke into low temperature (<200 °C) and high temperature (>350 °C) coke species. At low temperatures, coke retention results from strong adsorption, low volatility of the components. At high temperatures, PAHs are the main components of coke, and the pore size of the zeolite determines that they are trapped.[121] In addition, the acidity of the zeolite also has a direct impact on the formation of carbon deposits. Generally: (i) the stronger the acid site, the stronger the chemical interaction with a reagent, resulting in the intensive formation of coke precursors/molecules to accelerate the coking rate; (ii) The higher the density of acid sites, the higher the probability to get consecutive chemical steps that reactant molecules

undergo within the zeolite. Hence, this facilitates the occurrence of condensation reactions, resulting in rapid coking. Therefore, in order to obtain catalysts with long lifetime, the above factors must be incorporated into the modification design of zeolite catalysts.

1.3.3 Application of ZSM-5 Zeolite in MTO reaction

ZSM-5 zeolite is a highly siliceous aluminosilicate zeolite which consists of several pentasil units linked together, and the framework code is MFI. Inside the ZSM-5 zeolite framework, where two types of pores can be found (Figure 1.14): straight channels along the (010) direction and zigzag channels along the (100) direction. The latter pores cross each other at intersections; a three-dimensional pore network is obtained with the dimensions 5.1×5.5Å (straight channel) and 5.3×5.6Å (zigzag channel). It has been widely applied in industry as a catalyst. The chemical formula is $Na_nAl_nSi_{96-n}O_{192}\cdot 16H_2O$ ($0< n<27$).[122] In this formula the variable, n, can range from 0 to 27. That means the ratio of the amount of silicon molecules and aluminum molecules can be tuned in a large range, so acid sites of ZSM-5 zeolite with great adjustability can be obtained.

As a catalyst widely used in hydrocarbon activation reactions, ZSM-5 shows strong acidity, high activity and pronounced selectivity.[123] Therefore, the purpose of ZSM-5 zeolite optimization often focuses on the improvement of catalyst lifetime. Adjusting the acidity, expanding pore size and reducing the grain size, etc. are the main modification methods currently employed. They prolong the lifetime of a given zeolite by reducing the formation of aromatics and coke. These modification methods have been reviewed in detail in Section 1.2.

In general, ZSM-5 zeolite has great application potential in the MTO process. If the corresponding quantitative relationship between the acid sites amount, Brønsted acid or Lewis acids and the selectivity in the targeted product in the MTO and yield, an optimal adjusting of

the number of sites in ZSM-5 zeolite can be designed. In addition, ZSM-5 zeolite with a hierarchical structure exhibits good shape selectivity and diffusivity, which is of great application value in MTO reactions with strict diffusion requirements, and can yield good selectivity and stability. Therefore, the prepared ZSM-5 zeolite with moderate acidity, suitable particle size and hierarchical structure to meet the increasingly tense industrial demands of the MTO process has become the main research goal of ZSM-5 zeolite catalysts in the future.

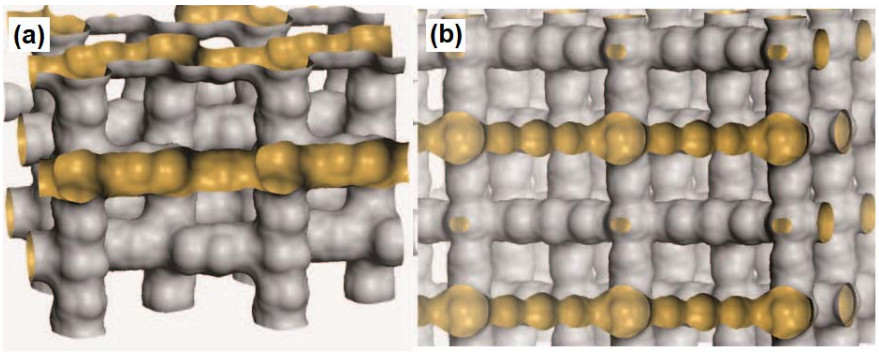

Figure 1.14 (a) shape and connection, (b) inner surface in the structures of H-ZSM-of the internal surface to the H-ZSM-5.[124]

Chapter 2. Experimental part

2.1 Materials and Pre-treatment

Materials

Trachydiscus minutus Algae was provided by the Institute of Chemical Process Fundamentals (ICPF, Prague, Czech Republic);

Tea is a kind of green tea from Guang Xi, China;

Lignin (DP-22666) was kindly provided by Borregaard (Norway). >90% polymer (<10% water); density 500-630 kg/m^3; high MW; medium S-content; 48.4 at% C; 5.0 at% H;

Grass was bought from the company Riga, France;

Perlite was provided by Radis et Capucine Company, France. It was washed, dried, and sorted by diameter (a: 4-3 mm, b: 3-1.5 mm, and c: 1.5-0.5 mm);

Pre-treatment

Raw materials for the preparation of zeolites: sodium aluminate anhydrous ($NaAlO_2$, Riedel de Haën), tetrapropylammonium hydroxide (TPAOH, 20 wt% in water, Sigma-Aldrich), anhydrous ethanol, tetraethyl orthosilicate (TEOS 99%, Sigma-Aldrich), ammonium nitrate (NH_4NO_3 98%, Acros Organics), hydrochloric acid (HCl 37%, Sigma-Aldrich) and methanol (≥99.9%, HPLC gradient grade, Fisher Chemical).

The preparation of Biochars: dry biomasses (Algae, Grass, Tea and Lignin) were firstly grinded and sieved (100 mesh), then the powders were heated at 300 ^oC for 1 h, 5 ^oC/min. As-obtained biochars were named as Algae-C, Grass-C, Tea-C and Lignin-C.

The preparation of Acid treated Biochar: with the aim to remove impurities, the biochar was treated with 2M HCl solution at 80°C for 2h.

2.2 Synthesis of ZSM-5 zeolite

All used ZSM-5 zeolites in this Thesis were synthesized according to the hydrothermal method. The addition ratio of raw materials and synthesis parameters were adjusted according to the requirements of the final targeted properties. The synthesis processes are discussed

separately for the biochar modified ZSM-5 zeolites and perlite-based structured ZSM-5 zeolites.

Biochar modified ZSM-5 zeolites:

0.13 g $NaAlO_2$ was dissolved in 20 g H_2O, then 12.7 g tetrapropylammonium hydroxide (TPAOH) was added. The obtained solution was kept under stirring until it turned clear. Finally, 10.4 g tetraethyl orthosilicate (TEOS) was slowly dropped into the solution and kept under stirring for 3 h. For the biochar-modified ZSM-5 zeolite, biochar was added to the above solution and stirred for 3 h to fully mix the biochar and the solution. In the next step, the mixed liquor was transferred to an autoclave for a hydrothermal treatment at 170 ^oC during several hours/days (the durations were varied). After this crystallization step, the solid was recovered by filtration and washed several times with deionized water until the pH reached 7. The final product was dried overnight and calcined in a muffle furnace under air flow at 550 °C for 12 h to remove both the organic template (TPAOH) and the hard template within the micropores of the samples. Finally, the powder was ion-exchanged with 1 mol l^{-1} NH_4NO_3 solution 3 times (1 h each). Finally, the exchanged zeolite was calcined again at 550 ^oC for 5 h to release ammonia. The biochar modified ZSM-5 zeolites were obtained. The whole synthesis strategy is summarized in Figure 2.1.

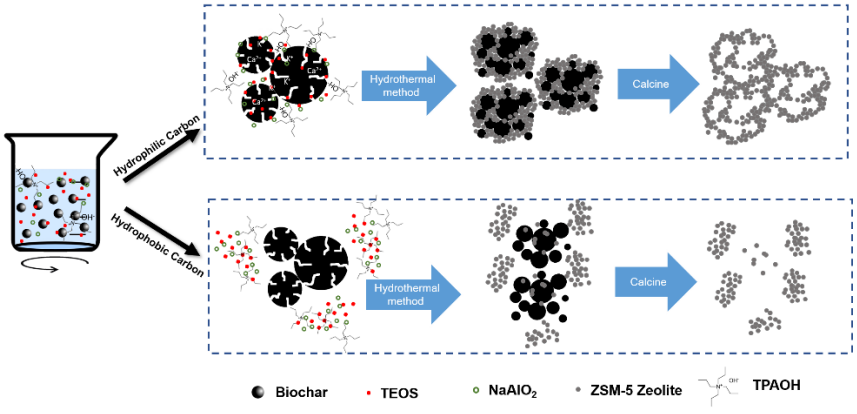

Figure 2.1 Synthesis strategy of Biochar modified zeolite.

Perlite-based structured ZSM-5 zeolite

To design this new family of structured catalyst, perlite was selected both as a support material and as the aluminum source for the synthesis; so no $NaAlO_2$ was added to the precursor solution. The ZSM-5 zeolite was synthesized as follows: 18.6 g TPAOH, 9.2 g ethanol and 13 g H_2O were mixed together. Then 10.4 g TEOS was slowly added to the solution under vigorous stirring. Finally, the clarified liquid and quantity of perlite were placed in a Teflon-lined stainless-steel autoclave. The hydrothermal treatment was undertaken in the oven at 170 °C and its duration was set to 3 days under autogenous pressure. After cooling, the obtained composite was filtered, washed several times with distilled water and calcined at 550 ◦C to remove the structure directing agent. As a reference sample, pristine zeolite without perlite addition was also synthesized following the same protocol. The zeolite was named Silicalite-1 because it did not contain any aluminum.

The synthetic strategy for preparing those ZSM-5/perlite structured materials is schematized in Figure 2.2. It should be noted that the adjustment of the synthesis parameters was detailed in the "experimental parts" of the corresponding chapters.

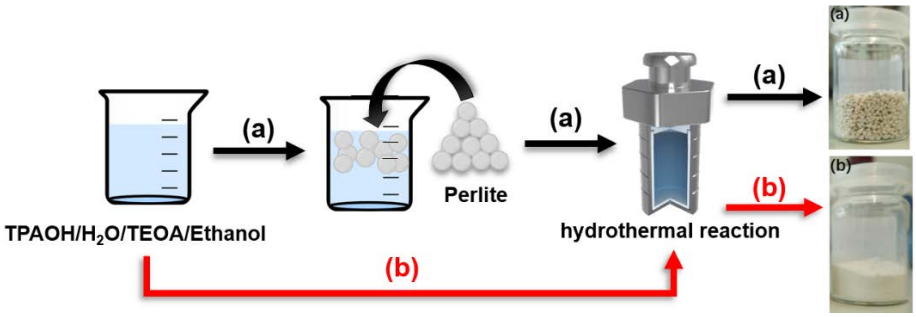

Figure 2.2 Synthesis strategy of (a) ZSM-5/x-n-Perlite and (b) silicalite-1.

2.3 Catalytic set-up

The MTO reaction catalyzed by zeolites was investigated using a fixed-bed reactor at atmospheric pressure. Prior to reaction, the catalysts were calcined at 450 °C for 1 h under Ar flow to remove impurities, after which the reactor temperature was adjusted to the reaction

temperature (between 300-450 °C). The amount of catalyst was set to 0.6 g, packed with quartz wool plugs in a quartz tubular reactor, as shown in Figure 2.3. The reactant methanol was fed using a saturator by a constant flow of Ar (20 ml/min). The temperature of the saturator was adjusted by means of a water bath to tune the desired weight hourly space velocity (WHSV). In this study, two feed velocites were selected: WHSV=2 and 8 g MeOH/g_{cat}·h^{-1}.

The products at the reactor outlet were analysed at regular time intervals (1 h) by GC equipped with a 50 m capillary column (PONA) and a flame ionization detector (FID). The GC program consisted in an isothermal mode at 40 ºC for 7 min, followed by an increase of 20 ºC/min until 280 ºC and an isothermal mode at this temperature for 10 min. In the calculated methanol conversion and selectivity (wt%), dimethyl ether (DME) is considered as unconverted methanol. The selectivity was expressed as the ability to direct the reaction to give a particular product under the same reaction conditions. Here, the selectivity was considered as the mole ratio of each product referred to the moles of converted methanol and DME. The expressions of conversion and respective selectivity were shown in Equations (1), (2) and (3). All the selectivities were expressed after 2 h on stream. Where n represents the quantity of the desired fraction and α is the number of C- atoms in products, ∑ means the calculation of the selectivity towards light olefins (C_2-C_4 olefins).

$$X = \frac{n\ MeOH\ in - (n\ MeOH\ out + 2 * n\ DME)}{n\ MeOH\ In} * 100\% \qquad (1)$$

$$S = \frac{(\sum)\alpha * n(CH_2)}{n\ MeOH\ in - (n\ MeOH\ out + 2 * n\ DME)} * 100\% \qquad (2)$$

$$\frac{\mathrm{C3}}{\mathrm{C2}} = \frac{n\ (C_3H_6)}{n(C_2H_4)} \qquad (3)$$

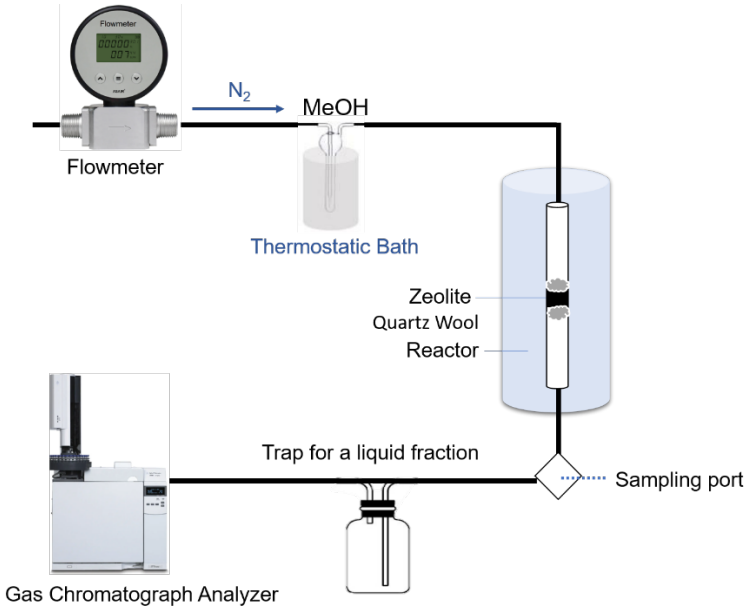

Figure 2.3 Experimental set-up for the MTO reaction.

2.4 Characterization techniques

2.4.1 X-Ray diffraction (XRD)

X-ray diffraction (XRD) is a powerful non-destructive technique primarily used for phase identification of a crystalline material. This technique allows to obtain the fingerprint of a given material, thus providing sound informations on unit cell dimensions, phases present, preferred crystal orientations, crystallite sizes and other structural parameters.[125] This technique is based on the Bragg's law as shown in Equation 4, where n is an integer, λ is the wavelength of the X-ray, d is the interplanar spacing where diffraction occurs, and θ is the diffraction angle.

$$2d \sin\theta = n\lambda \qquad (4)$$

Lattice parameters are obtained by detecting, processing and counting these diffracted X-rays. Due to the random orientation of the powder material, all possible diffraction directions of the lattice can be obtained from the scan results. Since each compound has a unique set of d-spacings, diffraction peaks can be converted to identify the structure of the materials.[126] This is achieved by comparing the XRD pattern to the Joint Committee on Powder Diffraction

Standards (JCPDS) files.[127]

In this Thesis, all powder XRD patterns were obtained with Bruker AXS D8 Advance diffractometer and LynxEye detector within the range of 2θ = 5 °-65 ° with a step size of 0.02° and a step time of 2 s. The analyses were performed with a source of X-ray (Cu Kα radiation, 1.5406 Å) and a power of 40 kV×40 mA.

2.4.2 Scanning electron microscopy (SEM)

A scanning electron microscope (SEM) is a type of electron microscope, which can use an electron beam to image samples with a resolution down to the nanometer scale. The principle of SEM is applying kinetic energy to produce signals on the interaction of the electrons. These electrons are either secondary electrons or backscattered electrons, which are used to view crystallized elements and photons. It is mainly used to observe the surface of materials and gives information about topography, morphology, roughness, composition, orientation of grains, crystallographic information, etc. of the material.

The morphologies of all samples in this study were acquired on a scanning electron microscope (Zeiss Gemini SEM 500) at 3 KeV equipped with a field emission gun. Energy-dispersive X-ray (EDX) analysis was performed to determine the elements contained in the samples.

2.4.3 N_2 adsorption/desorption

Gas adsorption is a common method for measuring the specific surface area and pore size distribution of materials. This method is based on the adsorption characteristics of gas on the solid surface, that is, the equilibrium adsorption capacity is measured under a certain pressure, and then the specific surface area, pore size distribution and physical quantities related to physical adsorption of the sample to be measured are obtained through theoretical calculation.

Among them, the widely used Brunauer-Emmet-Teller (BET) theory is applicable to the low-temperature nitrogen adsorption-desorption method.[128] The BET equation strictly describes a relationship between the adsorbed gas amount per gram of solid, the equilibrium

pressure, the temperature, the gas nature and the nature of the studied solid, as shown in equation 5.

$$\frac{P}{V(P_0 - P)} = \frac{1}{V_m C} + \frac{C-1}{V_m C} * \frac{P}{P_0} \qquad (5)$$

The surface adsorption capacity of N_2 on the solid surface depends on the relative pressure of nitrogen (P/P_0), where P is the partial pressure of N_2 and P_0 is the saturated vapor pressure of N_2 at 77 K. Adsorption and relative pressure P/P_0 fit the Brunauer, Emmett and Teller (BET) equations when P/P_0 is in the range of 0.05-0.35. Nitrogen adsorption can accurately analyze the mesopores (2~50 nm) and some macropores (50 nm) of the material.

The textural properties of the samples in this Thesis were measured by N_2 sorption isotherms measured at 77 K (ASAP 2020M equipment, Micromeritics). Total surface area was determined by the Brunauer-Emmett-Teller (BET) method using the relative pressure (P/P_0) in the range of 0.05-0.3. The total pore volume was calculated at $P/P_0 = 0.99$ while the micropore volume was estimated by t-plot method.

2.4.4 Temperature-programmed desorption (TPD) of NH_3

A temperature programmed desorption (TPD) technique has been developed especially in the field of catalysis, because the technique allows to study the interaction of probe molecules with solid surfaces, thereby being a powerful tool for the evaluation of active sites on catalyst surfaces.

NH_3-TPD uses ammonia gas as the probe molecule to quantitatively adsorb the sample at room temperature, and then uses He as the desorption medium to desorb adsorbed ammonia under the condition of raising temperature. There is a linear relationship between the adsorption force of ammonia on the sample and the acidity of the adsorption site. Generally, the stronger the adsorption site, the higher the adsorption energy of ammonia gas, and the higher the temperature required for desorption. Therefore, by analyzing the ammonia content in the adsorption and desorption gas at different temperatures, the distribution of acidic sites in

the sample can be characterized.

The acid sites analysis of zeolite was performed in a chemisorption analyser AutoChem II from Micromeritics. 0.05 g of the catalyst sample was purified in He at 700 ^{o}C for 10 min, cooled to 100 ^{o}C, then exposed to ammonia−helium mixture (10% NH_3-90% He) for 1 h. Physically adsorbed NH_3 was removed by He at 100 ^{o}C until the baseline became stable. The TPD curves were obtained at a heating rate of 30^{o}C from 100 to 700 ^{o}C. The desorbed ammonia was detected by gas chromatography with a thermal conductivity detector.

2.4.5 X-ray fluorescence (XRF) spectroscopy

X-ray fluorescence (XRF) is based on the emission of characteristic "secondary" (or fluorescent) X-rays from a material that has been excited by being bombarded with high-energy X-rays or gamma rays. The phenomenon is widely used for elemental analysis and chemical analysis. In this study, elemental analysis of the samples was performed by X-ray Flurorescence spectroscopy using Epsilon 3XL Panalytical apparatus. The fluorimeter holds a silver tube working at a maximum voltage of 50 kV. Samples were analyzed in the form of micrometer-sized pearls.

2.4.6 Fourier transform infrared spectroscopy (FTIR)

A molecule’s covalent bond will selectively absorb radiation of specific wavelengths, which changes the vibrational energy in the bond. The type of vibration (stretching or bending) induced by the infrared radiation depends on the atoms in the bond. Because different bonds and functional groups absorb different frequencies, the transmittance pattern is different in different molecules, which can be used to determining components in a mixture.[129]

FTIR spectra of surface functional groups of biochars were obtained by using a PerkinElmer infrared spectrometer model Spectrum 1000. Spectra were taken using 4 cm^{-1} resolution and 32 scans for statistical averaging.

2.4.7 Thermogravimetric analysis (TGA)

Thermogravimetric Analysis is a technique used to detect sample integrity changes under a

controlled temperature program in a controlled atmosphere.

The thermal decomposition processes of biomasses were evaluated by TGA. The biomasses were heated to 700 ^{o}C, at 5 ^{o}C/min, in a flow rate of air (99.99%) at 20 ml/min via using Q 5000IR from TA Instruments.

2.4.8 Dynamic light scattering (DLS)

Dynamic light scattering (DLS) is based on the Brownian motion of dispersed particles. In dynamic light scattering, the time-dependent fluctuations in the scattered light are measured by a single photon counting module. The rate of fluctuations is directly related to the rate of diffusion of the molecule through the solvent, which is related in turn to the particles' hydrodynamic radii. Smaller particles diffuse faster, causing more rapid fluctuations in the intensity than larger particles. Therefore, the fluctuation in light intensity contains information about the diffusion of the molecules and can be used to extract a diffusion coefficient and calculate a particle size. The biochar particle size analysis was performed using Litesizer™ 500 Particle Analyzer (Anton Paar) by DLS (Dynamic Light Scattering) method (ECPM, France). Biochar particles were dispersed in aqueous solution and then sonicated in a bath sonicator for 10 min. Particle size measurement was carried out at room temperature (25°C) and laser wavelength of 660 nm.

Chapter 3. Synthesis and characterization of biochar/zeolites

ABSTRACT

ZSM-5 zeolites with high external surface area and excellent performance by using biochar as hard template were studied in this chapter. The biochars used originated from four natural plants: grass, tea, algae and lignin.

The properties of the biochars and zeolites were comprehensively studied and compared using XRD, SEM, EDX, FTIR and other characterization techniques. The results show that these biochars exhibited significant differences in morphology, particle size, inorganic salts content and surface functional groups. Hence, the physicochemical properties of the zeolites were clearly affected due to biochar addition. Among them, Grass-C and Algae-C led to a positive effect on the modification of ZSM-5 zeolite, and the lifetime of the modified zeolite was prolonged, while the modification effect was not significant for Lignin-C and Tea-C.

3.1 Introduction

Hierarchical zeolites are modified materials with respect to the classical microporous zeolite.[130] Hierarchical zeolites possessing secondary structures such as mesopores or/and macropores which enable them to exhibit a high diffusion efficiency, catalytic activity and long catalyst lifetime.[131] Among them, an addition of hard template is a commonly used method for the hierarchical zeolites synthesis.[132-135]

Carbon materials, as hard templates (such as carbon black, carbon nanotubes/nanofibers, carbon aerogels, and various ordered mesoporous carbons), are often used to synthesize hierarchical zeolites.[136] Using the hard template method, hydrophilicity of the raw template is important, which can avoid the phase separation of the precursor solution and the template.[137] In addition, the nanocarbon materials tend to increase the mesoporosity of ZSM-5.[138] Considering that the internal pore size of ZSM-5, the coke formation often occurs first at the outer surface of the zeolite. The mass transfer rate between the products and the zeolite particles is particularly important and often overlooked. In addition, the cost relying to using an expensive nanocarbon template, complicating its high mass production, prevents its large-scale application.

Biochar is a green carbon material with a relative low-cost and more hydrophilic functional groups, which satisfy the basic conditions of being a hard template[139, 140] Such carbon materials are derived from the thermochemical decomposition of biomass such as lignin or cellulose under limited or fully anaerobic conditions.[141]

The most attractive feature of biochar is not just an inexpensive, sustainable and easy-to-produce hard template. It is more worth mentioning that the rich inorganic salts, such as calcium, potassium, sodium, phosphorus, etc. present are also beneficial for the modification of zeolites.[140] Studies have demonstrated that heteroatoms can be introduced into the framework, allowing tuning the structure, acidity, and particle size of the zeolite. For instance, Si^{4+} can be substituted by trivalent cations (i.e., B^{3+}, Al^{3+}, Fe^{3+}, and Ga^{3+}) in MFI-type zeolites

structure.[142] In addition, other elements, such as the main group metals, non-metals, and transition metals were also incorporated into the zeolite framework in form of TO_4 tetrahedrons to optimize the various physicochemical properties of zeolite.[80] The heteroatoms modified method was considered as an attractive route for the improvement of catalysis efficiency and adsorption selectivity.[84, 143-145] Hence, inorganic salts present in biochar can replace the additional step of adding heteroatoms, which can adjust the acidity of zeolite while acting as a hard template.

Currently, there are various types of biochar, which can be divided into the following six categories according to the main types of biomasses used in their production:

(1) Lignin-rich biochar: originated from biomass with high lignin content, such as wood, sawdust, etc.

(2) Cellulose-rich biochar: coming from biomass with cellulose as the main structural component, such as grass, straw, etc.

(3) Nutshell Biochar: obtained from seed shells, such as walnut shells, peanut shells, coconut shells, etc.

(4) Manure and sludge biochar: derived from the pyrolysis of manure and sludge.

(5) Algal Biochar: originated from freshwater and seawater algae.

(6) Black carbon: this category covers other biochars produced from biomass, not included in the above section and naturally occurring forms of carbon black.

So far, the studies devoted to ZSM-5 zeolite modified with biochar for the MTO reaction are still rare. In this chapter, the differences in physicochemical properties between biochars were compared, and explore the effects of different biochars on the catalytic performance of ZSM-5.

3.2 Experimental part

The biochar-modified ZMS-5 zeolite synthesized in this subsection followed the synthesis

procedure of "Biochar modified ZSM-5 zeolite" described in **Chapter 2.2.**

The specific synthesis parameters are as follows: The biochar used is Grass-C, Tea-C, Lignin-C and Tea-C. The addition amount of biochar in all zeolites was 400 mg, and the synthesized time was 3 days. The obtained sample was named: n biochar/ZSM-5 (n= 400, corresponding to the added amount of biochar). The operating parameters for the MTO reaction were: T=400 °C and WHSV=8.0 h^{-1}.

3.3 Result and discussion

3.3.1 Characterization of biochars

This subsection provides a comprehensive analysis of the physicochemical properties of the four biochars (Grass-C, Lignin-C, Tea-C, and Algae-C). The differences in inorganic composition among the biochars were investigated by XRD analysis (Figure 3.1). The XRD patterns indicated that the biochar samples of grass, algae and tea led to similar broad peaks in the 2θ = 20-30° region of the diffractogram. This broad diffraction peak can be attributed to the stacking structure of aromatic layers in graphite (002). It shows the successful conversion of biomass to biochar at 300 ^{o}C.

However, the heat-treated lignin under the same conditions was not completely converted into amorphous carbon. Indeed, few characteristic peaks of lignin could still be observed. This indicates that the required carbonization temperature of lignin is higher than that of the other biomass. This is one of the discrepancies between lignin and the other three types of biomasses. Furthermore, the three biochars of Grass-C, Algae-C and Tea-C exhibit sharp peaks, which undoubtedly assess the presence of crystals in the samples. The crystal compositions of biochars were confirmed by comparing these peaks with the Joint Committee on Powder Diffraction Standards (JCPDS) files. For the Grass-C, the characteristic peaks could be assessed to SiO_2 and two inorganic salts (KCl and $CaCO_3$). The diffractions in the Tea-C sample at 2θ = 15° and 24.5° correspond to calcium oxalate (CaC_2O_4). Algal carbon is rich in

$CaCO_3$. However, few characteristic peaks of other crystalline phases were displayed in the lignin-C, which implying the low content of inorganic salts in it.

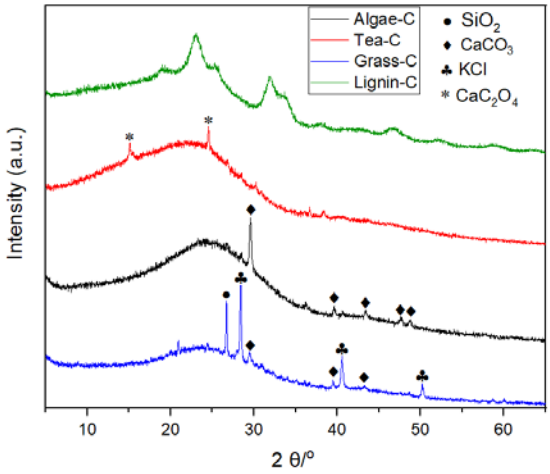

Figure 3.1 (a) XRD patterns of Grass-C, Lignin-C, Algae-C and Tea-C biochars.

The differences in carbonization of different biomasses at the same temperature were also observed in the thermogravimetric curves (TG), as shown in Figure 3.2. Grass, tea, algae, and lignin were heated to 700 ^{o}C under air, at a heating rate maintained at 10 °C/min. It can be clearly observed that biomasses start to lose weight at nearly 200 ^{o}C and stabilize at 500 ^{o}C. However, the weight loss profile among the four biomasses was significantly different. For the lignin it exhibits the slowest rate of carbonization, only about 20% of its mass was lost per 100 ^{o}C, between 200-500 ^{o}C. In contrast, the carbonization rate of algae and grass biomasses reached 30%. During the carbonization process of tea biomass, the thermogravimetric curve showed a stage changing. Prior 450 ^{o}C, the carbonization rate of tea was comprised between those of lignin and algae. But when the temperature remained higher than 450 ^{o}C, the characteristic of the tea mass loss shows a rapid decline again and a plateau at 500 ^{o}C.

These four thermogravimetric curves are closely related to the kinds of organic matter contained in the biomasses. Among them, the carbonization temperature of lignin is high and the carbonization rate is slow. On the other hand, the biomass rich in cellulose and polysaccharides exhibited a fast carbonization rate.

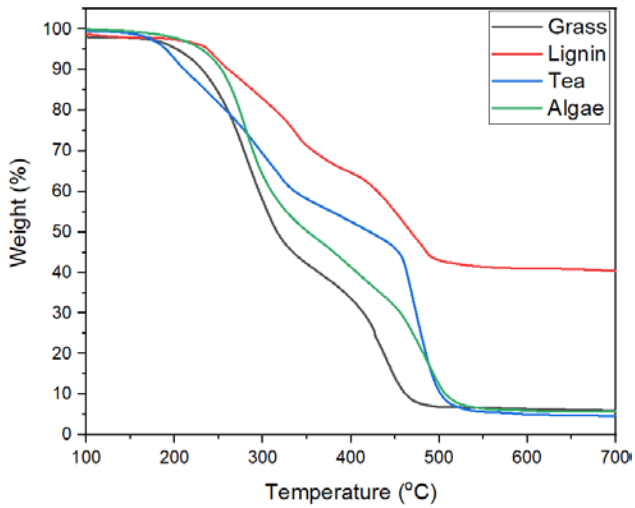

Figure 3.2 TG curves of Grass, Lignin, Algae and Tea biomasses.

Moreover, when the temperature reached 700 °C, lignin still retained 40% of its initial mass, whilst grass, algae and tea retained only about 6% of its mass. This result was affected by the type and proportion of organic matter in the biomass. The biomass with high cellulose content produced more gas and tar, but the yield of biochar was low. The biomass with a high lignin content could retain more biochar after carbonization. Table 3.1 shows the yield of biochar after being carbonized at 300 °C for 1 h of Grass-C, Tea-C, Lignin-C and Algae-C, which were 33%, 50%, 65% and 39%, respectively.

Table 3.1 The yield, S_{BET}, and particle diameter of biochars.

Samples	Yield (%)	S_{BET} (m^2/g)	Particle diameter (μm)
Grass-C	33%	14.4	1.7 (96%), 0.2 (4%)
Tea-C	50%	0.02	1.5 (81%), 6.0 (19%)
Lignin-C	65%	0.6	8.0 (83%), 1.2 (17%)
Algae-C	39%	3.3	2.0 (100%)

The macroscopic particle size distribution with respect to weight fraction of biochar was analyzed by a laser particle size analyzer, as shown in Figure 3.3 and Table 3.1. The results

demonstrate that the particle size of Tea-C ranged between 1 and 10 μm, with 81% of the particles exhibiting about 1.5 μm in size. Lignin-C showed the largest particle size among these biochar samples, with 83% of the particles exhibiting 8 μm in size. The particle size of Grass-C was small, 96% of the particles concentrated in the range of 1.7 μm, with few particles smaller than 0.2 μm. In addition, the particle size of Algae-C remained the most uniform, with almost all particles having about 2 μm in size.

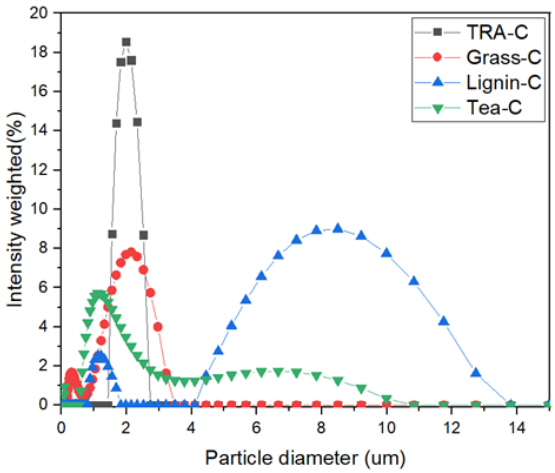

Figure 3.3 Hydrodynamic size distribution obtained by DLS measurement of Grass-C, Lignin-C and Tea-C biochars.

These results are closely related to the morphology and structure of the biomass, as shown in Figure 3.4. The tiny and uniform tissue structure of algae cells makes the biochar prepared with uniform particle size. The biochar prepared from grass with loose structure and easy to pulverize, so it also can obtain the small particle size. In contrast, for the Tea and Lignin, with large biological structure and hard texture, as-obtained biochars exhibited the larger particle size.

The SEM images (Figure 3.4) show the microstructure of the biochars. Four biochars exhibited micron-scale particle sizes. The Grass-C, compared with lignin biomass, presents abundant porosity (Figure 3.4 (a)). It preserves the basic morphology of the stem of the herb. The Tea-C particle shows a rough and irregular block-like structure, the particle size is

different (Figure 3.4 (b)). In contrast, the surface of lignin carbon is dense and smooth (Figure 3.4 (c)). The morphology of them are mostly irregular pebbles. The unique conch shell-like or bowl-like structure of Algae-C may be related to the original plant structure (Figure 3.4 (d)). It can be expected that the small particle size and rough surface of hard template are suitable as a matrix for zeolite crystal growth. The textural properties data (Table 3.1) also show that the Grass-C exhibits the highest specific surface area, reaching 14.4 m^2/g. Correspondingly, the specific surface areas of Tea-C and Lignin-C remained low, only about 0.8 m^2/g. The specific surface areas of Algae-C were about 3.3 m^2/g. These results are consistent with the SEM images.

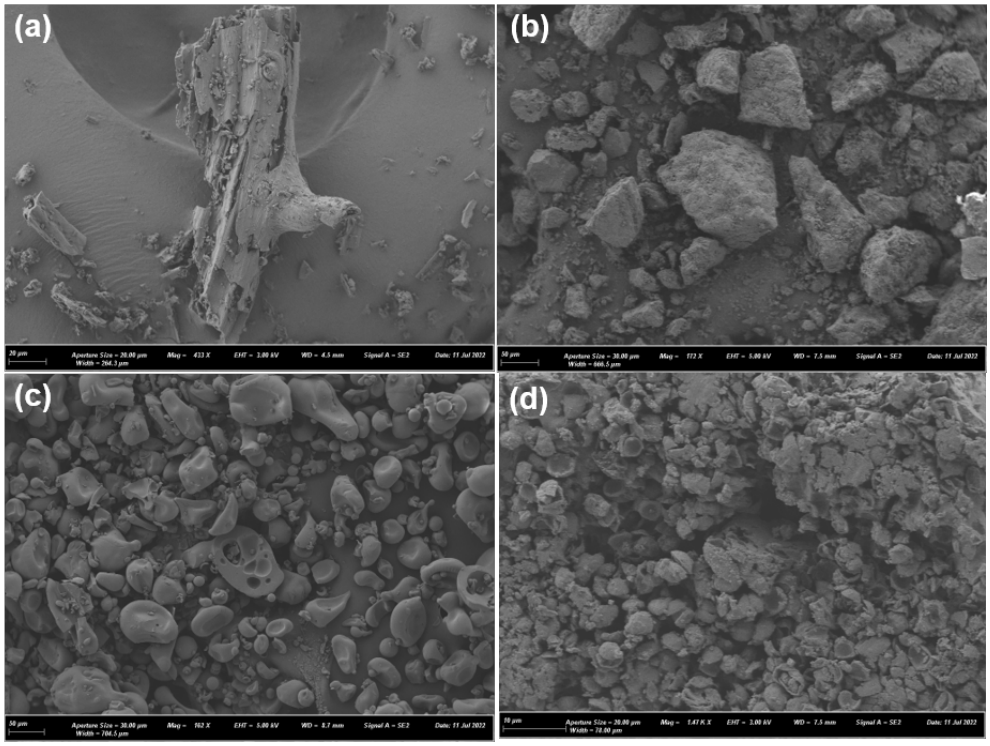

Figure 3.4 Scanning electron microscopy images (SEM) of (a) Grass-C, (b) Tea-C, (c) Lignin-C and (d) Algae-C.

In addition to the differences seen in their physical structure, there are also distinctions in the chemical composition of biochar. Due to the organic/inorganic salts of different types and contents present in the biochars, significant differences in the elements (nature and quantity)

could be found in biochars. The chemical elements, present in the four biomasses, were measured by means of EDX characterization, coupled with the SEM chamber, as shown in Figure 3.5 and Table 3.2. It is noteworthy that unlike conventional carbon templates such as carbon nanotubes, carbon black, and carbon nanospheres, biochars are rich in heteroelements, such as Mg, P, S, K and Ca.

Among them, the content of heteroatoms (Mg, P, S, K and Ca) in Grass-C was the highest, reaching 12.9%, while the content in lignin was the lowest, only 5.1%. The proportions of Algae-C and Tea-C were 9.4% and 6.4%, respectively. In addition, 7.7 % of K was detected in Grass-C. The content in P and Mg in the Algae-C was the highest, reaching 2.6% and 0.8% respectively. About 4.5% of S was concentrated in Lignin-C. Grass-C was enriched in potassium (7.7%) and calcium (1.6%) elements.

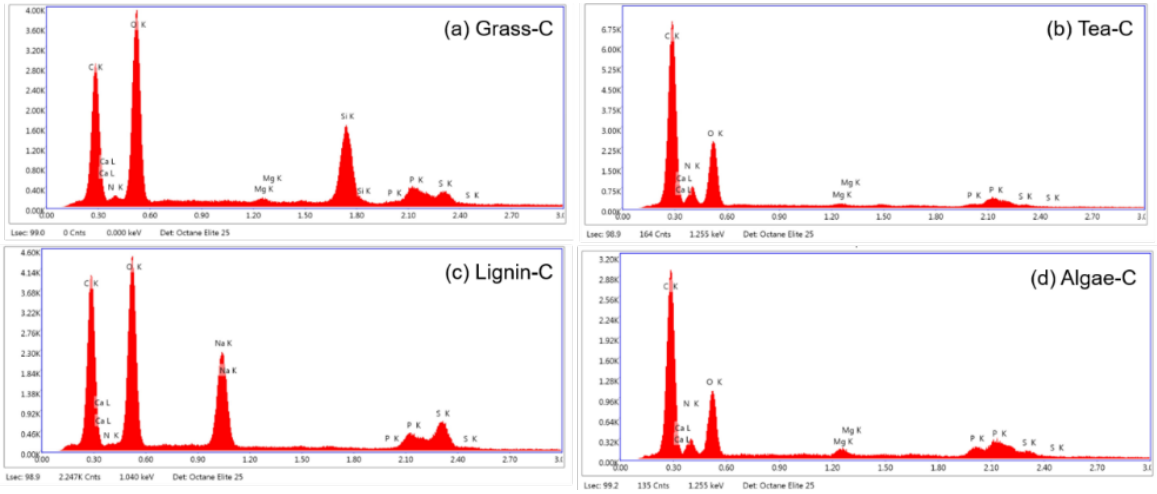

Figure 3.5 EDX elemental analyses of (a) Grass-C, (b) Tea-C, (c) Lignin-C and (d) Algae-C.

Another point that cannot be ignored is that biochar is rich in functional groups at the surface, such as hydroxyl, carboxylate, amino, phosphate and so on. FTIR (Figure 3.6) shows that a broad peak at 3341 cm^{-1} exists in biochars, corresponding to -OH bond stretching of the alcoholic and phenolic hydroxyl groups. The strength of this band is strong for Grass-C and Algae-C. However, its strength became negligible for Tea-C and Lignin-C samples. The

stretching vibrations of aliphatic -C=C- appeared at 1597 cm^{-1}, along with O-H bending vibration at 1384 cm^{-1}. The peak at 1086 cm^{-1} corresponds to C-O stretching vibration from carbohydrates. The presence of carbohydrates proves the hydrophilic nature of Grass-C and Algae-C compared with the other two samples.

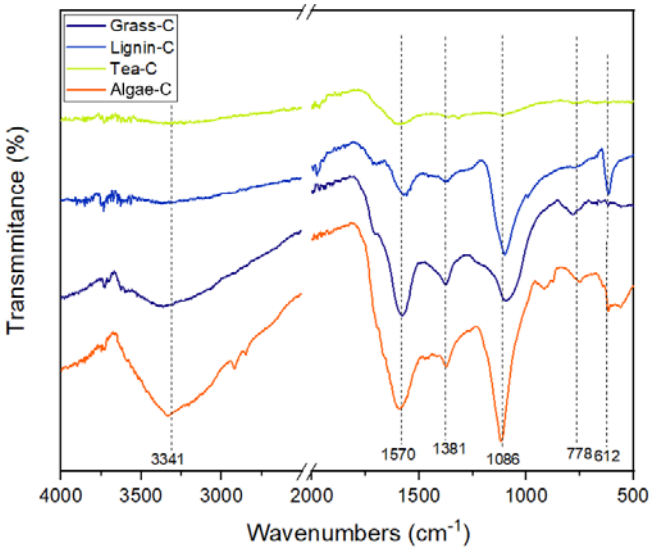

Figure 3.6 FTIR spectra of (a) Grass-C, (b) Tea-C, (c) Lignin-C and (d) Algae-C.

Table 3.2 The element composition in biochar samples quantified by EDX analysis

Sample	Mg	P	S	K	Ca
Grass-C	0.4	0.7	2.5	7.7	1.6
Tea-C	0.4	1.0	0.8	3.8	0.4
Lignin-C	0	0.5	4.5	0	0.1
Algae-C	0.8	2.6	1.6	3.3	1.1

3.3.2 Characterization of ZSM-5 zeolites

In order to explore the relationship between biochar, ZSM-5 physicochemical properties and performance in the MTO reaction, biochar modified zeolite and original H-ZSM-5 zeolite were analyzed by various techniques.

XRD pattern (Figure 3.7) confirms the fingerprint of the MFI crystalline of pristine ZSM-5 zeolite and ZSM-5 modified with biochars (Grass-C, Tea-C, Lignin-C and Algae-C). The addition of biochar was the same (400 mg) for all zeolites. The hydrothermal synthesis conditions were 170 ^{o}C during 3 days. The relative crystallinity of the molecular sieves was calculated from the peak area of the XRD pattern. Specifically, the relative crystallinity of MFI zeolites was calculated from the sum of the peak intensities of 23-25^{o}.

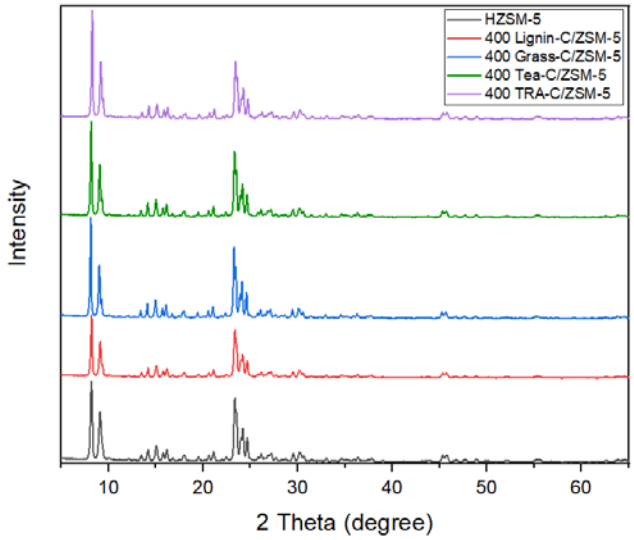

Figure 3.7 XRD patterns of H-ZSM-5, and biochars-C/ZSM-5.

The sample with the largest peak area was selected as the reference and arbitrarily set to 100% crystallinity. The relative crystallinity of each sample can then be obtained by the ratio between the sum of the peak area of the other samples referred to that sample, as shown in Table 3.4. The relative crystallinity of the zeolites modified with Tea-C and Grass-C were very high, reaching about 98%, and it was slightly lower for Lignin-C/ZSM-5 (97%). This confirms that an addition of 400 mg of biochars does not impact the crystallization of ZSM-5 zeolite. In stark contrast, the relative crystallinity of 400 Algae-C/ZSM-5 was only 80 %. The reason for this phenomenon is still unclear. It may be due to the influence of the introduction of some heteroelements.

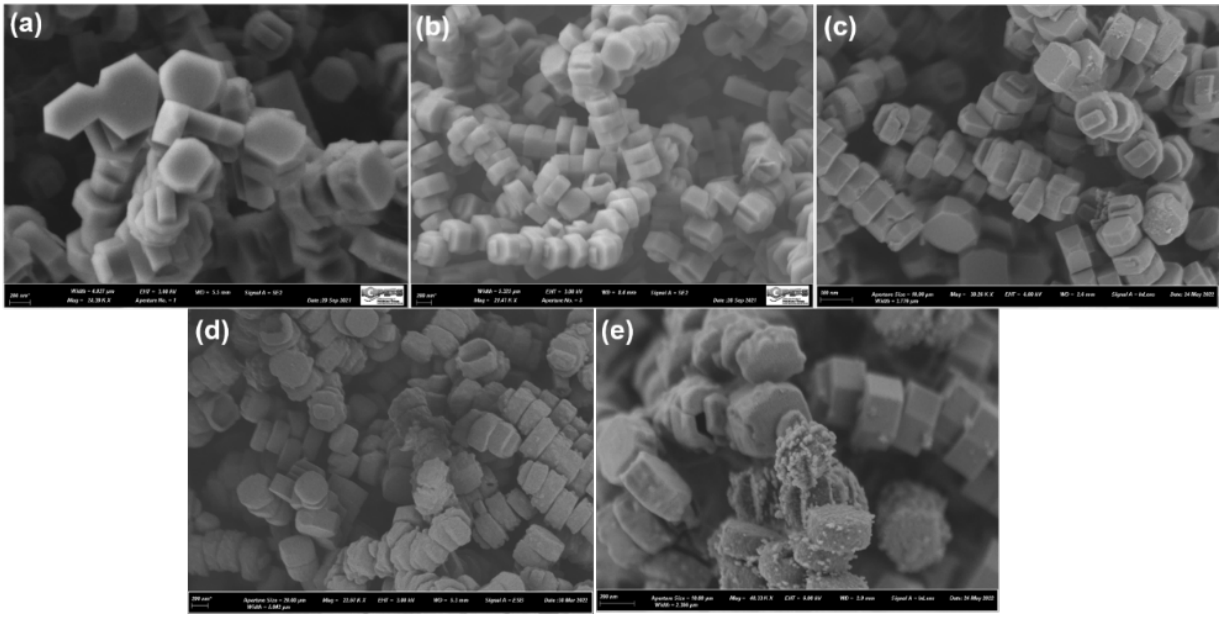

Figure 3.8 Scanning electron microscopy (SEM) of (a) HZSM-5, (b) 400 Grass-C/ZSM-5, (c) 400 Tea-C/ZSM-5, (d) 400 Lignin-C/ZSM-5 and (e) Algae-C/ZSM-5.

Furthermore, the microstructures of all zeolites were analyzed using SEM. The images (Figure 3.8) show that the size of all samples is in the nano-range, where the particle diameter is about 200 nm and the thickness is about 120 nm. The microstructure of all zeolites remained nearly the same. Zeolites exhibit the flat hexagonal prism-shaped particles with a uniform size and well-defined shape. However, the warty granules on some crystals could be observed for Algae-C/ZSM-5, which may be the reason of its lower relative crystallinity.

The XRF data (Table 3.3) shows the discrepancy in the chemical composition of these zeolites. Interestingly, after NH_4^+ ion exchange, heteroelements (P, Ca and Fe) were still detected in all samples, at different contents. Among them, Algae-C/ZSM-5 demonstrated the highest quantity of heteroelements, whereas the lowest was found in Lignin-C/ZSM-5 zeolite. In addition, K element was not detected in three zeolites. Through the comparison of SEM-EDX data of biochar, it can be observed that the difference of this chemical composition in the ZSM-5 zeolite samples has roughly a positive correlation with the content of inorganic salts in the biochar. These results demonstrate that metal or non-metal inorganic salts contained in

biochar can interact with the zeolite crystals, although their content remains low.

Table 3.3 Elemental composition of heteroelements in ZSM-5 zeolites measured by XRF.

Samples	P%	Ca%	Fe%
400 Algae-C/ZSM-5	0.182	0.35	0.28
400 Lignin-C/ZSM-5	0.068	0.09	0.06
400 Tea-C/ZSM-5	0.08	0.12	0.08
400 Grass-C/ZSM-5	0.09	0.20	0.10

Figure 3.9 and Table 3.4 reveal the textural properties of the synthesized catalysts such as total specific surface area (S_{BET}), micropore surface area (S_{micro}) and external surface area (S_{exter}). It can be clearly observed that S_{BET} of all zeolites are similar, about 370-390 cm^2/g. Among them, Tea and Grass led to slightly lower S_{BET} values. In addition, all biochar-modified zeolites presented a rising trend of S_{ext} with slightly different increase. The order of increase in external specific surface area is as follows:

Algae-C/ZSM-5 (171 m^2/g) > Grass-C/ZSM-5 (152 m^2/g) > Tea-C/ZSM-5 (123 m^2/g) > ZSM-5 (121 m^2/g) ≈ Lignin-C/ZSM-5 (120m^2/g)

Among them, Algae-C/ZSM-5 had the highest percentage of S_{exter} / S_{BET}, reaching 43%. This data for H-ZSM-5 was only 31%. Likewise, the improvement of the external specific surface of ZSM-5 zeolite by Tea-C and lignin was not significant, S_{exter} / S_{BET} was about 33%.

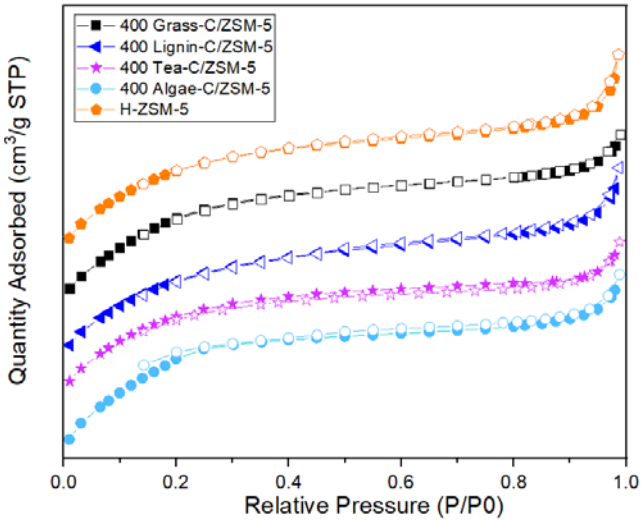

Figure 3.9 N_2 adsorption-desorption isotherms of H-ZSM-5 and ZSM-5 modified with different biochars (Grass-C, Tea-C, Lignin-C, and Algae-C).

Table 3.4 physical parameters of H-ZSM-5 and biochar-modified ZSM-5 zeolite.

Samples	**S_{BET} (m^2/g)**	**S_{micro} (m^2/g)**	**S_{exter} (m^2/g)**	**S_{exter}/S_{BET} (%)**	**Relative crystallinity %**
H-ZSM-5	387	266	121	31	100
Algae-C-400mg/ZSM-5	393	222	171	43	80
Lignin-C-400mg/ZSM-5	389	269	120	33	97
Tea-C-400mg/ZSM-5	390	267	123	34	98
Grass-C-400mg/ZSM-5	374	222	152	41	98

The external surface area of zeolite is related to the degree of bonding between the nuclei and the surface of biochar in the early stages of zeolite crystal formation. Generally, the higher affinity between hard template and precursor/initial nuclei of the zeolite, the greater probability of zeolite grows on its surface, which can build more additional pores. Considering the synthetic environment of the aqueous solution and the hydrophilicity of ZSM-5, the template

needs to be hydrophilic to guarantee such affinity.[136]

3.3.3 Catalytic performance in the MTO reaction

After completing the basic characterization, the catalytic performance of the zeolites was investigated in this section. Performed under the same conditions (400 ^{o}C, WHSV = 8 h^{-1}), the catalytic performance of the five catalysts is shown in Figure 3.10.

Zeolite was deemed to begin to deactivate when the conversion was below 95%. Figure 3.10 (a) shows that Algae-C/ZSM-5 exhibited the longest catalyst lifetime, able of reaching an astonishing 15 h. Although the lifetime of Grass-C/ZSM-5 was not as good as Algae-C/ZSM-5, the time to nearly 100% conversion still reached 9 h, which is slightly improved compared with H-ZSM-5 (8 h). However, the lifetime of Tea-C/ZSM-5 was not showing an increase (8 h), and the one of Lignin-C/ZSM-5 was further reduced to 6 h. It may be related to the non-improved external surface area and/or reduced crystallinity of Lignin-C/ZSM-5. The rate of deactivation could be sequenced as follows:

Lignin-C/ZSM-5 > Tea-C/ZSM-5 > H-ZSM-5 > Grass-C/ZSM-5 > Algae-C/ZSM-5

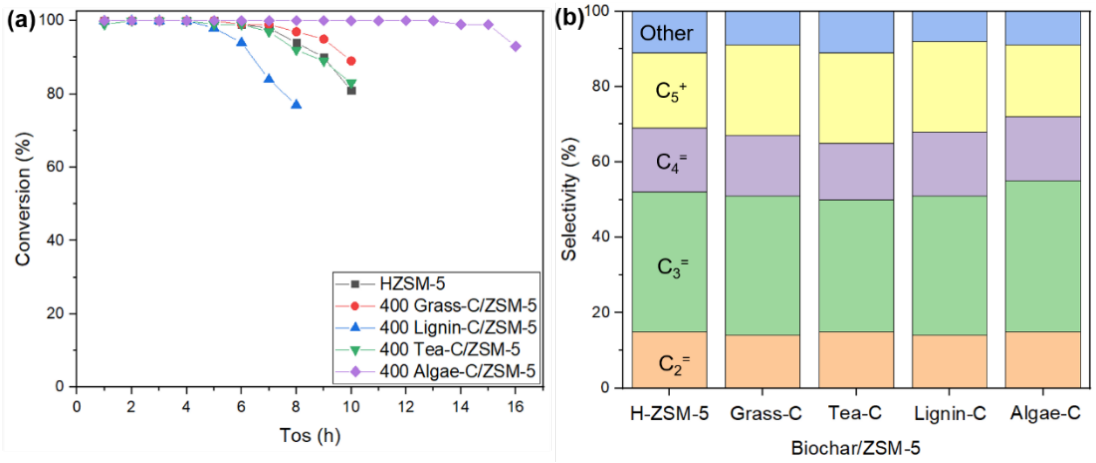

Figure 3.10 (a) Methanol conversion (b) product selectivity at T=400 °C and WHSV=8.0 h^{-1} over ZSM-5 catalysts with different biochar consumption.

Table 3.5 Catalytic result for the MTO reaction over ZSM-5 zeolites.

Catalyst	TOS (h)	Selectivity (%)				$C_3^=/C_2^=$	Lifetime (h)
		$C_2^=$	$C_3^=$	$C_4^=$	Total		
H-ZSM-5	2	15	37	17	69	2.5	8
Grass-C/ZSM-5	2	14	37	16	67	2.6	9
Tea-C/ZSM-5	2	15	35	15	65	2.3	8
Lignin-C/ZSM-5	2	14	37	17	68	2.6	6
Algae-C/ZSM-5	2	15	40	17	72	2.6	15

The selectivity of the products obtained over H-ZSM-5 and Biochar-C/ZSM-5 zeolites are displayed in Figure 3.10 (b) and Table 3.5. The selectivity is defined as the mole fraction of a given product per total mole fraction of all products formed. The selectivity to ethylene was similar for all zeolites, about 14-15%. The selectivity of propylene shows a slightly different trend. Among them, the propylene selectivity of Tea-C/ZSM-5d was the lowest, being 35%. The propylene selectivity of H-ZSM-5, Grass-C/ZSM-5 and Lignin-C/ZSM-5 was similar, about 37%. Algae-C/ZSM-5 yielded the highest selectivity to propylene, reaching 40%. In addition, Algae-C/ZSM-5 own the highest selectivity of total light olefins, including ethylene, propylene and butylenes.

3.4 Conclusion

This chapter related the use of four biochars (Grass-C, Algae-C, Lignin-C, Tea-C) as hard templates to modify ZSM-5 zeolites. The results showed that biochars possess different physicochemical properties due to the diversity of organic and inorganic compounds. Among them, grass, tea and algae rich in cellulose or polysaccharides required the lower carbonization temperature, and the synthesized biochars has small particle size, abundant pores, rich O-containing functional groups, and heteroelements. In contrast, lignin required a high carbonization temperature, yielding large particle size, dense structure, low content of O-containing functional groups and heteroelements. The characterization results proof that Grass-C and Algae-C can bring a higher external specific surface area. Biochar with these properties can allow zeolite crystals to grow better on its surface. Meanwhile, changes in the chemical composition of zeolite were also observed, thanks to the heteroelements from biochar introduced into the zeolite. The changes observed in the structure and composition of the zeolites directly impact on their catalytic performance. The catalytic results showed that a longer catalyst lifetime could be obtained when the zeolite presented a higher external surface area. The catalyst lifetime of pristine H-ZSM-5 zeolite was only 8 h, while the lifetime of the ZSM-5 zeolite with Algae-C was significantly enhanced to 15h. Grass-C/ZSM-5 exhibited a lifetime of 9 h. However, not all biochars showed a positive effect during the MTO catalytic reaction, which closely related to the physicochemical properties of biochars. In conclusion, it was possible to enhance the catalyst lifetime of ZSM-5 in the MTO reaction by adding the biochars.

Chapter 4. Modification of Algae-C and Grass-C assisted zeolites

ABSTRACT

By adjusting the amount of biochar addition, synthesis conditions, catalytic test operating conditions and other parameters, optimal conditions for the design of ZSM-5 zeolites were set. In addition, the influence of those parameters on the zeolite properties including acidity, chemical composition, crystallinity, porous texture was studied in-depth.

The results showed that the lifetime and the selectivity achieved by Algae-C and Grass-C modified ZSM-5 zeolites were importantly modified after the adjustment of parameters. Among them, the catalytic lifetime of Grass-C/ZSM-5 reached nearly 16 h at 350 ^{o}C, when biochar addition was raised to 500 mg. For Algae-C/ZSM-5, the lifetime was kept stable (16 h) even when its synthesis duration was limited to 2 days. In addition, inorganic salts and surface oxygen-containing groups in biochar proved to play a crucial role in optimizing the ZSM-5 catalyst, after comparing the effects of algal carbon, acid-treated Algae-C and carbon black.

4.1 Introduction

Coking has been considered as a pivotal reason for the deactivation of zeolites, because acid sites become inaccessible after the channel are clogged with coke. In catalytic reactions, the formation of coke was affected by the strength of the acid sites, thus their interaction with the reactants, but also by the type and residence time of the products.[110, 146]

Firstly, coke generally originates from complex carbonaceous deposits which cannot escape from the cage/channel of the zeolite, so they are named coke precursor. The formation of these products depends strongly on the reaction temperature. At “low” temperatures, the non-desorbed products generally formed non-polyaromatic molecules, strongly adsorbed within the zeolite framework, being unable to leave. At temperatures above 350 °C, these products, mainly constituted of highly polyaromatic compounds, cannot leave the channels due to steric constraints.[121] Therefore, the suitable reaction temperature is important for an acid-catalyzed reaction.

In addition, the composition of non-desorbed products depends also on time-on-stream in plug-flow reactors and the residence time of reactants/products in the reactor. The longer the residence time is, the larger non-desorbed products may become, raising their complexity and polyaromaticity.[121] Hence, the deactivation extent will be greatly advanced. It can be considered that small particle sizes and numerous pores are key parameters for improving products diffusion rate and prolonging the lifetime of the zeolite.

Besides, it is worthy to mention that the composition of coke depends also on the nature of the active sites (acid, base, acid-base, metal, etc.), since this nature determines the catalyzed reaction steps.[147] Extensive researches have demonstrated that the strong acidity catalyzes the methanol conversion. However, the coking rate can be accelerated with the acidity strength enhancement. Furthermore, the same may occur in the presence of a high density of acid sites. The high-density of acid sites usually leads to successive chemical reaction paths, along the diffusion of reactant molecules within the zeolite, thus favoring condensation reactions. In

addition, for the MTO reaction, both strong acid sites and weaker acid sites were suggested to act as active sites[148]. More importantly, appropriate proportion of weak acid content can efficiently avoid various hydrogen-transfer reactions, yielding small alkanes and aromatics, thus the zeolite shows a better resistance towards coking phenomenon.

In summary, a sound tailoring of peculiar features of ZSM-5 zeolite, such as crystal size, acidity, structure and so on, while changing the synthesis parameters can delay the coke formation.[146, 149] However, these physicochemical properties of zeolites are rather hard to be precisely controlled. Indeed, several parameters are inter-related, therefore one modification may impact more parameters. Besides, the crystal growth mechanism(s) of zeolites in hydrothermal environment remain(s) extremely complex. They are disturbed by various factors, including but not limited to: the nature of raw materials, temperature, time, aging process, etc. A 'in-depth' study of those parameters to make zeolite more efficient in a given application is therefore necessary.

In this chapter, Grass-C and Algae-C modified ZSM-5 zeolites were selected as samples to be modified. Several synthesis parameters and catalytic conditions were adjusted to explore their effects on catalyst lifetime and selectivity. Furthermore, the influence of heteroelements and O-containing groups presence in biochar were explored by comparing Algae-C/ZSM-5, acid-treated Algae-C/ZSM-5 and hydrophobic carbon black/ZSM-5 zeolites.

4.2 Experimental part

The research undertaken in this chapter reports a further optimization of Algae-C/ZSM-5 and Grass-C/ZSM-5 zeolites studied in **Chapter 3.** The parameters of optimization are: content of biochar addition, synthesis time, Si/Al and temperature of the MTO test.

Grass-C/ZSM-5: Based on the synthesis route reported in Chapter 3.2, 400, 500 and 600 mg of Grass-C were added to the zeolite precursors solution, and the hydrothermal temperature of these samples was kept at 170 ^{o}C. The synthesis duration was 3 days. The optimal quantity

of Grass-C addition was selected as a function of the lifetime. Based on the optimal Grass-C addition, Si/Al (30, 90, 120, 180) and synthesis time (1 d, 2 d, 3 d) were modified step by step. As-obtained samples were named: n Grass-C/ZSM-5-m (n is the amount of biochar, m is the synthesis time).

Algae-C/ZSM-5: The content of Algae-C in zeolite was varied: 200, 300 and 400 mg, respectively. The synthesis time (1 d, 2 d, 3 d) was further changed based on the optimal addition of Algae-C. In order to explore the effect of the physicochemical properties of carbon materials on final ZSM-5 zeolite, hydrophobic carbon black, acid-treated Algae-C were selected as model templates for this study. As-obtained samples were named: n Algae-C/ZSM-5-m (n is the amount of biochar, m is the synthesis time).

Four temperatures for the MTO reaction were selected: 300 ^{o}C, 350 ^{o}C, 400 ^{o}C and 450 ^{o}C. The influence of space velocity was also studied: WHSV=2.0 h^{-1} and 8.0 h^{-1} were compared.

4.3 Results and discussion of ZSM-5 modified with Grass-C

4.3.1 Influence of the Grass-C addition

XRD patterns of ZSM-5 zeolites obtained with 400 mg, 500 mg and 600 mg of Grass-C are similar, as shown in Figure 4.1. All the samples exhibit the sole MFI crystalline phase formation, indicating a successful synthesis. Moreover, the data of relative crystallinity, calculated from the XRD patterns, are presented in Table 4.1. The results show that the crystallinities of ZSM-5 zeolite modified with 400, 500 and 600 mg of Grass-C were 98%, 94% and 95%, respectively. The crystallinity of 500 and 600 mg Grass-C is similar and slightly lower than that of 400 Grass-C/ZSM-5. It seems therefore that the addition of biochar has a (limited) negative effect on the zeolite crystallinity.

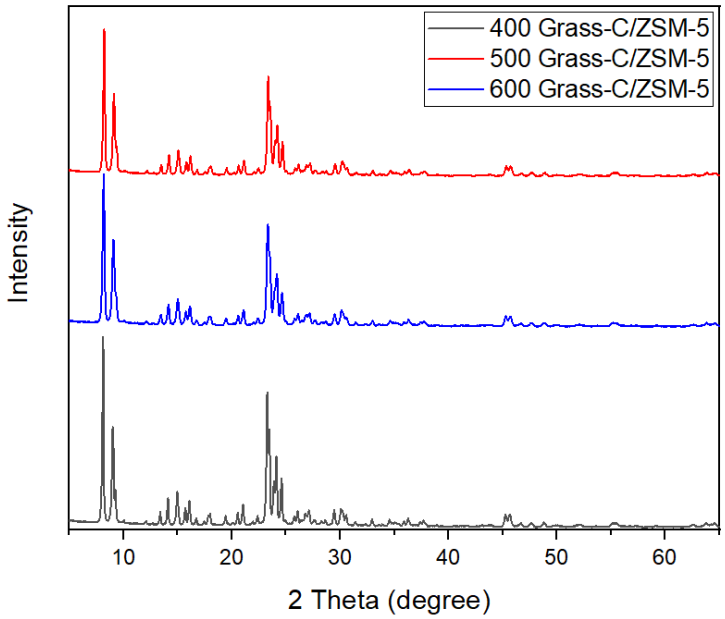

Figure 4.1 XRD patterns of Grass-C/ZSM-5 samples.

However, the specific surface areas of the samples exhibited marked discrepancies, in their textural properties (Figure 4.2 and Table 4.1). Firstly, the total specific surface area of all samples remained roughly the same. The value of S_{BET} of pristine H-ZSM-5 achieved 387 m^2/g, being slightly higher than the zeolites prepared with 400, 500, 600 mg Grass-C (about 375 m^2/g). However, there are significant differences in the microporous specific surface area and external surface area. It can be observed that the value of microporous specific surface area decreased with an increase of the biochar content. Compared with pristine H-ZSM-5, the microporous specific surface area of 400 Grass-C/ZSM-5 decreased from 266 m^2/g to 222 m^2/g. As the addition amount increased to 600 mg, the microporous specific surface area of the zeolite further dropped to 187 m^2/g.

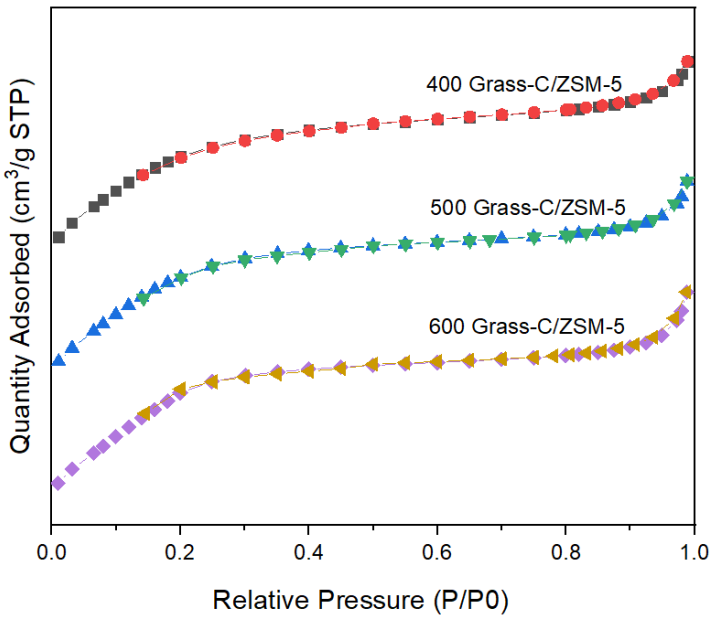

Figure 4.2 N_2 adsorption-desorption isotherms of Grass-C/ZSM-5 with different Grass-C addition (400, 500 and 600 mg).

The trend in the values of external surface areas (ESA) was the opposite. For pristine H-ZSM-5, the ESA value was only 121 m^2/g, while it increased to 152 m^2/g after 400 mg of Grass-C addition. ESA value was further enhanced with the Grass-C content increase. The ESA of 600 Grass-C/ZSM-5 reached an astonishing 189 m^2/g. It is therefore shown that biochar addition led to enhance external surface area of the zeolite, while led to a negative impact on the microporous structure, being possibly due to the presence of impurities.

XRF data about the elemental composition of impurities in zeolites are shown in Table 4.2. The results assessed that the presence of heteroatoms in zeolite was mainly due to Ca, P, Mg and Fe. The percentage of these heteroatoms showed a slight increase while raising the Grass-C content. Among them, the content of calcium increased significantly from 0.23 to 0.33% of oxide, ranging from 400 to 600 mg grass addition, respectively. These data confirm that the interaction between the inorganic elements in the biochar and the composition of the zeolites.[150]

Table 4.1 Physical parameters of ZSM-5 modified with different additions of Grass-C.

Samples	S_{BET} (m^2/g)	S_{Micro} (m^2/g)	S_{Exter} (m^2/g)	Relative crystallinity (%)
H-ZSM-5	387	266	121	100
400 Grass-C/ZSM-5-3d	374	222	152	98
500 Grass-C/ZSM-5-3d	373	207	167	94
600 Grass-C/ZSM-5-3d	376	187	189	95

The performances of 400, 500 and 600 Grass-C/ZSM-5 are presented in Figure 4.3. The results showed that the catalyst lifetime was extended when the zeolite was modified with Grass-C. For pristine H-ZSM-5, the conversion ability gradually decreased after 8 h, which was arbitrarily considered as the beginning of deactivation.

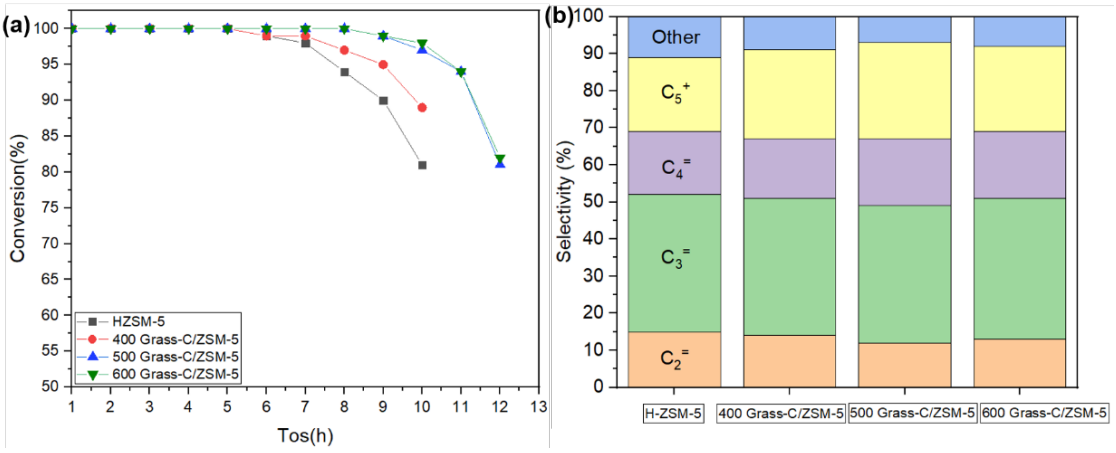

Figure 4.3 (a) Methanol conversion (b) product selectivity at T=400 °C and WHSV=8.0 h^{-1} over Grass-C/ZSM-5 catalysts with different Grass-C addition (400, 500, 600 mg).

Table 4.2 Elemental composition of ZSM-5 modified with different grass quantities.

Samples	P_2O_5%	CaO%	Fe_2O_3%	MgO
400 Grass-C/ZSM-5	0.09	0.23	0.12	0.02
500 Grass-C/ZSM-5	0.09	0.28	0.14	0.02
600 Grass-C/ZSM-5	0.10	0.33	0.15	0.05

As shown in Figure 4.3 (a), the catalyst lifetime of 400 Grass-C/ZSM-5 reached 9 h. When the addition of Grass-C was 500 mg, the catalyst stability was improved to 11 h. However, no further increase in catalyst life after an addition of 600 mg Grass-C to zeolite. Although the highest external surface area (189 m^2/g) was exhibited compared with all zeolites, the lowest microporous specific surface area (187 m^2/g) of it also cannot be ignored. According to the hydrocarbon pool mechanism, the catalytic conversion of methanol takes place in the internal channels of the MFI zeolite. Therefore, the high microporous specific surface area can provide abundant active sites within the zeolite. This may explain the rising interruption of catalyst stability for 600 Grass-C/ZSM-5.

Table 4.3 Catalytic data for the MTO reaction over Grass-C/ZSM-5 zeolites.

Catalyst	TOS (h)	Selectivity (%)				$C_3^=/C_2^=$	Lifetime (h)
		$C_2^=$	$C_3^=$	$C_4^=$	Total		
H-ZSM-5	2	15	37	17	69	2.5	8
400 Grass-C/ZSM-5	2	14	37	16	67	2.6	9
500 Grass-C/ZSM-5	2	12	37	18	67	3.1	11
600 Grass-C/ZSM-5	2	13	38	18	69	2.9	11

The addition of Grass-C to the zeolite did not yield significant differences in products selectivity. As shown in Figure 4.3 (b) and Table 4.3, the selectivity towards light olefins,

including ethylene, propylene and butylenes, was about 67-69% for all catalysts. In this experiment, 500 mg Grass-C is considered as a suitable amount for the optimization of ZSM-5 zeolite.

4.3.2 Influence of the Si/Al

Based on the addition of 500 mg of grass carbon, the Si/Al ratio in the zeolite was further adjusted by changing the addition of sodium aluminate source. The Si/Al ratios of 500 Grass-C/ZSM-5 zeolites were set to 30, 90, 120 and 180, respectively. Within that Si/Al ratio range, all zeolites were successfully synthesized (as shown in Figure 4.4). This confirms that the Al content in ZSM-5 zeolite could be (surprisingly) easily adjusted.

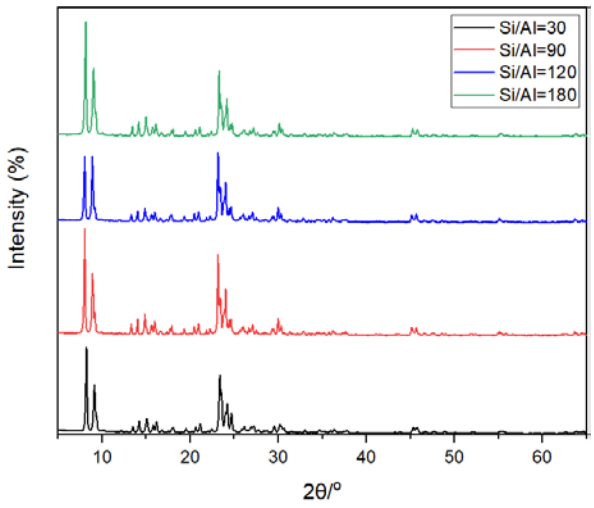

Figure 4.4 XRD patterns of Grass-C/ZSM-5 with different Si/Al ratios = 30, 90, 120 and 180.

The performance in the MTO reaction is shown in Figure 4.5. Figure 4.5 (a) shown that an increase in the Si/Al ratio led to gradually decrease the catalyst stability. For instance, at Si/Al = 30, 100% conversion could be maintained during 9 h and 95% conversion during 11 h for 500 Grass-C/ZSM-5 methanol. When the Si/Al ratio was increased to 90, the zeolite demonstrated full-methanol conversion in the first 3 h, then gradually decreased. Finally, it reached the same level as Grass-C/ZSM-5 (Si/Al=30) at 12 h. However, when the Si/Al ratio was further increased to 120, the zeolite could not achieve 100% conversion, thus no steady-

state behavior, with a decreasing trend versus time on stream. However, the deactivation rate of Grass-C/ZSM-5 (Si/Al=120) is slower than that of other zeolites, so the conversion ability after 12 h starts to be higher than Grass-C/ZSM-5 (Si/Al=30). Considering a long-term usage, the ZSM-5 zeolite (Si/Al=120) may outperform the zeolites that own lower Si/Al ratio. However, when the Si/Al ratio was 180, the conversion of methanol could only be maintained at about 90% in the early stage. After that, it gradually declined, with a more pronounced activity loss after 11 h. The catalytic stability of the zeolite for methanol could therefore be positively correlated with the Al-content in the zeolite. The higher the aluminum content was, the higher the catalytic activity of the zeolite was.

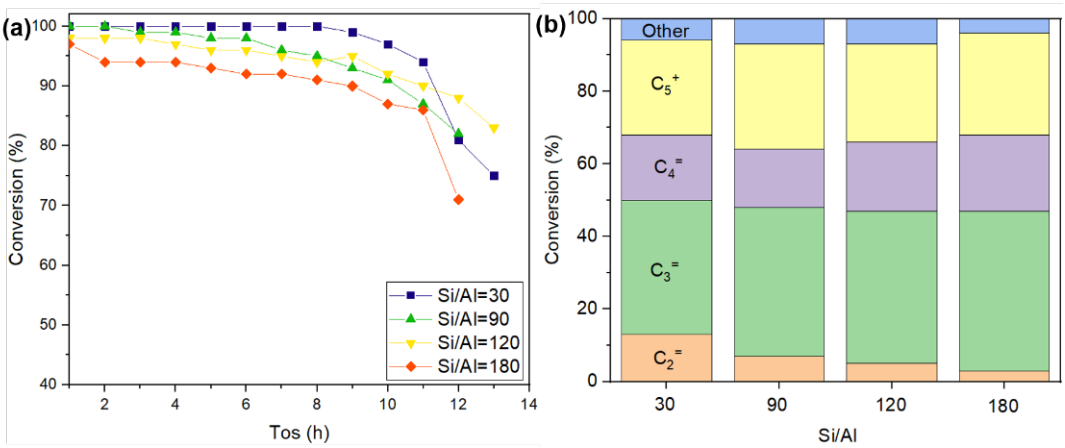

Figure 4.5 (a) Methanol conversion (b) product selectivity at T=400 °C and WHSV=8.0 h^{-1} over Grass-C/ZSM-5 catalysts with different Si/Al =30, 90, 120, 180.

In addition, the Si/Al ratio of the zeolite also significantly affected the selectivity towards the products, as shown in Figure 4.5 (b) and Table 4.4. All samples exhibited the highest selectivity to propylene and the lowest selectivity to ethylene. For ethylene alone, the selectivity increased while raising the aluminum content in the zeolite. For a Si/Al = 180, the selectivity to ethylene was only 3%. At Si/Al = 30, the selectivity of ethylene reached 14%. The selectivity in propylene as a function of Si/Al ratio followed an opposite trend, with a decrease in selectivity while raising the Al content. When the Si/Al ratio was 180, the propylene selectivity reached 44%, while at Si/Al = 30, the propylene selectivity dropped to

37%. In addition, for butylenes, the selectivity diminished with an increase in the Al content, following a similar trend than propylene. The overall selectivity to light olefins for all catalysts was similar, at about 65%. In practical applications, the silicon-aluminum ratio can be tuned according to final olefins fraction requirements.

Table 4.4 Catalytic data for the MTO reaction over Grass-CZSM-5 zeolites with different Si/Al ratio.

Catalyst	**Si/Al**	**Tos (h)**	**Selectivity (%)**				**$C_3^=/C_2^=$**
			$C_2^=$	$C_3^=$	$C_4^=$	Total	
500 Grass-C/ZSM-5	30	2	14	37	16	67	2.6
500 Grass-C/ZSM-5	90	2	7	41	16	64	5.9
500 Grass-C/ZSM-5	120	2	5	42	19	66	8.4
500 Grass-C/ZSM-5	180	2	3	44	21	65	14.7

4.3.3 Influence of the synthesis time

Until now, several synthesis parameters have been identified. The addition amount of Grass-C was kept constant at 500 mg, the synthesis temperature was kept at 170 ^oC, and Si/Al=30 was selected. Then, the synthesis duration was reduced from 3d to 2d and 1d to explore the effects on catalyst physicochemical properties and MTO reaction. Furthermore, the conditions of the catalytic reaction remain unchanged.

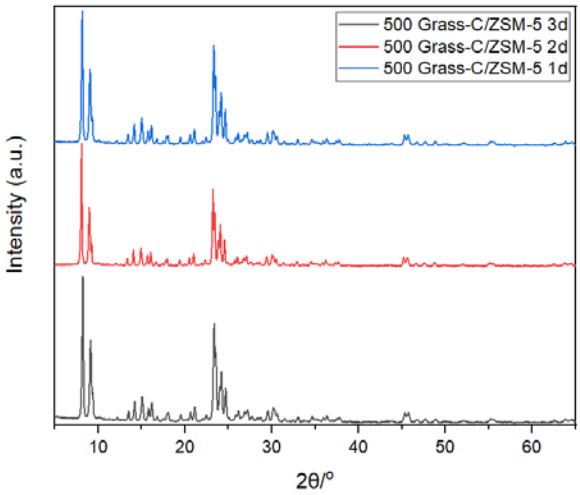

Figure 4.6 XRD patterns of Grass-C/ZSM-5 with different synthesis time (1, 2, 3 d).

The XRD patterns of the three zeolites (synthesis time is 3, 2 and 1 d) are presented in Figure 4.6. The characteristic peaks of the MFI structure are observed for all samples. However, the relative crystallinity of Grass-C/ZSM-5 zeolites decreased with the shortening of the crystallization time, as shown in Table 4.5. When the synthesis time was 3 d, the relative crystallinity of Grass-C/ZSM-5 was 95%. However, the relative crystallinity decreased to 91% when the synthesis duration was reduced to 2 d and 1 d.

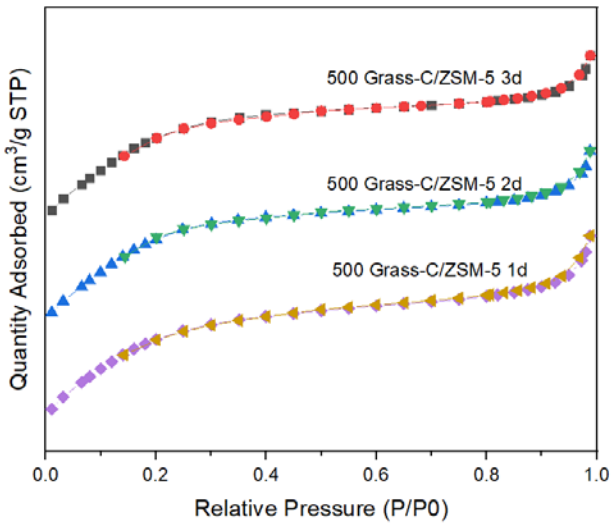

Figure 4.7 N_2 adsorption-desorption isotherms of Grass-C/ZSM-5 modified with different synthesis times (1, 2 and 3d).

Meanwhile, the N_2 adsorption/desorption isotherms (Figure 4.7) of the samples show only few differences. According to BET data in Table 4.5, the specific surface areas of the three samples remained similar, being roughly 370 m^2/g. However, the micropore surface area of Grass-C/ZSM-5-1d (217 m^2/g) was slightly increased compared compared to Grass-C/ZSM-5-3d (207 m^2/g) and Grass-C/ZSM-5-2 d (202 m^2/g). Unfortunately, Grass-C/ZSM-5-1d exhibited the lowest ESA, being only 152 m^2/g. These results may reveal the process of rapid formation of zeolite crystals in solution and slow growth on the surface of the hard template.

The MTO catalytic performance of zeolites with varying synthesis times were testes at two temperatures: 400 ^oC and 350 ^oC, at WHSV=8 h^{-1}. As shown in Figure 4.8 (a), at 400 ^oC and WHSV=8 h^{-1}, the catalysts lifetime decreased with the shortening of the synthesis duration. The lifetime of 500 Grass-C/ZSM-5-3d zeolite retained methanol conversion ability above 95% for 11 h. In contrast, when the synthesis time was reduced to 2d, the catalyst lifetime lasted on for 7 h. With the further shortening of the synthesis time to only 1 d, the catalytic lifetime was further reduced to 5 h. This reduction in the catalyst lifetime may be related to the change in the crystallinity or in certain crystal properties related to hydrothermal time, that still need to be further studied. In addition, these zeolites did not show significant differences in product selectivity. The selectivity towards light olefins was about 66% of all zeolites.

Table 4.5 Textural and structural properties of Grass-C/ZSM-5 zeolites obtained with different synthesis time.

Samples	**S_{BET} (m^2/g)**	**S_{Micro} (m^2/g)**	**S_{Exter} (m^2/g)**	**Relative crystallinity (%)**
500 Grass-C/ZSM-5-1d	371	219	152	91
500 Grass-C/ZSM-5-2d	373	202	171	91
500 Grass-C/ZSM-5-3d	373	207	167	95

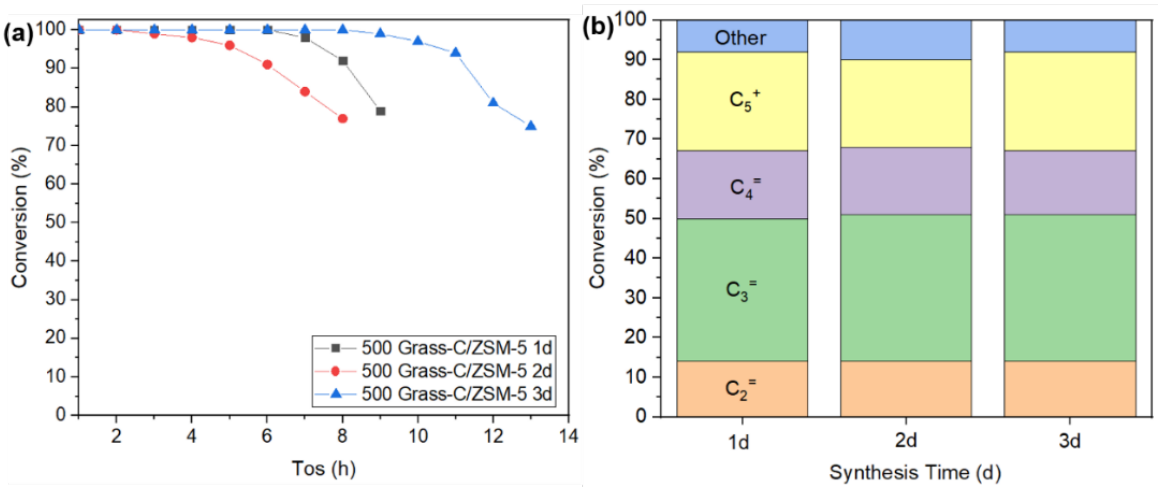

Figure 4.8 (a) Methanol conversion (b) product selectivity at T=400 °C and WHSV=8.0 h^{-1} over Grass-C/ZSM-5 catalysts with different synthesis time.

Furthermore, three Grass-C/ZSM-5 zeolites with different synthesis times were tested at 350 °C (Figure 4.9). Unexpectedly, these zeolites exhibited longer catalytic lifetimes compared to the reaction performance at 400 °C. Among them, the 500 Grass-C/ZSM-5-3d still showed the longest lifetime. Methanol conversion above 95% was maintained during 16 h, being significantly longer than the one at 400 °C. Similarly, the lifetime of Grass-C/ZSM-5 2d was also improved. Compared with the reaction performance at 400 °C, the lifetime of this zeolite was increased from 7 h to 12 h, at 350 °C. However, for the Grass-C/ZSM-5-1d catalyst, the opposite trend was observed. Its stability decreased from the start of the reaction, being less than 95% after 3 h on stream only. This may be related to the weak catalytic ability of Grass-C/ZSM-5 1d catalyst itself. A further reduction of the temperature could further weaken the catalytic activity of this zeolite.

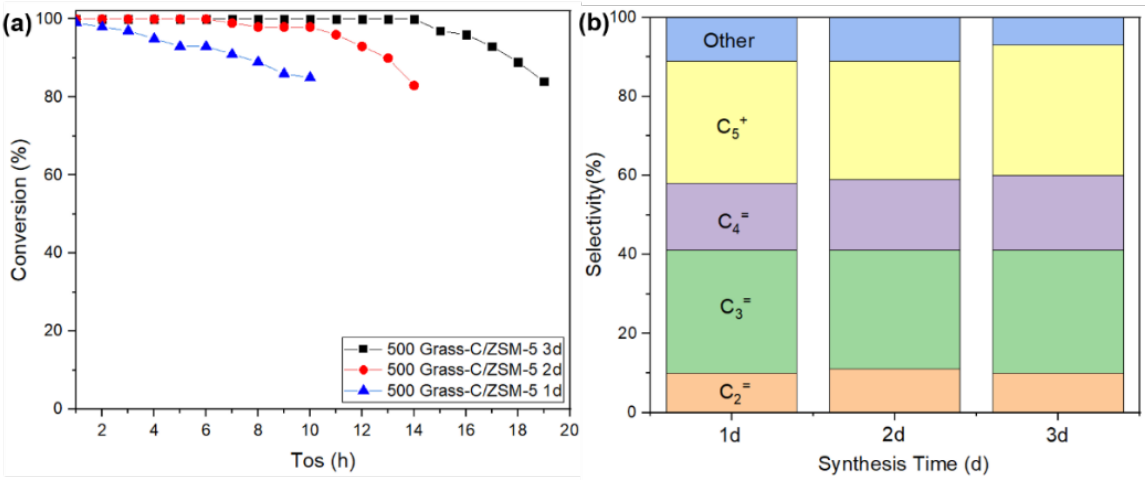

Figure 4.9 (a) Methanol conversion (b) product selectivity at T=350 °C and WHSV=8.0 h^{-1} over Grass-C/ZSM-5 catalysts with different synthesis time.

Table 4.6 and Figure 4.9 (b) show the selectivity of Grass-C/ZSM-5-(1 d, 2 d and 3 d) at 350 ^oC. The results show that the overall selectivity of Grass-C/ZSM-5 to light olefins declined while decreasing temperature. At 350 ^oC, all zeolites exhibited the lower selectivity to light olefins than at 400 ^oC, being about 58%. This indicates a weak activity for the catalysts at this temperature.

Table 4.6 Catalytic result for the MTO reaction over Grass-CZSM-5 zeolites with different synthesis time.

Catalyst	**Synthesis time**	**Reaction temperature**	**Selectivity (%)**			
			$C_2^=$	$C_3^=$	$C_4^=$	Total
500 Grass-C/ZSM-5	1d	350 ^oC	10	31	17	58
		400 ^oC	14	36	17	67
500 Grass-C/ZSM-5	2d	350 ^oC	11	30	18	59
		400 ^oC	14	37	17	68
500 Grass-C/ZSM-5	3d	350 ^oC	10	31	19	60
		400 ^oC	14	37	16	67

4.3.4 Influence of the catalytic temperature

For 500 Grass-C/ZSM-5-3d zeolite, an unexpectedly result shows that the catalytic lifetime of Grass-C/ZSM-5 could be further improved while reducing the reaction temperature; however, the selectivity in light olefins showed an opposite trend. It can be concluded that the temperature has a direct influence on the ZSM-5 performance.

As shown in Figure 4.10 (a), the conversion to methanol remained complete during 14 h and was maintained above 95% during 16 h on stream for 500 Grass-C/ZSM-5-3d zeolite, at 350 ^{o}C. When the reaction temperature was enhanced to 400 ^{o}C, the catalyst lifetime was reduced to 11 h. With a further temperature increase to 500 ^{o}C, the deactivation rate of the zeolite was further intensified. After 4 h of reaction, the conversion was less than 95%.

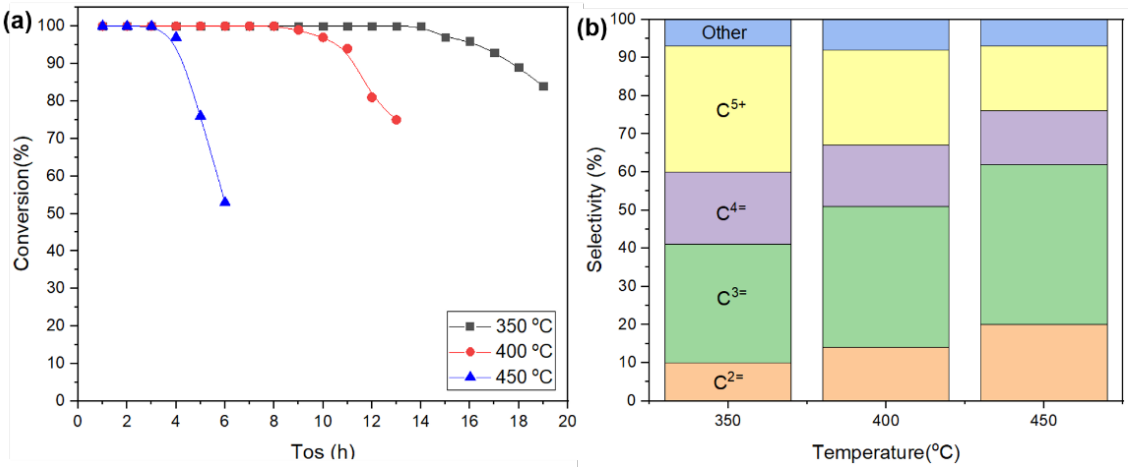

Figure 4.10 (a) Methanol conversion (b) product selectivity at different temperature (350, 400, 450 ^{o}C) and WHSV=8.0 h^{-1} over Grass-C/ZSM-5 catalysts.

The reaction temperature also affected the selectivity of the catalysts towards the products, as shown in Figure 4.10 (b) and Table 4.7. The selectivity to light olefins increased with the reaction temperature, although the catalytic lifetime was significantly damaged. At 350 ^{o}C, the selectivity in light olefins was 60 %. When the temperature raised to 450 ^{o}C, the selectivity increased to 76 %. Among them, the improvement of ethylene and propylene was most significantly. The selectivity towards ethylene increased from 10 % to 20 %, while the

selectivity for propylene increased from 31 % to 42 %. However, the selectivity in butylenes presents a downward trend, with a decrease from 19 % to 14 %. Although the effect of temperature on product selection is complex, it can be confirmed that the high temperature can improve the activity of the zeolite but also accelerate the formation of coke. That is the reason for the rapid deactivation of zeolite at 450 ºC.

Table 4.7 Catalytic data for the MTO reaction over Grass-C/ZSM-5 zeolites at different reaction temperature.

Catalyst	**Reaction temperature (ºC)**	**Selectivity (%)**			
		$C_2^=$	$C_3^=$	$C_4^=$	Total
500 Grass-C/ZSM-5	350	10	31	19	60
500 Grass-C/ZSM-5	400	14	37	16	67
500 Grass-C/ZSM-5	450	20	42	14	76

4.4 Results and discussion of Algae-C/ZSM-5

4.4.1 Influence of the Algae-C addition

First, the effect of different Algae-C additions on the physicochemical properties of ZSM-5 zeolite was investigated. XRD patterns of pristine H-ZSM-5 zeolite and Algae-C modified ZSM-5 with different amounts of Algae-C (200, 400, 600 mg) were compared in Figure 4.11 The results showed that all diffraction peaks appeared, thus confirming the sole formation of MFI structure for all samples.

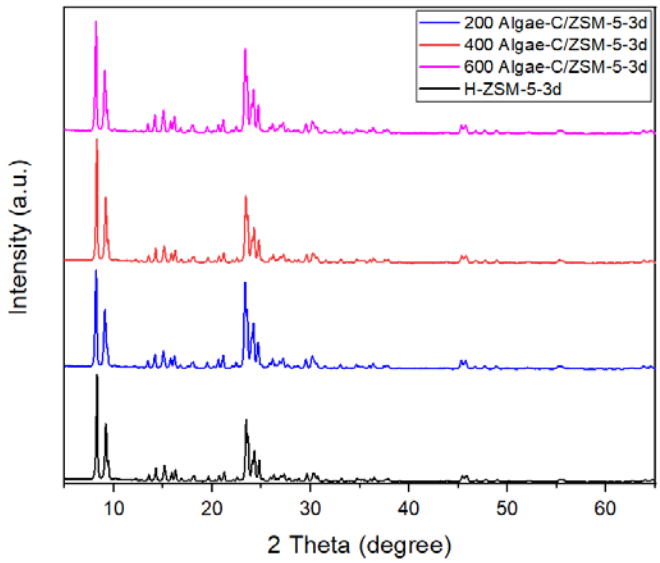

Figure 4.11 XRD patterns of synthesized Algae-C/ZSM-5 with different Algae-C addition (200, 400, 600mg).

However, differences between the crystals were found by further estimation of the relative crystallinity of those samples. The relative crystallinity of the molecular sieves was calculated from the sum of the peak intensities between 23-25°. The sample with the largest peak area was selected as the reference and arbitrarily set to 100% crystallinity. The relative crystallinity of each sample can then be obtained by the ratio between the sum of the peak area of the other samples referred to that sample, as shown in Table 4.8. Compared to pristine H-ZSM-5 zeolite, the relative crystallinity of the zeolite with the addition of Algae-C was reduced. The relative crystallinity of 200 Algae-C/ZSM-5 was 84 %, but with a further increase of Algae-C addition, the relative crystallinity of 400 Algae-C/ZSM-5 and 600Algae-C/ZSM-5 diminished to 80 %. These data demonstrate that the addition of Algae-C led to a negative impact on the crystallization process of the zeolite.

Table 4.8 Textural properties of the samples determined by N_2 adsorption/desorption measurements.

Sample	S_{BET} (m^2/g)	S_{Micro} (m^2/g)	S_{Exter} (m^2/g)	S_{Ext}/S_{BET} (%)	Relative crystallinity (%)
H-ZSM-5	387	266	121	31	100
200 Algae-C/ZSM-5	373	217	157	42	84
400 Algae-C/ZSM-5	393	223	171	43	80
600 Algae-C/ZSM-5	340	186	154	45	80

The N_2 adsorption/desorption isotherms (Figure 4.12) of the samples clearly show differences. According to BET data in Table 4.8, the specific surface areas of pristine H-ZSM-5 and 200 Algae-C/ZSM-5-3d zeolite remained similar, about 370 m^2/g. With an Algae-C addition raise to 400 mg, the specific surface area surprisingly increased to 393 m^2/g. However, the specific surface area of ZSM-5 zeolite with the highest amount of Algae-C (600 mg) decreased, reaching only 340 m^2/g.

Further comparison of the microporous specific surface area and external specific surface area of all samples highlighted that the micropores specific surface area of pristine H-ZSM-5 was the highest, reaching 266 m^2/g. The micropore specific surface areas of 200Algae-C/ZSM-5 (217 m^2/g) and 400 Algae-C/ZSM-5 (223 m^2/g) were similar and lower than that of HZSM-5. The value of 600 Algae-C/ZSM-5 was the lowest, reaching only 186 m^2/g. In contrast, the external surface area of ZSM-5 zeolites obviously increased with Algae-C addition. For 200 Algae-C/ZSM-5 and 400 Algae-C/ZSM-5 zeolites, the ESA reached 157 m^2/g and 171 m^2/g, respectively, being much higher than that of parent HZSM-5 zeolite (132 m^2/g). When Algae-C addition further increased to 600 mg, the ESA (154 m^2/g) was still higher than that of pristine H-ZSM-5, but lower than the sample with 400 mg Algae-C.

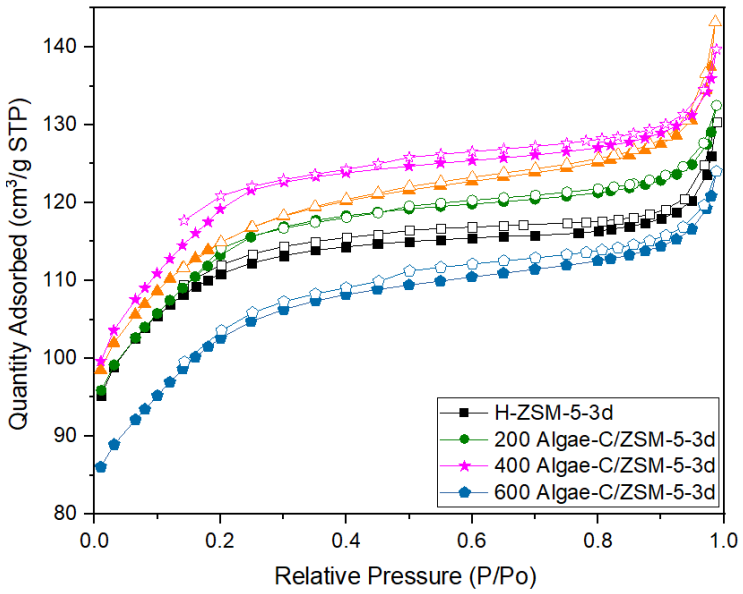

Figure 4.12 N_2 adsorption-desorption isotherms of Algae-C/ZSM-5 with different Algae-C addition.

This result confirms that the addition of Algae-C is beneficial to increase the generation of macropores in the zeolite, but it will cause certain damage to the microporous channels. This may be caused by the blockage of the pores or the influence of crystallization by the heteroelements present in Algae-C.

The XRF data (Table 4.9) showed differences in the chemical composition of these zeolite samples. The first thing to note is that after NH_4^+ ion exchange, heteroatoms, such as P, Ca, Fe and Mg, were still detected in all Algae-C/ZSM-5 zeolites, although the content remained low. In addition, the percentage of heteroelements contained in the zeolite showed an interesting regularity, it showed an upward trend with an increase of Algae-C addition. This result further confirms the influence of heteroelements present in biochar on the zeolite synthesis. Among them, the content of Fe and Ca was higher than P and Mg. These four elements may have a certain effect on the zeolite crystallinity and acidity.

Considering that Algae-C/ZSM-5 zeolite was affected by Algae-C heteroelements, the acidity of Algae-C/ZSM-5 zeolite was characterized by NH_3-TPD method. Figure 4.13 shows the acidity of H-ZSM-5 and *n* Algae-C/ZSM-5-3d (n=200, 400, 600) zeolite samples. The

NH_3-TPD profiles are usually deconvoluted to two Gauss fitting distribution peaks. The low and high temperature peak of all zeolites corresponded to mild acid sites (Si-OH bonds) and strong acid sites (Si-OH-Al bonds), respectively. Generally, the strength of the acid sites affects the activity of catalysts in MTO processes.

Mild acid sites play the main role in the initial C-C bound formation and enhance alkylation and methylation reactions that directly guide propylene selectivity, because they favor light olefins production. Those mildly acidic sites put off undesirable secondary reactions such as hydrogen transfer. The hydrogen transfer reaction increased the selectivity in paraffins and aromatics which is unwanted for MTO.

Table 4.9 Elemental composition of ZSM-5 zeolites measured by XRF.

Samples	P_2O_5%	CaO%	Fe_2O_3%	MgO%
200 Algae-C/ZSM-5	0.11	0.15	0.22	0.04
400 Algae-C/ZSM-5	0.18	0.35	0.28	0.07
600 Algae-C/ZSM-5	0.35	0.56	0.40	0.25

Compared with all NH_3-TPD profiles, the peak intensity presented a decreasing trend with an increase of Algae-C addition, suggesting an acidity decrease.[151] In addition, the peak temperature of the desorption peak at the strong Brønsted acid site also showed a decreasing trend. Among them, the strong acid site desorption temperature of pristine H-ZSM-5 is 558 ^oC, the desorption temperatures of 200 Algae-C/ZSM-5 and 400 Algae-C/ZSM-5 were reduced to about 527 ^oC, and this temperature for 600 Algae-C/ZSM-5 remained only 518 ^oC. The decrease in NH_3 desorption temperature meant that the strength of Brønsted acid site in the sample was weakened.

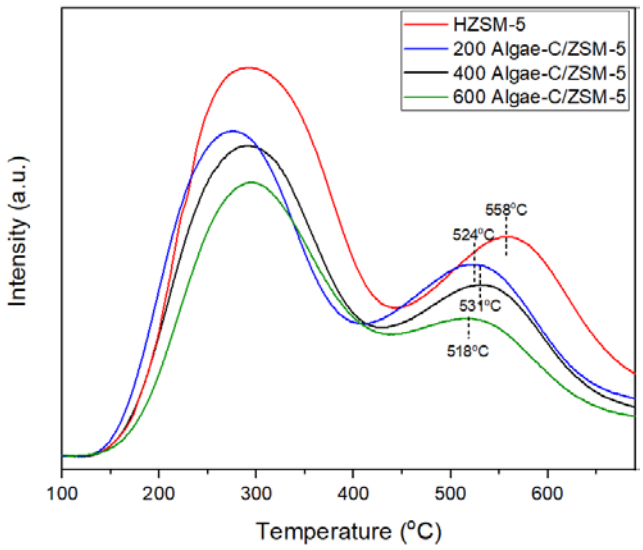

Figure 4.13 NH_3-TPD profiles of pristine H-ZSM-5, Algae-C/ZSM-5-3d (200, 400, 600 mg).

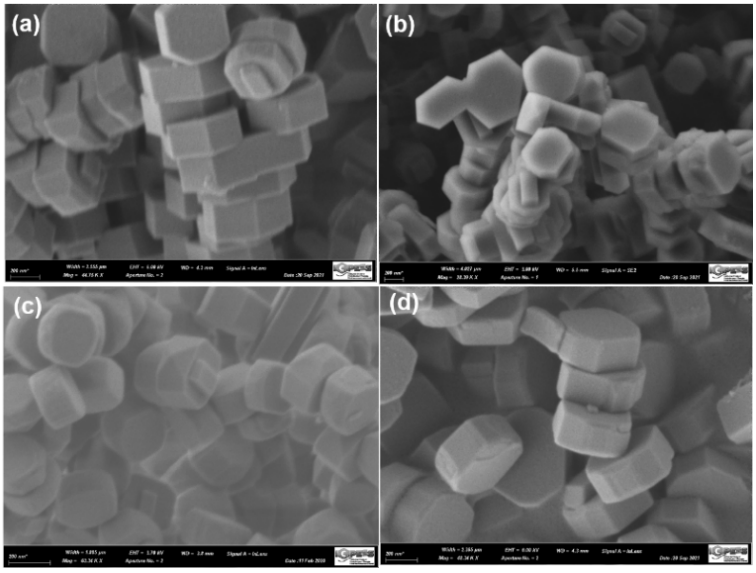

Figure 4.14 SEM images of (a) pristine H-ZSM-5, (b) 200 Algae-C/ZSM-5, (c) 400 Algae-C/ZSM-5 and (d) 600 Algae-C/ZSM-5.

The SEM images (Figure 4.14) of the four samples all showed coffin-shape of complete single crystals, which is one of the typical crystal morphologies of ZSM-5 zeolite. Even with the addition of algae carbon, the crystals of the samples did not show significant changes, indicating that an addition of algae carbon did not affect the overall crystallization process of

the zeolite. This result is consistent with the results shown in the XRD patterns.

The catalytic performance of the catalysts in the MTO reaction was evaluated in a fixed bed reactor. Figure 4.15 presents the conversion and selectivity reached over H-ZSM-5 and 200 Algae-C/ZSM-5-3d at different temperatures (350, 400 and 450 ^{o}C) and two different space velocities (WHSV=2 h^{-1} and 8 h^{-1}). The data were collected after 30 min of reaction. The point plots correspond to the methanol conversion over HZSM-5 and 200 Algae-C/ZSM-5-3d at different reaction temperatures. The corresponding bar chart below the dot plot shows a high selectivity in light olefins.

Both samples exhibited excellent catalytic activity under all conditions. The conversion of methanol was almost 100% for both catalysts in the reaction time of 30 min. However, the selectivity of the two catalysts to light olefins under different conditions was significantly different. Obviously, the temperature has a large effect on product selectivity. The higher the temperature was, the higher the selectivity towards light olefins was.

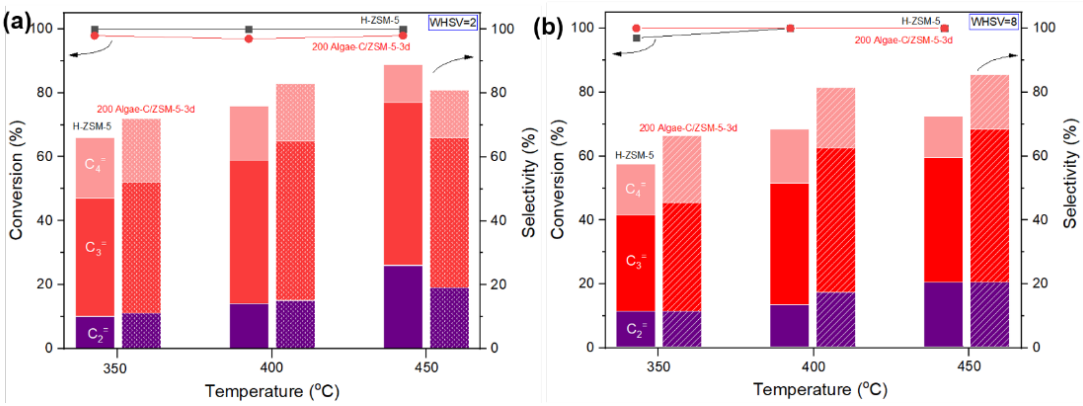

Figure 4.15 Conversions and selectivities achieved over H-ZSM-5 and 200 Algae-C/ZSM-5-3d catalysts in the MTO after 30 min on stream (a) WHSV=2 h^{-1} (b) WHSV=8 h^{-1}.

Table 4.10 shows the C_4 hydrogen transfer index (C_4-HTI) of the two samples under different operating conditions. It is noteworthy that a temperature raise favored the cracking of C_{5+} hydrocarbons, inhibiting hydrogen transfer reactions and hence improving the selectivity in ethylene and propylene. The C_4-HTI index of both samples diminished significantly with

increasing reaction temperature. However, elevated temperature does not only raise energy consumption, but also accelerates the formation of carbon deposits on the catalyst surface, thus shortening its lifetime. Furthermore, 200 Algae-C/ZSM-5-3d generally led to higher light olefins selectivity than parent H-ZSM-5. Especially at high space velocity (WHSV=8 h^{-1}) and high temperature (400 and 450 ^{o}C), the selectivity of 200 Algae-C/ZSM-5-3d towards light olefins was about 11% (absolute value) higher than over H-ZSM-5.

It can be considered that the addition of Algae-C is beneficial, yielding an increase in the selectivity towards light olefins. This is also attributed to the inhibition of hydrogen transfer reactions by Algae-C/ZSM-5 which exhibits mild acidity. The change in the space velocity had little impact on the selectivity.

Table 4.10 C_4-Hydride transfer index of H-ZSM-5 and 200 TRA-C/ZSM-5 at different catalytic conditions

Space velocity	**Temperature**	**C_4-Hydride transfer index (C_4-HTI)**	
		H-ZSM-5	200 Algae-C/ZSM-5
WHSV=2 h^{-1}	350 ^{o}C	0.30	0.29
	400 ^{o}C	0.26	0.18
	450 ^{o}C	0.20	0.21
WHSV=8 h^{-1}	350 ^{o}C	0.40	0.32
	400 ^{o}C	0.35	0.27
	450 ^{o}C	0.24	0.23

[a] The hydride transfer index was calculated from the alkane selectivity (C_4-) and the alkene selectivity (C_4=) in terms of the formula of C_4-/(C_4-+ C_4=).

The selection of suitable conditions was based on the results shown in Figure 4.15. Relatively low reaction temperature was chosen for performing stability tests, since the temperature is positively correlated with the rate of carbon deposition and energy consumption.

Two sets of test conditions (WHSV=2 h^{-1}, T=350 ^{o}C and WHSV=8 h^{-1}, T=400 ^{o}C) were selected. The performances in the methanol conversion and targeted products selectivity for all samples (HZSM-5 and 200, 400, 600 Algae-C/ZSM-5) were compared during the long duration period, as shown in Figure 4.16.

It is noteworthy that H-ZSM-5 and Algae-C/ZSM-5 catalysts exhibited significantly different lifetimes (Figure 4.16 (a)). For 400 Algae-C/ZSM-5 (at 350°C and WHSV=2 h-1), the methanol conversion still demonstrated an astonishing 90 % after a reaction run of 100 h. 200 Algae-C/ZSM-5-3d still achieved 94% conversion of methanol after 50 h. The lifetime of these two Algae-C modified catalysts was much higher than that of pristine H-ZSM-5, which significantly declined after 26 h on stream. However, when the addition of Algae-C increased to 600 mg, the catalyst lifetime was comparable to H-ZSM-5 without significant improvement. This may be caused by the destruction of the micropores in 600 Algae-C/ZSM-5 zeolite and the presence of only few acid sites. Furthermore, Figure 4.16 (b) presents the product selectivity of 400 Algae-C/ZSM-5-3d under these catalytic conditions for different time periods. The results show that the selectivity in light olefins first increased and then gradually decreased. The selectivity towards light olefins was the highest at around 25 h, reaching 66%, and then slowly decreased. After 100 h on stream, the selectivity to light olefins was still 63%.

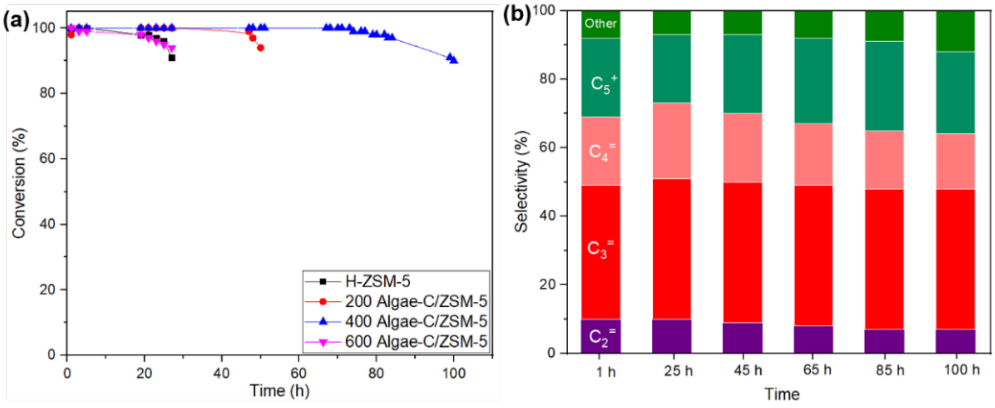

Figure 4.16 (a) Methanol conversion and (b) product selectivity of Algae-C/ZSM-5-3d with different Algae-C addtion in the MTO at 350 °C, WHSV=2 h^{-1}.

After a further increase in the space velocity (WHSV=8 h^{-1}) and temperature (400 ^{o}C), the lifetime of all samples decreased sharply (Figure 4.17 (a)). For 400 Algae-C/ZSM-5, the conversion of methanol became lower than 95% after 16 h. This time was reduced to 12 h for 200 Algae-C/ZSM-5 zeolite. H-ZSM-5 and 600 Algae-C/ZSM-5 still showed similar lifetimes, being worse than 200 Algae-C/ZSM-5 and 400 Algae-C/ZSM-5 zeolites, maintaining 95% conversion capacity only during 10 h on stream.

Likewise, the product selectivity of 400 Algae-C/ZSM-5 at different reaction times is shown in Figure 4.17 (b). After 5 h, the catalyst exhibited the highest selectivity to light olefins, reaching 71%, being higher than the selectivity of the catalyst at low temperature and low space velocity. When the catalyst began to deactivate gradually, the catalyst's selectivity towards light olefins also showed a decreasing trend. At 15 h, the selectivity to light olefins dropped to 62%. The catalytic results of ZSM-5 catalysts with different algae carbon additions in the MTO reaction confirm that the improvement in the catalyst lifetime shows a positive correlation with an increase of the external surface area of the modified catalysts, which is beneficial for enhancing mass transfer of the products within the zeolite particles. Short dwell time of products can greatly avoid coke formation, which will render the active sites inaccessible. In addition, mild acidity can also delay the deactivation by reducing the formation of polyalkyl and/or polycyclic aromatics that are difficult to be desorbed from the pores.

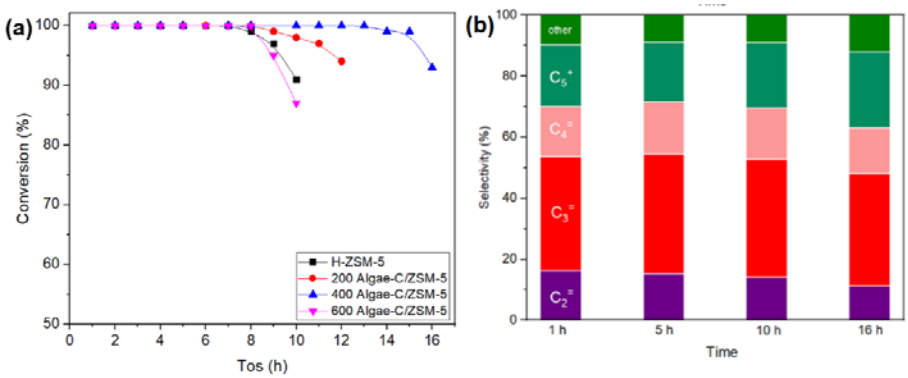

Figure 4.17 (a) Methanol conversion and (b) product selectivity of Algae-C/ZSM-5-3d with different Algae-C addtion in the MTO at 400 °C, WHSV=8 h^{-1}.

4.4.2 Influence of the catalytic temperature

The effect of different catalytic temperatures on the performance of Algae-C/ZSM-5 was explored. Figure 4.18 (a) shows that the reduction of catalytic temperature affects the catalytic activity of Algae-C/ZSM-5, which was also proved for Grass-C/ZSM-5 zeolite. The degree of methanol conversion could not reach 100 % unless the catalytic temperature was higher than 350 ^{o}C. In addition, the reaction temperature was also correlated with the catalyst lifetime of Algae-C/ZSM-5. At 350 ^{o}C, the conversion of the catalyst continued to decline over time. When the catalytic temperature was enhanced to 400 ^{o}C, the catalyst showed excellent lifetime. The conversion was kept above 95 % within 16 h. However, with a further temperature increase, the methanol conversion could reach 100 % in the early stages, but only for a shorter duration (4 h). The lifetime was reduced to 1 h at 500 ^{o}C, with a methanol conversion of only 55% in the second hour.

In addition, the selectivity of light olefins with temperature increase also shows a trend of increasing first and then decreasing (Figure 4.18 (b)). At 350 ^{o}C, the catalyst with the lowest selectivity to light olefins, only has about 65%. Its selectivity to light olefins at 400, 450, 500 ^{o}C is similar, reaching 72%, 74% and 71%, respectively. Among them, the selectivity to ethylene increases continuously with the increase of temperature, while the selectivity to propylene decreases at 500 ^{o}C, and the selectivity to butenes decreases with the increase of temperature.

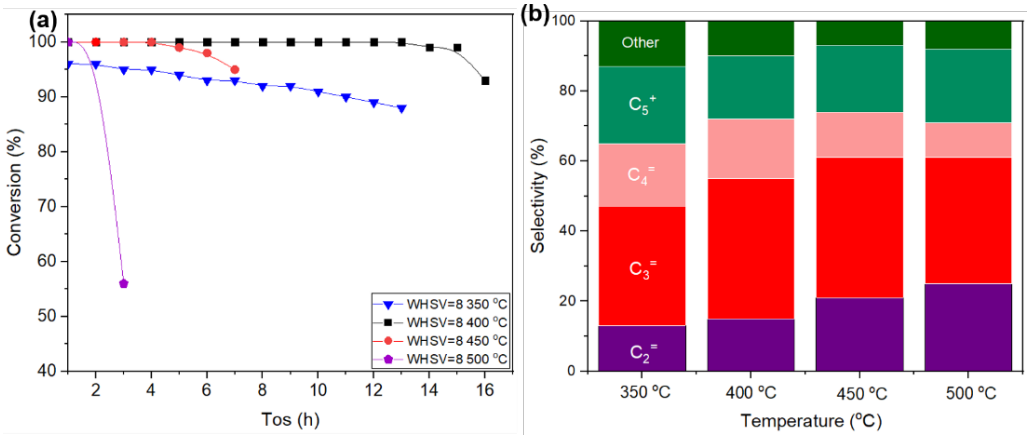

Figure 4.18 Methanol conversion of (a), products selectivity of 400 Algae-C/ZSM-5(3d) in the MTO at different temperatures (350 °C, 400 °C, 450 °C, 500 °C), WHSV=8 h^{-1}.

4.4.3 Influence of the synthesis time

In order to further optimize the catalyst which led to the promising performance, the effect of 400 Algae-C/ZSM-5 zeolite synthesis duration on its physicochemical properties was explored. In this study, 1d, 2d and 3d of hydrothermal treatment were selected for comparison. Although the XRD patterns (Figure 4.19 (a)) demonstrated that all samples were highly crystalline, consistent with the typical MFI structure, the relative crystallinity still highlighted differences, as shown in Table 4.11 Compared with the samples with synthesis time of 1d and 3d, 400 Algae-C/ZSM-5-2d led to the highest relative crystallinity, reaching 86 %. The relative crystallinity of 400 Algae-C/ZSM-5-1d was only 64%. This result shows that the crystallinity of the zeolite and the synthesis time are not completely correlated. However, a too short synthesis time remains unfavorable for a complete crystallization.

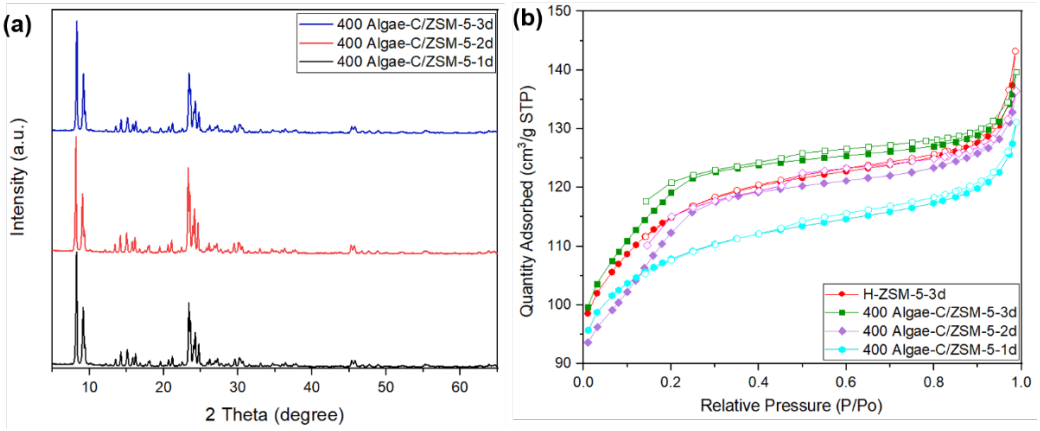

Figure 4.19 (a) XRD patterns and (b) N_2 adsorption-desorption isotherms of 400 Algae-C/ZSM-5 with different hydrothermal time (3d, 2d, 1d).

In addition, N_2 adsorption-desorption isotherms of these catalysts also showed differences, as shown in Figure 4.19 (b) and Table 4.11. The specific surface areas of 400 Algae-C/ZSM-5-3d and 400 Algae-C/ZSM-5-2d remained similar with respect to H-ZSM-5, around 390 m^2/g. In contrast, when the synthesis duration was limited to one day, the specific surface area significantly diminished to 349 m^2/g. In parallel, the micropore specific surface area and external specific surface area of the zeolite showed a more complex trend. Indeed, the changes induced in the textural and structural properties of those zeolites may be affected by several factors as crystallinity, particle size and the amount of Algae-C added. However, the NH_3-TPD profiles (Figure 4.20) of the three samples showed that the synthesis time had no significant effect on the acidity of the samples.

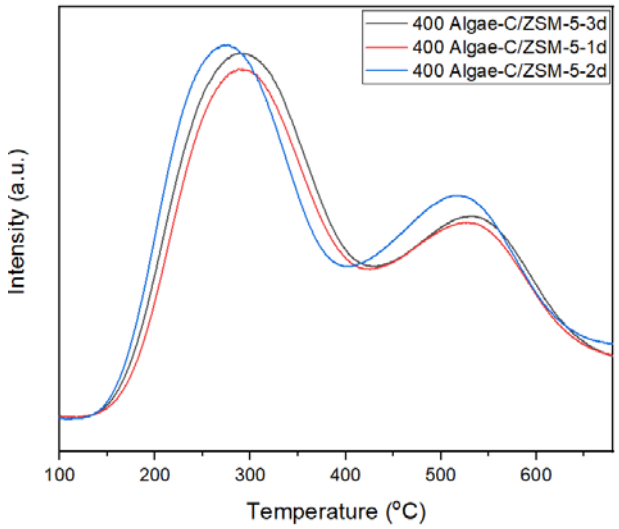

Figure 4.20 NH_3-TPD profiles of 400 Algae-C/ZSM-5 with different hydrothermal times (3d, 2d, 1d).

Regarding the catalytic activity, it can be clearly seen that the lifetimes of Algae-C/ZSM-5 materials were drastically impacted by monitoring the synthesis duration (Figure 4.21 (a)). Indeed, after 3 days or 2 days, the lifetimes were similar, being roughly 16 h. However, the lifetime of the catalyst prepared for 1 d was greatly shortened, with a significant deactivation observed after only 5 h on stream. This may be related to low micropore area (89 cm^2/g) and poor crystallinity (64%). In terms of light olefins selectivity (Figure 4.21 (b)), 400 TRA-C/ZSM-5 2d was slightly lower than 400 Algae-C/ZSM-5-3d.

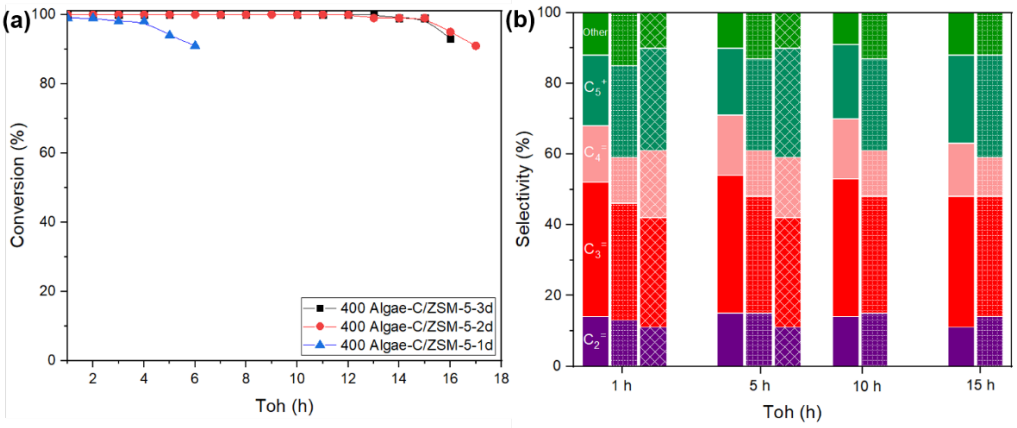

Figure 4.21 Methanol conversion of different catalysts (a), products selectivity of 400 Algae-C/ZSM-5(3d, 2d, 1d) in the MTO at 400 °C, WHSV=8 h^{-1}.

Table 4.11 Textural properties of the Algae-C/ZSM-5 determined by N_2 adsorption/desorption measurements.

Sample	S_{BET} (m^2/g)	S_{Micro} (m^2/g)	S_{Exter} (m^2/g)	S_{Exter}/S_{BET} (%)	Relative crystallinity %
H-ZSM-5	387	266	121	31	100
400 Algae-C/ZSM-5-3d	393	223	171	43	80
400 Algae-C/ZSM-5-2d	387	213	174	45	86
400 Algae-C/ZSM-5-1d	349	260	89	26	64

The differences in the catalytic properties of the three zeolites may be caused by changes in the physical structure of the zeolites caused by different hydrothermal times, such as crystallinity, micropore specific surface area and external specific surface area. Such difference is revealed in the N_2 adsorption and desorption isotherm studies of the samples. However, the factors affecting the catalytic performance of zeolites are complex. The MTO data can only allow us to speculate that too low ESA will cause a rapid deactivation of the zeolite. Hence, being able to increase the ESA of a given zeolite appears as an effective method to prolong its lifetime.

4.4.4 Influence of the physicochemical properties of carbon materials

4.4.4.1 Characterization of carbon materials

The difference between biochar and pure carbon materials in the attempts for modification of ZSM-5 zeolite was further explored. The 400 mg biochar powder containing rich inorganic salts and ash was treated with 2M HCl for 2h to obtain 240 mg pure carbon. Furthermore, hydrophobic carbon black (240 mg) was included as a reference material too.

In order to further explore the effect of unique physicochemical properties (presence of heteroelements and surface functional groups) of Algae-C on ZSM-5 zeolite, acid-treated Algae-C and hydrophobic carbon black (CB) were used as reference materials to prepare

Algae-C/ZSM-5, Acid Algae-C/ZSM-5 and CB/ZSM-5. The XRD patterns of Algae-C, acid treated Algae-C and carbon black were shown in Figure 4.22. Compared with Algae-C, acid treated Algae-C and carbon black only exhibited broad peak corresponding to amorphous carbon, showing that the two carbon materials hardly contain inorganic salt impurities.

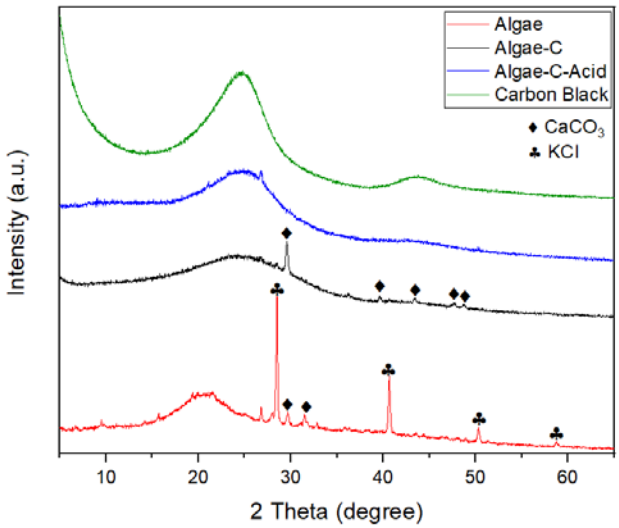

Figure 4.22 XRD patterns of Algae, Algae-C, Algae-C-Acid and Carbon black.

The microscopic particle size distribution of biochar was analyzed by a laser particle size analyzer, with respect to weight fraction, as shown in Figure 4.23. The experimental results show that the three carbon materials show relatively uniform particle size distribution, but there are differences in particle size. Among them, carbon black exhibited the largest particle size, with an average particle size of about 2.6 μm. The average particle size of Algae-C was about 1.9 μm. The average particle size of Algae-C after acid treatment was reduced again to only about 1.2 μm.

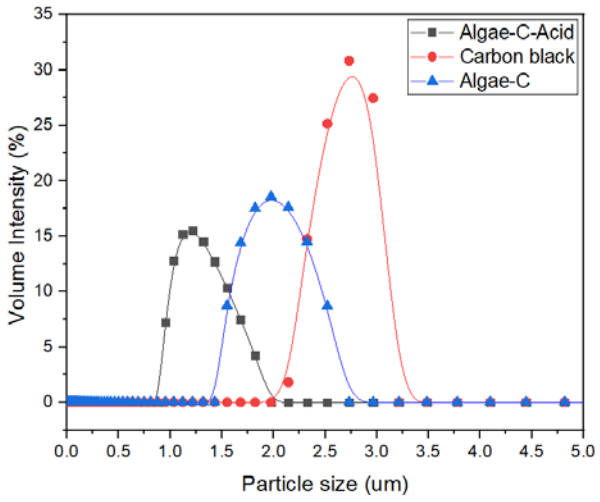

Figure 4.23 DLS grading curves of TRA-C, TRA-C-Acid and carbon black.

In addition, Figure 4.24 presents the N_2 adsorption-desorption isotherms for Algae-C, Algae-C-Acid and carbon black. It can be seen from these isotherms that carbon black and Acid-TRA-C led to higher adsorption capacities. Among them, the specific surface area of carbon black reached 77 m^2/g, while Acid treated Algae-C reached 149 m^2/g (Table 4.11). However, the specific surface area of Algae-C reached only 2.3 m^2/g. Compared with Algae-C, the high specific surface area of Acid-Algae-C was attributed to the fact that hydrochloric acid dissolved the inorganic salts present in Algae-C particles, resulting in an etching effect on the Algae-C surface, thus greatly enhancing the particle porosity and surface roughness.

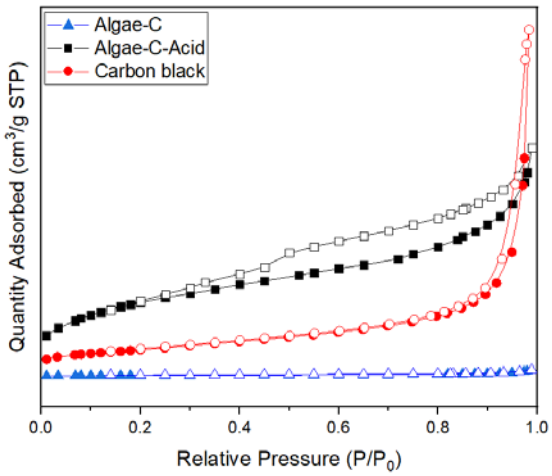

Figure 4.24 N_2 adsorption/desorption isotherms of Algae-C, Algae-C-Acid and Carbon black.

Figure 4.25 presents the infrared absorption spectroscopy of Algae-C and Acid treated Algae-C. Algae-C exhibited higher -OH and C-O-C, C-O-P bond vibrations than acid Algae-C. The presence of these abundant functional groups usually originates from polysaccharides, phosphates and soluble proteins in Algae-C. In contrast, for hydrophobic carbon black, no vibrational peaks of surface groups could be detected.

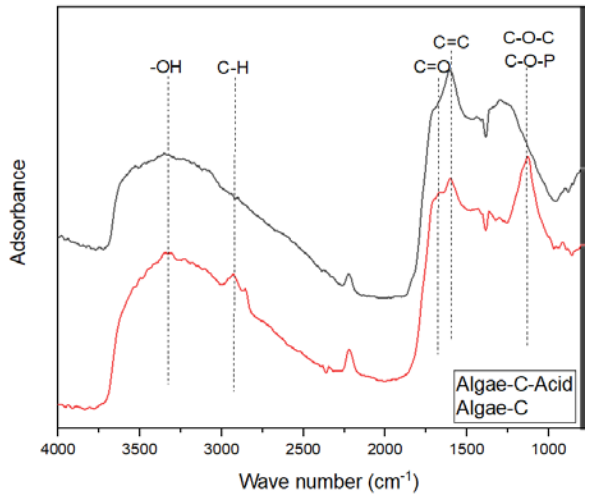

Figure 4.25 Infrared absorption spectroscopy of TRA-C, TRA-C-Acid and Carbon black.

Finally, EDX mapping of the elements (Figure 4.26) assessed that Algae-C contained much oxygen and metal cations, whilst Acid-Algae-C and carbon black almost possessed exclusively C and O elements; the O-content being significantly lower than that of Algae-C.

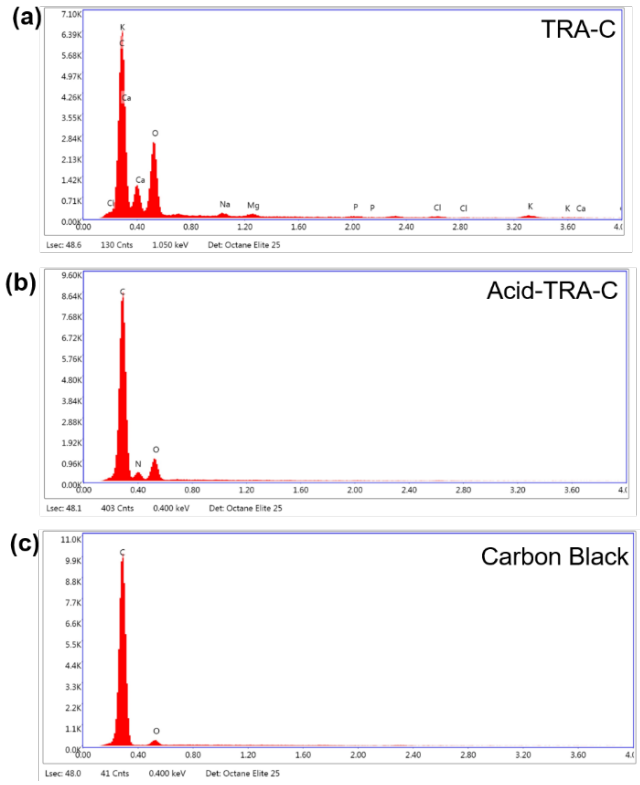

Figure 4.26 EDX images of (a) Algae-C, (b) Acid treated Algae-C and (c) Carbon black.

4.4.4.2 Synthesis of carbon modified ZSM-5

ZSM-5 zeolites were synthesized using these three types of carbon materials, and synthesis time of 2 days was selected. As-obtained catalysts were named 400 Algae-C/ZSM-5-2d, 240 Acid-Algae-C/ZSM-5-2d, and 240 Carbon Black/ZSM-5-2d. The XRD patterns (Figure 4.27) confirmed that all samples exhibited clearly MFI type characteristic diffraction peaks, thus assessing that the presence of carbon materials did not have an influence on the zeolite formation.

However, Table 4.12 shows some differences with respect to relative crystallinity. Among them, the relative crystallinity of Algae-C/ZSM-5 was the lowest, only 86%. The relative crystallinity of Acid Algae-C/ZSM-5 was similar (88%). Carbon Black/ZSM-5 exhibited the highest relative crystallinity, reaching 95%. From this data, it can be seen that the addition of

carbon template did not yield an effect on the relative crystallinity of ZSM-5 zeolites. In addition to carbon particles, impurities such as other inorganic salts contained in the carbon matrix may further affect the crystallization of the ZSM-5 zeolite.[89] Indeed, the amount of acid sites and specific surface areas of these samples exhibited significant differences.

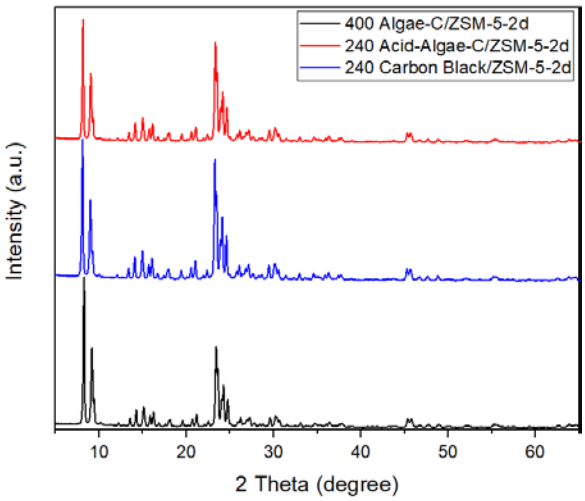

Figure 4.27 XRD patterns of 400 Algae-C/ZSM-5-2d, 240 Acid-Algae-C/ZSM-5-2d, and 240 Carbon Black/ZSM-5-2d.

As shown in Figure 4.28, the strength of NH_3 desorption peaks of both 240 Acid-Algae-C/ZSM-5-2d and 240 Carbon Black/ZSM-5-2d were rather similar, indicating roughly the same number of acid sites in both samples. In stark contrast, the peak strength of 400 Algae-C/ZSM-5-2d was much lower than that of the two other samples, especially the high temperature peak corresponding to strong acid sites. As ‘a priori’ expected, these results demonstrate that inorganic salts from the biochar influenced the acidity, especially the strong Brønsted acid sites. In addition, the maximum desorption temperature peak at the strong acid site of algae-C modified zeolite lower than that of Carbon black and acid treated algae-C modified samples.

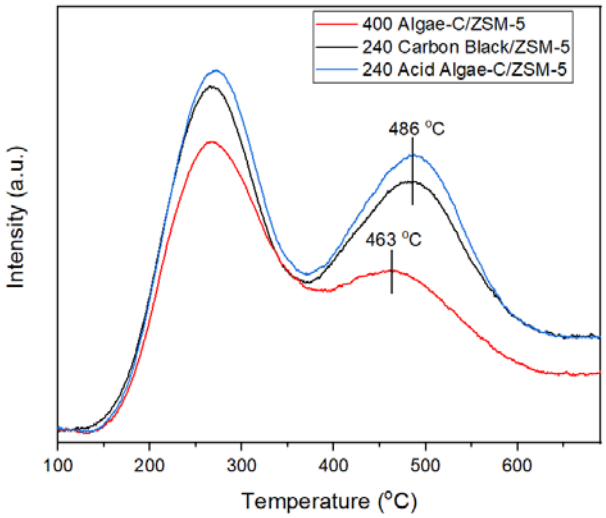

Figure 4.28 NH_3-TPD of 400 Algae-C/ZSM-5-2d, 240 Acid-Algae-C/ZSM-5-2d, and 240 Carbon Black/ZSM-5-2d.

Furthermore, Figure 4.29 and Table 4.12 showed that the total specific surface area of 240 (Acid-Algae-C, Carbon Black)/ZSM-5, 400 Algae-C/ZSM-5-2d and HZSM-5 zeolite were rather similar, whereas their microporous area and ESA remained different. 240 (Acid-Algae-C and Carbon Black)/ ZSM-5-2d zeolites 'micropore area was much higher than their external surface area, similar to parent ZSM-5 zeolite. However, 400 Algae-C/ZSM-5-2d showed high ESA. It might possible that carbon black and Acid-Algae-C have no pore-forming ability, due to the less hydrophilic group (such -OH) on the surface area of both templates.

Table 4.12 Textural properties and relative crystallinity of the ZSM-5 zeolites.

Sample	S_{BET} (m^2/g)	S_{Micro} (m^2/g)	S_{Exter} (m^2/g)	S_{ext}/S_{BET} (%)	Relative crystallinity (%)
400 Algae-C/ZSM-5-2d	387	213	174	45	86
240 Acid Algae-C/ZSM-5-2d	373	246	127	34	88
240 Carbon Black/ZSM-5-2d	387	268	119	31	95

The affinity between template and gel precursors plays a key role in the pore-forming process. The zeolite nuclei containing -SiOH groups can effectively connect to the -OH group

on the biochar surface by hydrogen bonding or condensation reaction. However, the acid treated biochar and carbon black will rather induce phase separation with zeolite nuclei.

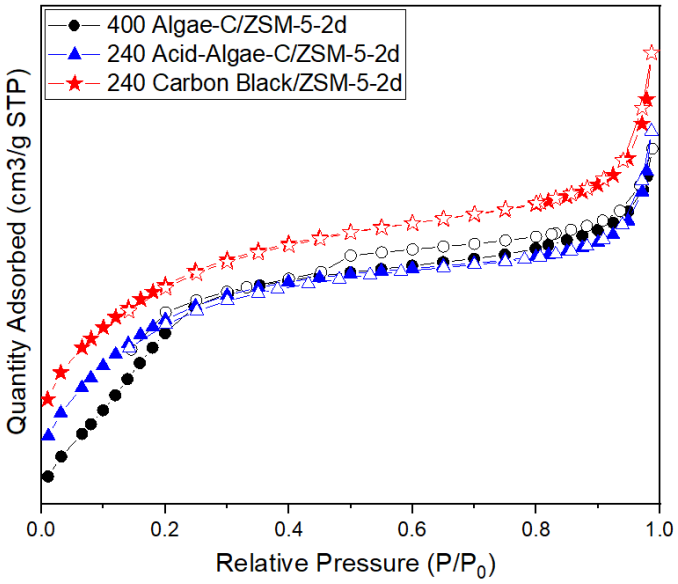

Figure 4.29 N_2 adsorption/desorption isotherms of samples 400 Algae-C/ZSM-5-2d, 240 Acid-Algae-C/ZSM-5-2d, and 240 Carbon Black/ZSM-5-2d.

The catalytic behavior in the MTO reaction (Figure 4.30 (a)) showed that 400 Algae-C/ZSM-5-2d with high external surface area and low acidity exhibited the longest catalyst lifetime. However, for Carbon Black and Acid-Algae-C/ZSM-5-2d catalysts, their conversion rate gradually decreased after 10 h. In addition, the selectivity in light olefins over 400 Algae-C/ZSM-5-2d was higher than that over Carbon Black and Acid-Algae-C/ZSM-5-2d catalysts due to the presence of mild acidity in 400 Algae-C/ZSM-5-2d (Figure 4.30 (b)).

As a result, biochar from algae did not only act as a suitable hard template as a pore-forming agent for ZSM-5 zeolite, but also as a suitable mean to diminish (and tune) the acidity of ZSM-5 zeolite due to presence of metal elements. The latter elements yielded a positive influence in the MTO reaction.

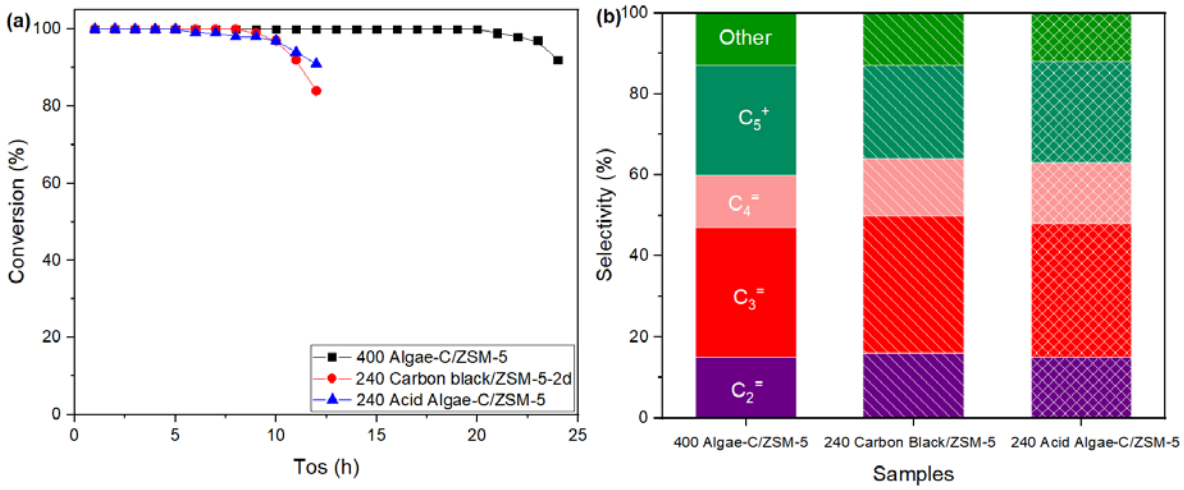

Figure 4.30 Methanol conversion (a), products selectivity of of 400 (Acid-Algae-C, Carbon Black, Algae-C)/ ZSM-5-2d and 400 TRA-C/ZSM-5-2d catalysts.

4.5 Conclusion

The catalytic performance of Algae-C/ZSM-5 and Grass-C/ZSM-5 was further optimized by adjusting the parameters of synthesis and reaction, including the amount of biochar added, Si/Al, synthesis duration, reaction temperature, space velocity.

The results showed that the external surface area of the zeolite was directly affected by the amount of biochar added. The high ESA can be obtained by several types of biochar addition, which yielded a longer lifetime to the zeolites. However, the microporous structure of the zeolite was partially destroyed with an excessive amount of biochar, resulting in the loss of active sites. Hence, it yielded adversely effects to the performances of the zeolites. It is therefore important to select an appropriate amount of biochar. Among them, 400 mg of Algae-C and 500 mg of Grass-C were suitable choices. In addition, the acidity of the zeolite showed a decreasing trend with the addition amount of biochar, inducing an increase in the content of heteroatoms in the zeolite. A negative correlation between those heteroelements content and the zeolite acidity could be assessed. The catalytic data in the MTO reaction showed that moderately reducing the acidity of the zeolite was beneficial to prolong the catalyst lifetime.

Except to the introduction of heteroelements, a proper tailoring of the Si/Al also led to changes in acidity. The variation of this parameter showed a significant effect on the selectivity and the catalytic activity of ZSM-5 zeolite. The results confirmed that at low Al content, the selectivity to ethylene dropped sharply, but the selectivity to propylene increased rapidly. Meanwhile, the acid sites of the zeolite decrease while reducing the Al content, which led to the weakening of the catalytic activity. For short-term use, Grass-C/ZSM-5 with Si/Al=30 exhibited better catalytic activity in the early stages of the reaction, but it rapidly deactivated. Although Grass-C/ZSM-5 with Si/Al=120 could not reach 100 % conversion, its deactivation rate was slower. So, the latter catalyst is therefore more suitable for long-term use.

The crystallinity of zeolite was affected by synthesis time. The short synthesis time was not sufficient to achieve fully crystalline zeolite materials. Crystallinity also influenced the

catalytic performance, but it a lower extent than external surface area and acidity. In addition, there is also a correlation between reaction temperature and performance. At high temperature, the selectivity of the catalysts in light olefins fraction exhibited significant improvement. When temperature was increased from 350 ^{o}C to 450 ^{o}C, for Grass-C/ZSM-5, the selectivity towards ethylene increased from 10 % to 20 %, and the selectivity for propylene increased from 31 % to 42 %. However, the coking rate was accelerated at high reaction temperatures, thus leading to rapid deactivation of the zeolite.

Furthermore, the importance of hydrophilicity and heteroelements for zeolite modification was proved by comparing the effect of Algae-C, acid-treated Algae-C (without inorganic salts) and hydrophobic carbon black (without surface functional groups) on ZSM-5. Hydrophilicity is a necessary condition for hard templates to play a pore-forming role in a hydrothermal environment. With this property, zeolite crystals can better interact with biochar surface. When the template was removed, the pore can be left perfectly in zeolites. In addition, inorganic salts acted as a mean to weaken the acidity of the ZSM-5 zeolite, thus yielding a positive effect on the MTO behavior.

Chapter 5. Structured ZSM-5 zeolite coatings on perlite support

ABSTRACT

ZSM-5 zeolite crystals were grown via an *in situ* hydrothermal synthesis on perlite supports. In this study, cheap perlite mineral, which mainly contains SiO_2 and metal oxides (Al_2O_3, CaO, MgO), was used as aluminum source and support material for binderless zeolite crystals growth. Hence, this synthesis strategy neither needs the introduction of Al, nor support surface functionalization steps, which may diminish the cost. Besides, the highly porous structure and the big particle size of ZSM-5 / perlite composites are beneficial to reduce the pressure drop along the catalyst bed, rendering easier the heat and mass transfers of the products. In addition, the influence of different particle sizes (4-3, 3-1.5 and 0.5-1.5 mm) and quantities (1-3 g) of ZSM-5/perlite without any further modification were successfully evaluated in the Methanol-To-Olefins reaction (MTO). An optimized ZSM-5/ Perlite structured catalyst exhibited a high stability at full methanol conversion during 14 h on stream, along with an 80% selectivity towards light olefins at 475 ^oC. In addition, this catalyst still exhibited an excellent catalytic activity at relatively low temperature (350 ^oC), the methanol conversion remaining 96% after 28 h on stream. Finally, the conversion was maintained at 95% during 8 h on stream at WHSV=8h^{-1} with a propylene selectivity of 38%.

5.1 Introduction

In general, zeolites are used as nanoparticles with hundreds of nanometers in size, thus leading to problems for an industrial implementation in fixed-bed reactors as: high pressure drop, limited heat and mass transfers or difficult of recovery. In particular, light olefins have to be quickly removed from the catalyst surface to prevent them from reacting further. Moreover, the formation of un-anticipated hot spots in the fixed-bed reactor, as a result of limited heat transfer in the catalyst particles, may deactivate the zeolite catalyst rapidly, since MTP or MTO reactions are highly exothermic.[152]

The use of highly porous materials (SiC foams, porous glass or silica beads) as zeolite

support became a serious option to improve the light olefins yield and the catalyst resistance to deactivation. Valtchev *et al.*[153] synthesized structured ZSM-5@silica catalyst beads without using a binder. This kind of zeolite composite not only improved the catalyst recovery but also avoided an activity loss due to aggregation. Ivanova *et al.* [154, 155] prepared ZSM-5 / *β*-SiC foam structured catalysts, which demonstrated an excellent and stable conversion of several alcohols into olefins. Unfortunately, silica beads and SiC foams involved complex preparation steps, inducing a high cost. For instance, Louis *et al.* prepared promising structured catalytic beds made of 3D tri-modal glass supports. ZSM-5 zeolite crystals were successfully grown on hierarchized glass scaffolds and exhibited improved catalysts activity and selectivity in n-hexane cracking, but suffered from mechanical stability issues.[156]

Perlite is a volcanic glass, mainly composed of amorphous aluminum silicate. This kind of light weight glass material with porous structure exhibits interesting physical properties, such as high thermal, flame and chemical resistance[157]. Perlite can therefore be used as a support material and filter aid. Kasai *et al.* [158] synthesized zeolite surface-modified perlite to adsorb heavy metals. It appeared that perlite acts as an excellent support medium due to the complex and irregular shape of its glass flakes. In addition, perlite also contains about 75 % SiO_2 and a variety of metal elements (Al, K, Na…). Especially, aluminum accounts for nearly 11 % of total composition. Perlite can therefore be used as an aluminum source for a cost-efficient zeolite synthesis. Pergher *et al.* [157]synthesized zeolite from expanded perlite and evaluated its performance in Rhodamine B adsorption. Corregidor *et al.* [159]synthesized ZSM-5/MCM-41 zeolites from perlite, which were then used as catalysts for the reaction between vinyl acetate and isoamyl alcohol. Since for these zeolite syntheses, the natural mineral was used both as silica and alumina sources, leading to their dissolution, thus the original structure of perlite particles could not be maintained. At present, there are few reports on the synthesis of ZSM-5 zeolite directly using perlite particles as supprot and aluminum source.

In this study, we report the binderless synthesis of ZSM-5 crystals on Perlite particles. Perlite was used both as an aluminum source and as a support. Thanks to an open cell structure and rich Al content, perlite offers a high diffusivity for both reactants and products throughout its highly porous structure. To assess its viability, the MTO reaction was selected as a model acid-catalyzed reaction. Indeed, we thought worthy to evaluate if those structured composite catalysts can help to overcome stability and selectivity issues encountered in fixed-beds. Meanwhile, we also studied the effect of different additive amounts, various particle sizes of perlite, reaction temperature and space velocity in the MTO reaction.

5.2 Experimental part

The Perlite-modified ZSM-5 zeolite synthesized in this subsection followed the synthesis procedure of "biochar-based structured ZSM-5 zeolite" in Chapter 2.2. The perlite particles with: (a) 4-3 mm, (b) 3-1.5 mm, and (c) 1.5-0.5 mm diameter was used as a support for ZSM-5 crystals growth, and determine the suitable particles size for the MTO reaction. Then, the amount of perlite (1 g, 2 g, 3 g) was modified. As-obtained samples were named ZSM-5/x-n-Perlite; with x (=1, 2, 3 g) and n (a: 4-3 mm, b: 3-1.5 mm, c: 0.5-1.5 mm) defined the mass of perlite and its particle size, respectively. For the MTO reaction, the influence of space velocity (2 h^{-1}, 8 h^{-1}, 12 h^{-1}) were studied. The whole synthesis strategy was summarized in Figure 5.1

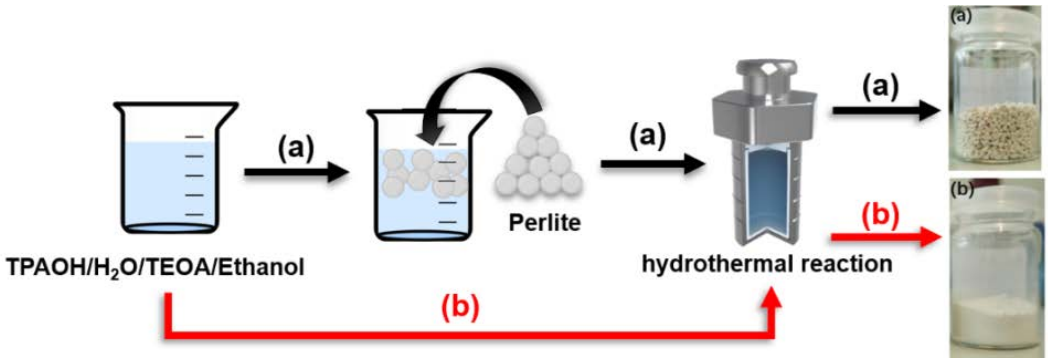

Figure 5.1 Synthesis strategy of (a) ZSM-5/*x*-*n*-Perlite and (b) silicalite-1.

5.3 Results and discussion

5.3.1 Characterization of perlite

Perlite is a kind of amorphous volcanic glass formed by rapid cooling, with pearl fissures. The granules are irregular lumps with a lighter texture, and exhibit a rather large size distribution, as shown in Figure 5.2. The perlites screened in this study were 0.5-4 mm in diameter.

Figure 5.2 Picture of perlite particles.

The SEM image (Figure 5.3) shows the microscopic structure of perlite particles. It can be seen that perlite has an extremely open pore structure, the pore size being non uniform. In addition, thin pore walls endow perlite with a lighter mass.

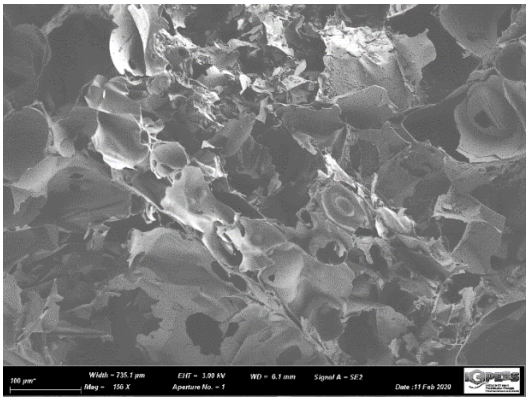

Figure 5.3 SEM image of perlite.

In addition, BET surface area of perlite was only 0.9 $m^2 \cdot g^{-1}$ (Table 2), meaning that it is a non-porous solid. In a practical sense, perlite did neither exhibit micropores (< 2 nm) nor mesopores (> 2 nm and <50 nm). Its sole porosity was due to the presence of macropores (> 50 nm). Perlite has a sponge-like alveolar structure, providing sufficient space for the growth of zeolite crystals.

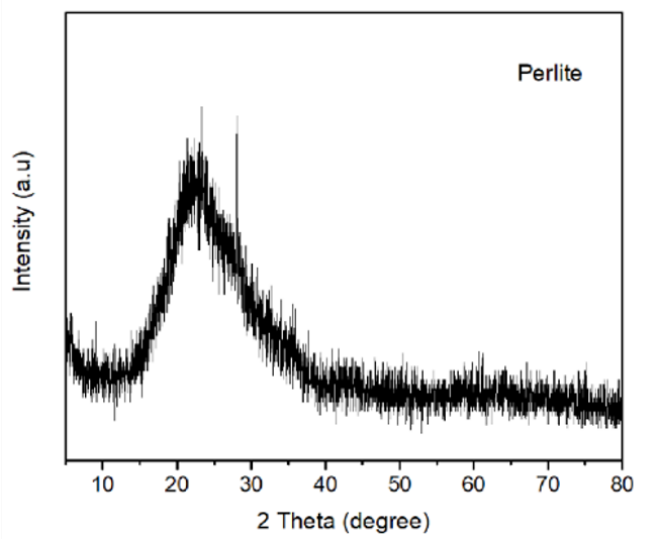

Figure 5.4 XRD pattern of perlite.

At the same time, the resulting of XRD pattern (Figure 5.4) is consistent with XRF data. The main constituent of perlite is amorphous silica.

Perlite chemical composition is presented was analyzed using XRF spectroscopy (Table 5.1). The major components present in perlite were SiO_2 (78.0 wt%). In addition, it contains a variety of metal oxides: Al_2O_3 (11.7 wt%), K_2O (3.5 wt%), Fe_2O_3(1.3 wt%), Na_2O (3.9 wt%), CaO (0.9 wt%), TiO_2 (0.4 wt%) and MgO (0.2 wt%). It appears that aluminum content is much higher than other elements. Likewise, the XRD pattern (Figure 5.4) is consistent with XRF data. The main constituent of perlite is amorphous silica.

Table 5.1 Chemical composition of perlite determined by XRF.

Oxide	SiO_2	Al_2O_3	K_2O	Fe_2O_3	Na_2O	CaO	TiO_2	MgO
Content (wt%)	78.0	11.7	3.5	1.3	3.9	0.9	0.4	0.2

The textural and structural properties of Silicalite-1 sample were also characterized. Figure 5.5 presents the SEM image (Figure 5.5 (a)) and the XRD pattern (Figure 5.5 (b)) of Silicalite-1. Silicalite-1 crystals exhibit hexagonal nanoparticles structure, with a size of 250 nm. XRD pattern proved that Silicalite-1 zeolite is highly crystalline, being consistent with typical MFI structure with two main peaks between 2θ = 7°-10° and three peaks between 2θ = 23°-25°. Likewise, Table 5.2 shows that Silicalite-1 sample exhibits a high specific surface area (381 m^2 g^{-1}), which may provide active sites and fast transport rate for the reactants and products.

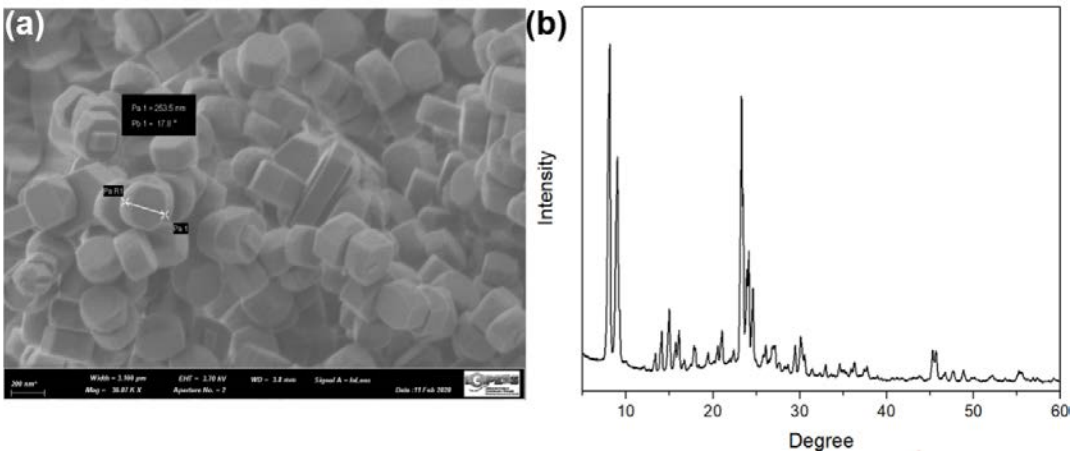

Figure 5.5 (a) SEM image and (b) XRD pattern of Silicalite-1 zeolite.

Silicalite-1 zeolite exhibits a mild acidity due to the absence of Al in the framework. However, a mild acidity can reduce the formation of heavy hydrocarbons in the pores, which may increase the catalyst life-time. However, due to the absence of strong acid sites, the catalytic activity of Silicalite-1 remained low, being limited to 4-5 % methanol conversion (Figure 5.6).

NH_3-TPD further confirmed the weak acidity of Silicalite-1 zeolite, as shown in Figure5.12. Compared with ZSM-5/Perlite catalysts, the position of silicalite-1 desorption peak appeared at low temperature (242 ^oC), and the peak intensity diminished sharply. Hence, in order to obtain high stability and elevated light olefins selectivity, the presence of strong acid sites is suitable for the MTO reaction. It is important to mention here that perlite alone did not convert methanol.

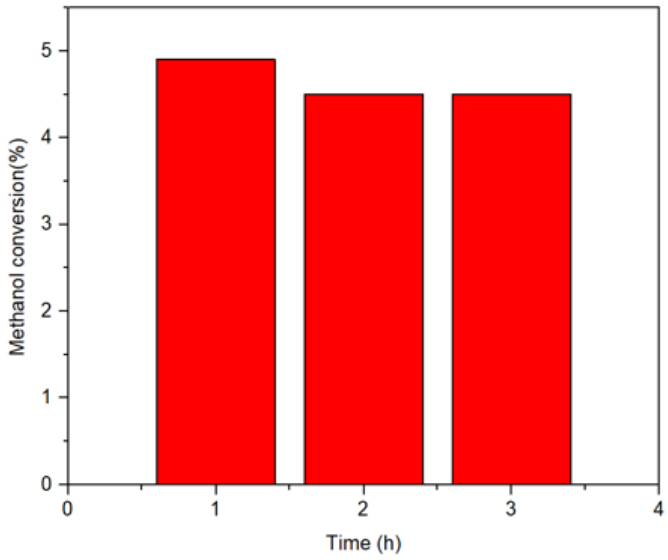

Figure 5.6 Methanol conversion as a function of time on stream over Silicalite-1.

5.3.2 Characterization and performance of ZSM-5/Perlite catalysts

5.3.2.1 Influence of the perlite particle size

In order to systematically study the influence of perlite on the catalytic performance of ZSM-5 / Perlite composites, perlite with different particle sizes was used. The particle sizes of perlite *a*, *b* and *c* were 4-3 mm, 3-1.5 mm, and 0.5-1.5 mm, respectively.

Figure 5.7 shows the XRD patterns of ZSM-5/*1-a, b, c*-Perlite composites. The characteristic peaks of all ZSM-5 / Perlite composites proved that the three samples exhibited the MFI topology. However, a decreasing peak intensity of ZSM-5/*1-a, b, c*-Perlite composites

with respect to pristine ZSM-5 assessed an influence of perlite addition.

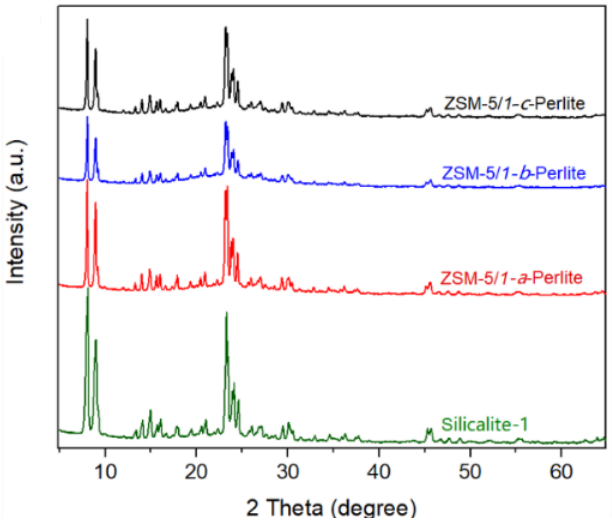

Figure 5.7 XRD patterns of Silicalite-1 and ZSM-5/*1-a, b, c*-Perlite composites.

Nitrogen adsorption-desorption measurements have been performed over shaped perlite beads (Figure 5.8). The latter isotherms were all of type I according to the IUPAC classification, isotherms with a small hysteresis loop, which indicate that samples have high microporosity and inter-crystal mesoporosity possibly related to the aggregation of the crystals and pores in perlite.

Furthermore, it appears from N_2 adsorption-desorption isotherm, the presence of a hysteresis loop at relative pressures higher than $P/P_0 > 0.4$, indicating also the presence of mesopores. The analysis of textural properties showed that both specific surface areas and microporous areas followed the order ZSM-5/*1-a*-Perlite < ZSM-5/*1-b*-Perlite < ZSM-5/*1-c*-Perlite (Table 5.2). Those results are in line with an increase in the zeolite loading onto perlite support.

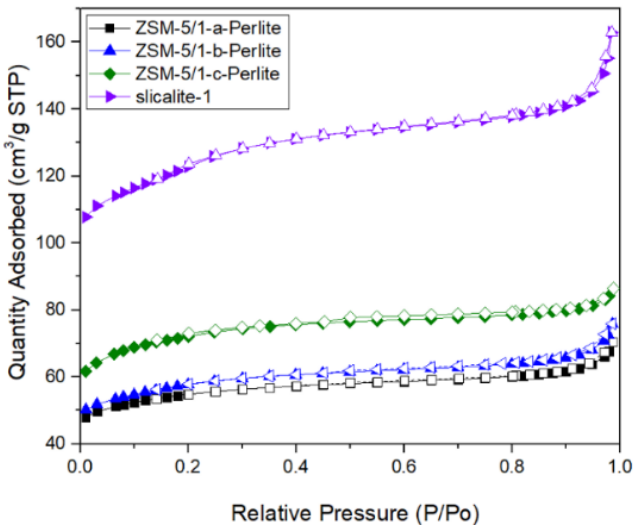

Figure 5.8 N_2 adsorption-desorption isotherms of Silicalite-1 and ZSM-5/*1-a, b, c*-Perlite composites.

Table 5.2 Textural properties of the samples determined by N_2 adsorption / desorption measurements at -196°C.

Samples	S_{BET} (m^2/g)	S_{Micro} (m^2/g)	V_{Total} (cm^3/g)	V_{micro} (cm^3/g)	Amount of zeolite coating (%)[a]
Perlite	1	-	-	-	-
Silicalite-1	404	261	0.233	0.127	-
ZSM-5/1-a-Perlite	179	126	0.102	0.062	40
ZSM-5/1-b-Perlite	189	125	0.109	0.061	60
ZSM-5/1-c-Perlite	236	163	0.128	0.079	68
ZSM-5/2-c-Perlite	138	91	0.081	0.045	37
ZSM-5/3-c-Perlite	108	76	0.067	0.037	13

[a] determined by mass difference after and prior to the hydrothermal synthesis

ZSM-5 / *1-c*-Perlite exhibits the highest specific surface area (236 m^2 g^{-1}). The slight

differences observed in the micropore volume and average pore width of ZSM-5/*1-a, b, c*-Perlite catalysts may be due to differences in the perlite sizes. Besides, the loading of ZSM-5 on *b* and *c*-Perlite was similar, about 0.6 g. For ZSM-5 /*1g-a*-Perlite, the loading was slightly lower, being approximately 0.4 g zeolite. This difference may be due to the specific surface area of perlite. Large particle sizes generally led to lower surface areas, thus inducing a lower amount of material coated on perlite.

Figure 5.9 presents the SEM images of ZSM-5/1-*n*-Perlite samples. According to Figures 5.9 (a-c), it can be observed that ZSM-5 crystals uniformly covered the surface of perlite particle. Moreover, it is worthy to mention that all samples exhibited a high homogeneity and the same morphology.

Figure 5.9 (d) shows the morphology of ZSM-5 crystals on perlite. ZSM-5 crystals exhibit a clear microstructure of a six-prism, having a particle size of nearly 150-200 nm, being the same as Silicalite-1 material. This result means that hydrothermal synthesis of the zeolite was not significantly influenced by perlite addition whatever its size and quantity. Meanwhile, a closer look at higher magnification (Figures 5.9 (d-e)) confirmed that zeolite crystals mainly grew on the perlite surface rather than simply mixing, meaning that the latter crystals were stabilized and probably covalently bonded to the perlite surface.

Furthermore, Figures 5.9 (d) and (e) show that as-obtained ZSM-5 crystals are *b*-oriented and build a chain-like superstructure perpendicularly to the perlite surface, having few microns in length. It has already been reported that *b*-oriented ZSM-5 crystals led to higher permeation properties in membrane applications [19]. It appears therefore that our strategy consisting of converting the external part of perlite support, acting as a reservoir of Al (and Si) nutrients, induced support self-transformation at the interface [20], leading to peculiar zeolite crystal growth.

A tailorable growth of zeolite crystals in a peculiar direction has already been achieved

using covalent linkers or proteins [23-25] to guide the assembly of zeolite crystals. However, we were here able to successfully demonstrate that zeolite nanocrystals can, by themselves, build a regular chain-like structure without any linker use. This is a meaningful finding since such specific growth and orientation usually lead to specific properties[160]. Ma *et al.* [160]reported that TPAOH and the scaffold created synergistic interactions, inducing the self-assembly of inorganic precursors into three-dimensional *b*-oriented MFI superstructures. SEM / EDX analysis (Table 5.3) confirms that using perlite as Al source led to its introduction within as-grown zeolite crystals.

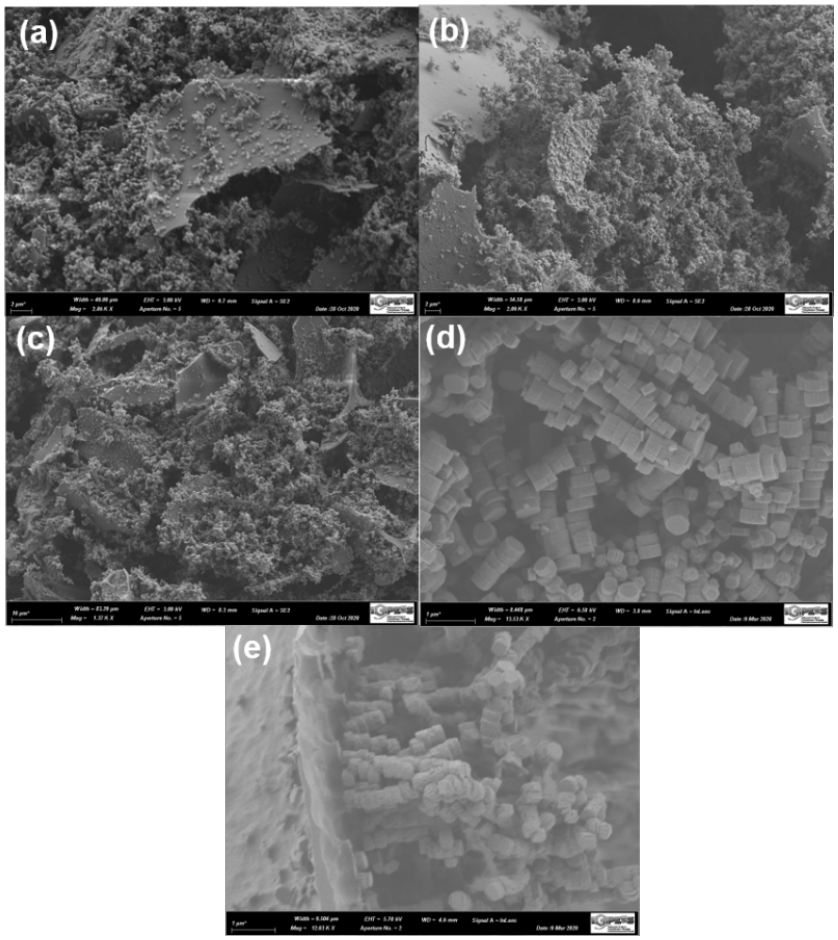

Figure 5.9 SEM micrographs of (a) ZSM-5/*1-a*-Perlite, (b) ZSM-5/*1-b*-Perlite, (c) ZSM-5/*1-c*-Perlite, higher magnification (d) ZSM-5 on the surface of perlite, (e) showing the interface between ZSM-5 crystal and perlite.

The catalytic performance of the three ZSM-5/1-*a*, *b*, *c*-Perlite samples were evaluated at 475 °C (Figure 5.10 (a)). During the MTO reaction, the conversion of methanol over the samples was close to 100% after 2 h on stream, which is by far higher than over Silicalite-1. So, the presence of Al provided the necessary acidity to the zeolite for performing efficiently the reaction. The methanol conversion over ZSM-5/1-*a*-Perlite and ZSM-5/1-*b*-Perlite showed a slight decrease after 6 h. In contrast, ZSM-5/1-*c*-Perlite exhibited a longer catalyst life-time. The catalyst life-time obtained at 100% methanol conversion over the later catalyst was approximately 14 h. Such stability is higher than the one observed over benchmark ZSM-5 catalysts at the same WHSV value, provided by Zeolyst (CBV3024) or home-made, exhibiting 15 < Si / Al < 25, which already exhibited a methanol conversion < 98% after 10h on stream. [27]

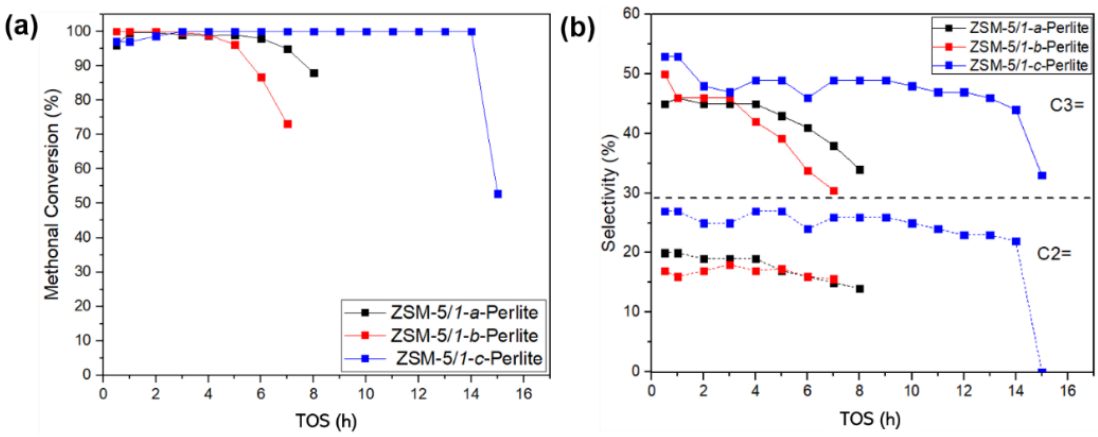

Figure 5.10 (a) Methanol conversion, (b) Ethylene and propylene selectivities in the MTO process at 475 °C over ZSM-5/1-*n*-Perlite (*n*=*a*, *b*, *c*) samples.

Figure 5.10 (b) shows the selectivities towards ethylene and propylene over those catalysts, respectively. It is important to highlight here that all catalysts demonstrated initial high propylene selectivity, ranging from 45 to 53 %. Especially for ZSM-5/1-*c*-Perlite, the highest propylene and ethylene selectivities were achieved, being 53 % and 27 %, respectively. In acid catalysis, the deactivation of the zeolite can be generally attributed to coke deposition

due to the formation of aromatics during the reaction. However, in this study the loading of ZSM-5 catalyst and contact time between the catalyst and the methanol in fixed-bed were closely related to the catalytic performance[161]. Large particles led to greater accumulation in the pores in the reactor, as shown in Figure 5.11, which may cause the methanol to flow too fast in the reactor and fail to insure a proper contact with the catalyst. Hence, this may also lead to diminish methanol conversion.

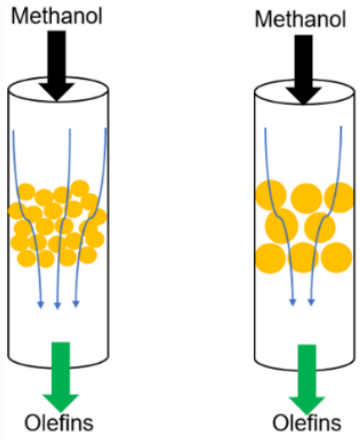

Figure 5.11 Scheme of the MTO process at 475 °C over ZSM-5/1-*n*-Perlite (*n=a, b, c*) samples.

5.3.2.2 Influence of the quantity of perlite

An increasing addition of perlite may improve the yield in light olefins over ZSM-5 / *n-x*-Perlite catalysts. Hence, 1, 2 or 3 g perlite were respectively added during the synthesis of the zeolite. Considering that ZSM-5/*n-c*-Perlite allowed achieving prominent light olefins selectivity, this sample was selected to explore the effect of perlite addition on the MTO reaction. Figure 5.12 (a) shows that all ZSM-5/ *n-c*-Perlite (*n*=1, 2, and 3 g) samples exhibited the MFI structure, meaning that the addition of perlite did not influence the formation of the zeolite. However, with a higher amount of perlite, the peak of amorphous silicon (2θ =23°) gradually increased. This is directly related to the content of amorphous silica in the perlite. In addition, the strength of the characteristic peak diminished while enhancing the perlite amount.

Figure 5.12 (b) also highlights that ZSM-5/*1*, *2*-*c*-Perlite catalysts exhibited weaker acid sites than ZSM-5/*3*-*c*-Perlite, which mainly relates to the low content of ZSM-5 in the composite catalyst. In contrast to the other samples, ZSM-5/*2*-*c*-Perlite exhibited two kinds of acidity patterns. A low ammonia desorption peak at 311°C and a high temperature one at 536 °C, corresponding to weak and strong acidity, respectively.

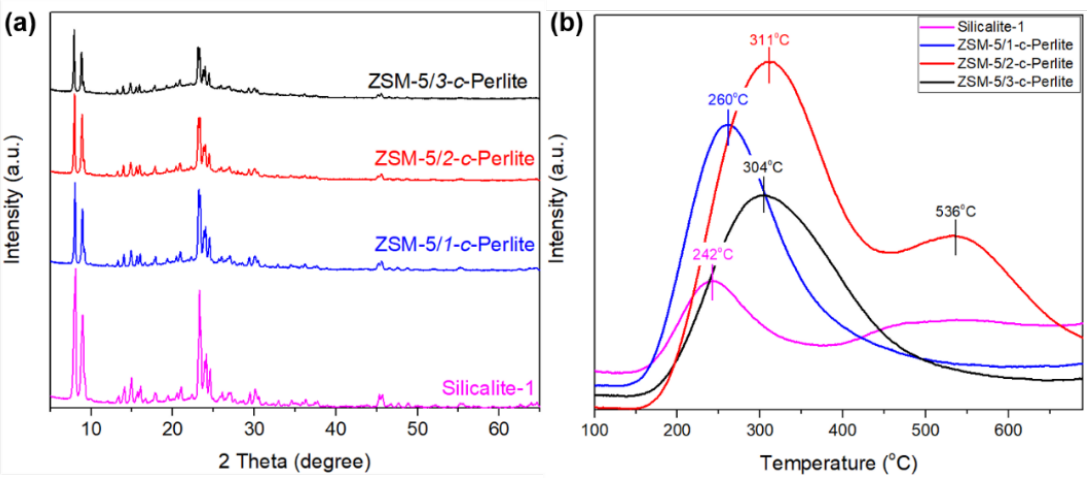

Figure 5.12 (a) XRD patterns and (b) NH_3-TPD profiles of ZSM-5/*x*-c-Perlite (*x*=1, 2, and 3).

At the same time, the unit load of ZSM-5 on perlite diminished while increasing the perlite content. The unit load of ZSM-5/*1*, *2*, *3*-*c*-Perlite was 60, 38 and 13 %, respectively. The reason can be due to uneven mixing between solution and perlite particles, since sponge-like structure of perlite make them floating in the precursor solution. At the same time, the specific surface area also changed according to the same trend, from 236 down to 108 m^2 g^{-1}. It is worthy to mention here that the quantity of zeolite coating onto perlite led to approximately the same loadings based on BET surface area calculations (Table 5.3).

Table 5.3 Elemental composition of ZSM-5/ x-c-Perlite catalysts obtained from EDS spectra coupled with the SEM.

Elements	Atomic (%)		
	ZSM-5/1-c-Perlite	**ZSM-5/2-c-Perlite**	**ZSM-5/3-c-Perlite**
O	59.3	58.6	49.2
Al	1.6	1.5	1.4
Si	33.6	27.1	24.2
K	4.4	12.5	14.2
Na	0	0	0.3

Figure 5.13 (a) shows that methanol conversion profiles yielded significant differences among ZSM-5/*1*,*2*-c-Perlite and ZSM-5/*3*-c-Perlite. Compared with ZSM-5/*3*-c-Perlite, ZSM-5/*1*-c-Perlite and ZSM-5/*2*-c-Perlite exhibited longer catalyst life-time and higher selectivity towards light olefins (Figure 5.13 (b)). There was a slight decrease in propylene selectivity over ZSM-5/*2*-c-Perlite, compared to ZSM-5/*1*-c-Perlite. Ethylene selectivity remained similar over ZSM-5/*1-c*-Perlite and ZSM-5/*2-c*-Perlite catalysts. Obviously, when the loading of ZSM-5 on perlite was superior to 36 %, no significant effect on methanol conversion could be observed. Nevertheless, when the loading of ZSM-5 was too low, like ZSM-5/*3*-c-Perlite (13 %), the catalytic performance in the MTO reaction was dramatically affected.

It is noteworthy that the peak intensity of the stronger acid sites is much lower than that of the weak acid sites. Compared with literature reports, low-silica ZSM-5 zeolites (Si/Al ratio < 30) having a low proportion of strong acid sites appeared quite unusual.[162]

Our findings may therefore be attributed to the presence of heteroelement, leached out from the perlite, to the ZSM-5 zeolite (Table 5.3).[163, 164] Indeed, EDX analysis coupled with the SEM chamber assessed the presence of K element in the zeolite. The high content of

perlite and low unit load of ZSM-5 zeolite of ZSM-5/*3*-*c*-Perlite may be the reason of high percentage of K, thus leading to the decrease in the acidity. Hence, the latter acidity of ZSM-5/Perlite catalysts was therefore governed by a combination of aforementioned factors.

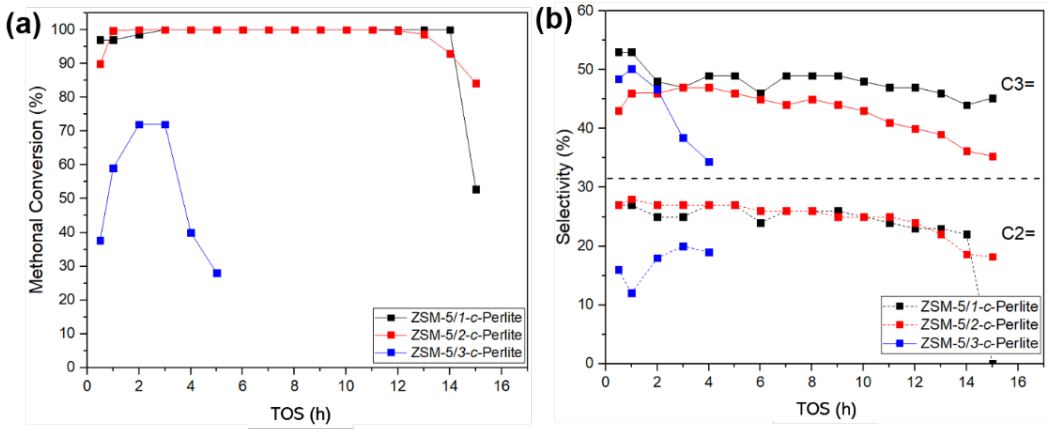

Figure 5.13 (a) Methanol conversion versus time on stream in the MTO at 475 °C over ZSM-5/*x*-*c*-Perlite (*c*=1, 2, 3) samples, (b) Ethylene and propylene selectivities.

5.3.2.3 Influence of the reaction conditions

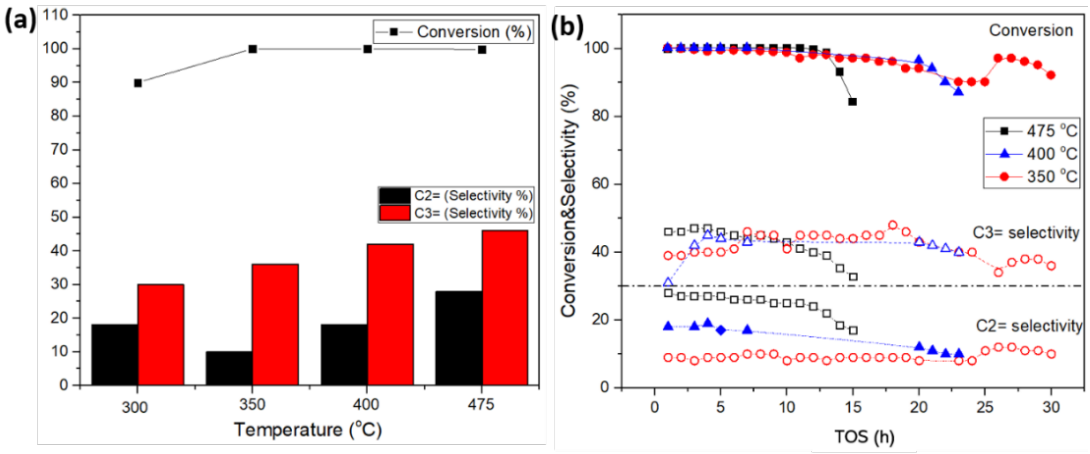

Figure 5.14 (a) Conversions and selectivities achieved over ZSM-5/*2*-*b*-Perlite catalyst in the MTO after 1 h on stream, WHSV = 2 h^{-1}, (b) Methanol conversion, Ethylene and propylene selectivities versus time on stream at 350 °C (red), 400 °C (blue) and 475 °C (black).

The catalytic performance of as-prepared catalysts was also investigated at different temperatures, ranging from 300 to 475 °C. As shown in Figure 5.14 (a), the methanol

conversion over ZSM-5/*2*-*c*-Perlite reached 90% at 300°C. When the reaction temperature was increased to 350 ºC, a full methanol conversion could be observed. These results confirm the high intrinsic activity of ZSM-5/*2*-*c*-Perlite catalyst. With a further raise in the temperature, the conversion remained stable (100%). At the same time, the selectivity towards ethylene gradually increased, while the selectivity in propylene remained stable. The global selectivities towards $C_2^=$ and $C_3^=$ at 350, 400 and 450 were 46%, 60% and 74%, respectively.

Compared with methanol conversion at different temperatures, the life-time of ZSM-5/*2*-*c*-Perlite catalyst was negatively correlated with temperature (Figure 5.14(b)). At 350 ºC, the methanol conversion did not show significant decline during 30 h on stream. In stark contrast, the life-time of ZSM-5/*2*-*c*-Perlite diminished to 20 h and 12 h on stream at 400 °C and 475 ºC, respectively. In the early stages of the reaction, the selectivity in propylene showed a slight growth at 350°C and 400 ºC. At 350 ºC, the highest selectivity of propylene reached 47 %, being stable for a long time. The dramatic loss in activity at high temperature (475 ºC) is usually associated to the formation of large amounts of coke deposits in the pores. Hence, the low temperature reaction appeared beneficial for improving the catalyst life-time.

Further experiments were conducted to understand the performance of ZSM-5/*2*-*b*-Perlite catalyst at different space velocities (2, 8 and 12 h^{-1}). At all space velocities, ZSM-5/*2*-*b*-Perlite exhibited an excellent MTO performance. As shown in Figure 5.15 (a), even at a space velocity up to 12 h^{-1}, methanol was almost completely converted at 350 ºC, and the selectivity in $C_2^=$-$C_3^=$ reached 38%. With an increase in the reaction temperature or a decrease in the space velocity, ZSM-5/*2*-*b*-Perlite yielded higher catalytic activity.

Furthermore, at 400 ºC and high space velocity (8 h^{-1}), as shown in Figure 5.15 (b), ZSM-5/*2*-*b*-Perlite still demonstrated a long catalyst life-time, while keeping the methanol conversion above 95% for 8 h. The selectivity towards propylene showed a slight increase during the reaction, raising from 27% to 38% after 4 h on stream and then remaining stable

during 8 h. At high WHSV, the presence of macropores in the perlite may increase the reaction intermediates and products diffusion in this composite catalyst to yield more light olefins as already observed by Lee *et al.* [162]

Table 5.4 provides a summary of the results presented herein as well as recent reports dealing with ZSM-5 coatings or chemically modified catalysts for the MTO reaction. Compared to the simple synthesis procedure reported in our study, the listed catalysts required rather complex pre-treatments or additional modification steps. The MTO results reached by ZSM-5/*2*-*b*-Perlite, synthesized from green source and avoiding the cationic exchange step, remains highly competitive compared to traditional catalysts.

To summarize, we were able to design ZSM-5/Perlite catalysts able to selectively convert methanol into light olefins. Those results are in line with former studies on similar catalytic systems from Wang *et al.* able to efficiently enhance the FCC naphtha aromatization reaction. However, the robustness of our strategy relies on avoiding the cationic exchange step (since no external Al source was used as $NaAlO_2$).

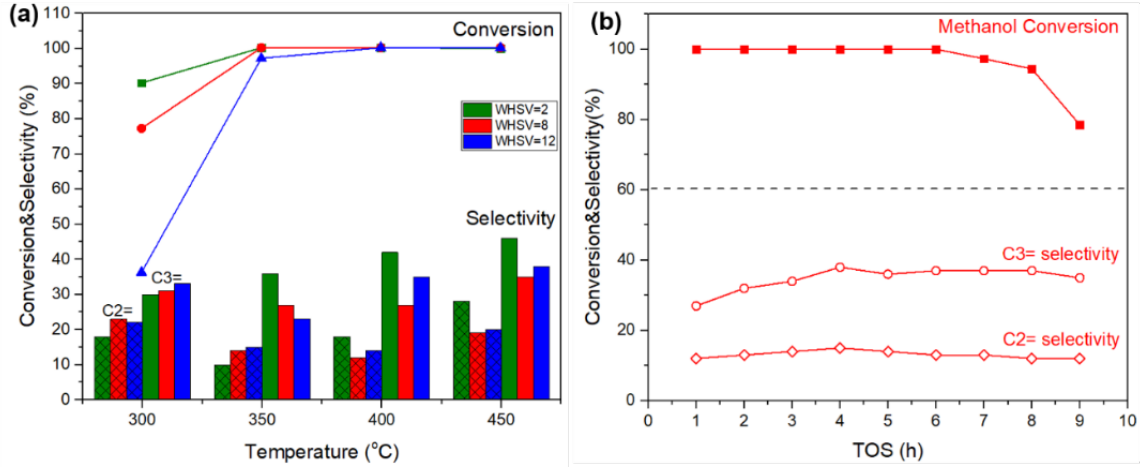

Figure 5.15 (a) Conversions and selectivity achieved over ZSM-5/*2*-*b*-Perlite catalyst in the MTO at different temperatures after 1 h on stream, WHSV=2 h^{-1} (green), 8 h^{-1} (red) and 12 h^{-1} (blue), (b) Methanol conversion, Ethylene and propylene selectivities versus time on stream in the MTO at 400 °C (WHSV=8 h^{-1}).

Table 5.4 Summary of the MTO performance for ZSM-5 catalysts at different conditions.

Sample	WHSV (h^{-1})	Reaction temperature (°C)	Conversion (%)	Selectivity (%)	Ref
ZSM-5/*2-b*-Perlite	2	350	100	$C^{2=}$ 10 $C^{3=}$ 36	This work
		400	100	$C^{2=}$ 18 $C^{3=}$ 42	
		475	100	$C^{2=}$ 28 $C^{3=}$ 46	
	8	350	100	$C_2^=$ 14 $C_3^=$ 27	
		400	100	$C_2^=$ 12 $C_3^=$ 27	
		475	100	$C_2^=$ 19 $C_3^=$ 35	
ZSM-5 (Polyurethane Sponge)	2.55	400	100	$C_2^=$ 12 $C_3^=$ 24	[162]
	2.5	350	~90	$C_2^=$ ~20 $C_3^=$ ~10	
	8	350	~52	$C_2^=$ ~18 $C_3^=$ ~18	
SS-fiber@HZSM-5	5	450	100	$C_2^=$ ~11 $C_3^=$ ~43	[165]
ZSM-5/SiC foam composite	4.4	500	100	$C_3^=$ ~35	[166]
GaZSM-5 treated with 0.2 M NaOH	10	320	99	$C_2^=$ ~12 $C_3^=$ ~17	[167]
SnZSM-5 (Si/Sn=200)	5	450	100	$C_2^=$ ~9.8 $C_3^=$ ~42	[161]
ZSM-5 treated by NaOH/H_3PO_4	3	450	~98	$C_3^=$ 23	[162]

5.4 Conclusion

In addition to the zeolite crystals' successful growth on perlite support, our synthesis strategy induced successful aluminum transfer from perlite into the zeolite crystals. ZSM-5/*x*-*n*-Perlite composite did not only exhibit the advantages of easy handling (recovery) and low pressure drop, but also demonstrated excellent catalytic activity. Under commonly used MTO reaction conditions (475 ^{o}C, WHSC=2 h^{-1}), ZSM-5/*1*-*c*-Perlite composite allowed achieving the longest catalyst lifetime (14 h) and the highest C_2-C_4 light olefins selectivity (80 %). An exceptional 53% selectivity towards propylene was reached, competing with the best values reported to date for ZSM-5 zeolites. Surprisingly, this composite catalyst also demonstrated excellent catalytic performance at low temperature and high space velocity (up to 12 h^{-1}). ZSM-5/*2*-*c*-Perlite exhibited a life-time of up to 30 h at 350 ^{o}C. Meanwhile, the selectivity in propylene reached 46%. These promising catalytic properties did not only benefit from the three-dimensional skeleton structure of expanded perlite, but also were closely related to the dissolution of potassium from perlite.

Chapter 6. General conclusions and future prospects

6.1 Conclusions

In this Thesis, the modification and structuring of ZSM-5 zeolites were investigated. Among them, the purpose of modification of zeolite is to prolong the catalytic lifetime, which was achieved by intruding biochars to optimize the structure and acidity of the zeolite. The experiments of this subject were detailed in Chapter 3 and Chapter 4, including the nature of biochar screening and parameters optimization. In addition, a new kind of structured ZSM-5 zeolite coatings was presented in Chapter 5. The innovation of this zeolite catalyst structuration relied on the first-time use of perlite, being a cheap and stable nature mineral as a support.

Firstly, the type of biochar led to different effects on the modification of the zeolite. Characterization results showed that biochars derived from different types of biomasses (Grass, Algae, Tea and Lignin), yielding significant differences in their microstructure, particle size, functional groups and chemical composition. Compared with other biochars, Grass-C and Algae-C exhibited porous structures, smaller and uniform particle sizes, and the presence of more hydrophilic groups and heteroelements. Compared with H-ZSM-5, Tea-C/ZSM-5 and Lignin-C/ZSM-5, the zeolites modified by Grass-C and algae-C showed higher external specific surface areas and lower acidities. In addition, the lifetime of ZSM-5 zeolite with Algae-C, Grass-C was significantly longer than that of H-ZSM-5, Tea-C/ZSM-5, and Lignin-C/ZSM-5. This result proved a positively correlated lifetime of the catalyst with its external surface area, but negatively correlated with its acidity. Meanwhile, Grass-C and Algae-C were selected as effective hard templates for the next research. A related specific discussion was presented in Chapter 4. After completing the biochar screening, this study further allowed to optimize the properties of Grass-C/ZSM-5 and Algae-C/ZSM-5 zeolites (Chapter 3).

After completing the biochar screening, the properties of Grass-C/ZSM-5 and Algae-C/ZSM-5 zeolites as a function of different parameters of synthesis and catalysis were further

studied in Chapter 4. These parameters included the addition amount of grass carbon and algal carbon, synthesis time, Si/Al ratio and reaction temperature. The results showed that the understanding of the influence of the addition of biochars on the zeolite was rather complicated. With an increase in biochar amount, the ESA of the zeolite was improved, its acidity became weaker, and its microporous structure was partially destroyed. With a proper tailoring of biochar addition, the performance of the zeolite could be improved. This phenomenon further demonstrated the direct correlation between biochar addition and changes induced in zeolite physicochemical properties. In addition, Si/Al ratio and catalytic temperature could impact the catalytic activity of the zeolite. Low Al content means less acidic sites, which led to a decrease in methanol conversion capacity and a slower deactivation rate. Likewise, lower reaction temperature also yielded a similar behavior. This result proved that the catalytic activity is strongly correlated to the zeolite acidity and reaction temperature. Unfortunately, high activity also leads to faster coking rate and therefore catalyst deactivation.

In addition, by comparing the effects Algae-C, acid-treated Algae-C and hydrophobic carbon black on zeolite, it was shown that the presence of numerous hydrophilic functional groups and heteroelements in biochar led to a positive effect on the catalytic performance. This property could not be observed in conventional carbon-based hard templates.

In order to solve the problems in the application of zeolite powders, a new kind of monolithic zeolite structured catalyst was studied in Chapter 5. This monolithic zeolite involved the use of perlite, a natural mineral, as a carrier material. The aluminum present in perlite could be successfully used as a raw Al source providing the acidity to the zeolite. This method presents the advantages of environmental friendliness and low cost. Moreover, the abundant heteroelements in perlite also contributed to tune the acid strength of the zeolite. ZSM-5/perlite composites did not present the advantages of easy catalyst recycling and low pressure drop, but also yielded an excellent catalytic activity. Under the reaction conditions

commonly used in the MTO reaction, the ZSM-5/Perlite composite achieved the longest catalyst lifetime (14 h) and the highest selectivity to C_2-C_4 olefins (80%). An exceptional selectivity of 53% towards propylene was achieved, rivaling the best values reported to date for ZSM-5 zeolites powder. Surprisingly, this composite catalyst also demonstrated excellent catalytic performance at low temperature and high space velocity. ZSM-5/Perlite presented a lifetime of up to 30 h at 350°C. Meanwhile, the selectivity of propylene achieved 46%. These promising catalytic properties not only benefited from the three-dimensional skeletal structure of expanded perlite, but were also closely related to the dissolution of the heteroelements from the perlite.

For the biochar modification method, the importance of hydrophilicity of hard template (biochar) is demonstrated to increase the external surface area of zeolite under the hydrothermal condition. Besides, increasing the ESA as well as reducing the acidity and density of Brønsted acid sites was key parameters for prolonging the catalyst's life. In addition, the performance of zeolite was also affected by the synthesis protocol and operating MTO conditions. For the perlite modification method, it confirms that it is feasible to use a natural porous mineral containing silicon and aluminum as a carrier and aluminum source. Perlite/ZSM-5 zeolite still showed suitable acidity even without introduction of additional aluminum source, and it presents excellent catalytic performance in MTO reaction. In general, these results proved that the idea of modifying zeolite properties while using natural or waste materials is feasible. Adhering to the synthesis concept of environmental friendliness and low cost, the obtained modified zeolite exhibited catalytic performance far exceeding the one of an unmodified sample. These results serve therefore as a foundation for subsequent studies based on waste-modified zeolites.

6.2 Perspectives

Dealing with this MTO reaction which has a research history of nearly five decades, the

research on MTO process has achieved fruitful results. It covers catalyst screening, design, optimization, process improvement, and now the exploration of reaction mechanisms relying on advanced characterization techniques.

At present, due to the increasing demand for light olefins in industry, the catalytic performance of zeolite is required to be higher and higher. Further reducing the synthesis cost and reducing the pollution during the synthesis process are the basic principles of zeolite production. In addition, optimizing product selectivity, improving reaction efficiency, and extending catalytic lifetime are the goals of next-generation catalyst development. In addition, in response to the diverse demands of the international olefins market, there is an urgent need to control selectivity for the development of processes such as MTE (methanol-to-ethylene) and MTP (methanol-to-propylene).

Furthermore, although numerous studies have made great contributions to the mechanistic findings of the MTO reaction, still mysteries remain unsolved. Those include: the formation path of the first C-C bond at the early stage of the reaction, the nature of the hydrocarbon pool species, etc. The exploration of these peculiarities can facilitate the directional design of new generation catalysts to improve the catalytic performance and reduce coke production.

In addition, the research and development of practical application process is also crucial, and the problems it brings are more complicated. Including the scale-up of zeolite synthesis process, powder structuring or granulation, and reaction process and reactor design. In actual industrial applications, more difficulties and challenges will arise.

References

[1] D. Breck, J. Smith, Scientific American, **200** (1959) 85.
[2] C. Colella, A.F. Gualtieri, Microporous and Mesoporous Materials, **105** (2007) 213.
[3] N. Kosinov, J. Gascon, F. Kapteijn, E.J.M. Hensen, Journal of Membrane Science, **499** (2016) 65.
[4] B. Yue, S. Liu, Y. Chai, G. Wu, et al., Journal of Energy Chemistry, **71** (2022) 288.
[5] L. Pauling, Proceedings of the National Academy of Sciences, **16** (1930) 453.
[6] J.V. Smith, Zeolites, **4** (1984) 309.
[7] N. Eroglu, M. Emekci, C.G. Athanassiou, Journal of the Science of Food and Agriculture, **97** (2017) 3487.
[8] Y.T. Tran, J. Lee, P. Kumar, K.-H. Kim, et al., Composites Part B: Engineering, **165** (2019) 354.
[9] L.J. Spencer, Annual Reports on the Progress of Chemistry, **20** (1923) 261.
[10] G.W. Morey, W.T. Chen, American Mineralogist, **40** (1955) 996.
[11] A. Rabenau, Angewandte Chemie International Edition in English, **24** (1985) 1026.
[12] P. Bai, U.J. Etim, Z. Yan, S. Mintova, et al., Catalysis Reviews, **61** (2019) 333.
[13] R.M. Barrer, Journal of the Chemical Society (Resumed), (1948) 2158.
[14] M. Faustini, L. Nicole, E. Ruiz-Hitzky, C. Sanchez, Advanced Functional Materials, **28** (2018) 1704158.
[15] J.A. Rabo, M.W. Schoonover, Applied Catalysis A: General, **222** (2001) 261.
[16] G.T. Kerr, Inorganic Chemistry, **5** (1966) 1537.
[17] G.T. Kerr, G.T. Kokotailo, Journal of the American Chemical Society, **83** (1961) 4675.
[18] R. L. Wadlinger, G. T. Kerr, E. J. Rosinski, United States Patent OfficeUnited States, 1967.
[19] S.T. Wilson, B.M. Lok, C.A. Messina, T.R. Cannan, et al., Journal of the American Chemical Society, **104** (1982) 1146.
[20] J. Landers, G.Y. Gor, A.V. Neimark, Colloids and Surfaces A: Physicochemical and Engineering Aspects, **437** (2013) 3.
[21] R. Gans, Jahrb. Preuss. Geol. Landesanstalt, **26** (1905) 1905.
[22] R. Gans, Jahrb. Preuss. Geol. Landesanstalt, **27** (1906) 63.
[23] R. Millini, G. Bellussi, RSC Catalysis Series, **28** (2017) 1.
[24] J.D. Sherman, Proceedings of the National Academy of Sciences, **96** (1999) 3471.
[25] W. Vermeiren, J.P. Gilson, Topics in Catalysis, **52** (2009) 1131.
[26] R. Millini, G. Bellussi, (2017).
[27] F. Collins, A. Rozhkovskaya, J.G. Outram, G.J. Millar, Microporous and Mesoporous Materials, **291** (2020) 109667.
[28] V. Van Speybroeck, K. Hemelsoet, L. Joos, M. Waroquier, et al., Chemical Society Reviews, **44** (2015) 7044.
[29] J. Li, A. Corma, J. Yu, Chemical Society Reviews, **44** (2015) 7112.
[30] Y. Kamimura, K. Itabashi, T. Okubo, Microporous and Mesoporous Materials, **147** (2012) 149.
[31] Y. He, S. Tang, S. Yin, S. Li, Journal of Cleaner Production, **306** (2021) 127248.
[32] C.S. Cundy, P.A. Cox, Chemical Reviews, **103** (2003) 663.
[33] M. Park, C.L. Choi, W.T. Lim, M.C. Kim, et al., Microporous and Mesoporous Materials, **37** (2000) 91.
[34] M. Król, P. Rożek, D. Chlebda, W. Mozgawa, Solid State Sciences, **94** (2019) 114.
[35] S. Chandrasekhar, P.N. Pramada, Microporous and Mesoporous Materials, **108** (2008) 152.
[36] H. Tanaka, A. Miyagawa, H. Eguchi, R. Hino, Industrial & Engineering Chemistry Research, **43** (2004)

6090.
[37] S. Ma, Z.-P. Liu, Topics in Catalysis, **65** (2022) 59.
[38] C.S. Cundy, P.A. Cox, Chemical reviews, **103** (2003) 663.
[39] G. Demazeau, A. Largeteau, Zeitschrift für anorganische und allgemeine Chemie, **641** (2015) 159.
[40] K. Byrappa, M. Yoshimura, Handbook of hydrothermal technology, (2013) 331.
[41] G. Yang, S. J. Park, Materials (Basel), **12** (2019) 1177.
[42] L. Zhang, S. Xie, W. Xin, X. Li, et al., Materials Research Bulletin, **46** (2011) 894.
[43] S. Z. Patuwan, S. E. Arshad, Materials, **14** (2021) 2890.
[44] C. I. Round, S. J. Hill, K. Latham, C. D. Williams, Microporous Materials, **11** (1997) 213.
[45] S.M. Alipour, R. Halladj, S. Askari, Reviews in Chemical Engineering, **30** (2014) 289.
[46] Z. A. Pour, K.O. Sebakhy, Chemistry, **4** (2022) 431.
[47] Z. Asgar Pour, K.O. Sebakhy, Chemistry, **4** (2022) 431.
[48] O. Cheung, N. Hedin, RSC Advances, **4** (2014) 14480.
[49] A.R. Loiola, J.C.R.A. Andrade, J.M. Sasaki, L.R.D. da Silva, Journal of Colloid and Interface Science, **367** (2012) 34.
[50] K.S. Hui, C.Y.H. Chao, S.C. Kot, Journal of Hazardous Materials, **127** (2005) 89.
[51] O. Eljam, R. Eljam, I. Maamoun, A. Khalil, et al., Chemosphere, **287** (2022) 131990.
[52] M. Jiménez-Reyes, P.T. Almazán-Sánchez, M. Solache-Ríos, Journal of Environmental Radioactivity, **233** (2021) 106610.
[53] E. Han, Y.-G. Kim, H.-M. Yang, I.-H. Yoon, et al., Chemistry of Materials, **30** (2018) 5777.
[54] G. Park, C. Ahn, S. Park, Y. Lee, et al., Applied Catalysis A: General, **607** (2020) 117840.
[55] C. Martínez, A. Corma, Coordination Chemistry Reviews, **255** (2011) 1558.
[56] A. Palčić, V. Valtchev, Applied Catalysis A: General, **606** (2020) 117795.
[57] A. Corma, Journal of Catalysis, **216** (2003) 298.
[58] M. Stöcker, Microporous and Mesoporous Materials, **82** (2005) 257.
[59] E. Koohsaryan, M. Anbia, Chinese Journal of Catalysis, **37** (2016) 447.
[60] S. Mitchell, A.B. Pinar, J. Kenvin, P. Crivelli, et al., Nature Communications, **6** (2015) 8633.
[61] J. Pérez-Ramírez, C.H. Christensen, K. Egeblad, C.H. Christensen, et al., Chemical Society Reviews, **37** (2008) 2530.
[62] R. Srivastava, M. Choi, R. Ryoo, Chemical Communications, (2006) 4489.
[63] J. Kim, M. Choi, R. Ryoo, Journal of Catalysis, **269** (2010) 219.
[64] T. Ennaert, J. Van Aelst, J. Dijkmans, R. De Clercq, et al., Chemical Society Reviews, **45** (2016) 584.
[65] X. Jia, W. Khan, Z. Wu, J. Choi, et al., Advanced Powder Technology, **30** (2019) 467.
[66] D. Kerstens, B. Smeyers, J. Van Waeyenberg, Q. Zhang, et al., Advanced Materials, **32** (2020) 2004690.
[67] S. Mardiana, N.J. Azhari, T. Ilmi, G.T.M. Kadja, Fuel, **309** (2022) 122119.
[68] J.-B. Koo, N. Jiang, S. Saravanamurugan, M. Bejblová, et al., Journal of Catalysis, **276** (2010) 327.
[69] A.H. Janssen, I. Schmidt, C.J.H. Jacobsen, A.J. Koster, et al., Microporous and Mesoporous Materials, **65** (2003) 59.
[70] J.O. Abildstrøm, M. Kegnæs, G. Hytoft, J. Mielby, et al., Microporous and Mesoporous Materials, **225** (2016) 232.
[71] N. Chu, J. Wang, Y. Zhang, J. Yang, et al., Chemistry of Materials, **22** (2010) 2757.
[72] H. Xin, J. Zhao, S. Xu, J. Li, et al., The Journal of Physical Chemistry C, **114** (2010) 6553.
[73] I. Schmidt, A. Boisen, E. Gustavsson, K. Ståhl, et al., Chemistry of Materials, **13** (2001) 4416.
[74] R. Wei, C. Li, C. Yang, H. Shan, Journal of Natural Gas Chemistry, **20** (2011) 261.
[75] L.H. Ong, M. Dömök, R. Olindo, A.C. van Veen, et al., Microporous and Mesoporous Materials, **164** (2012) 9.

[76] C. Sun, Y. Yang, J. Du, F. Qin, et al., Chemical Communications, **48** (2012) 5787.
[77] M. Khanmohammadi, S. Amani, A.B. Garmarudi, A. Niaei, Chinese Journal of Catalysis, **37** (2016) 325.
[78] J. Dedecek, V. Balgová, V. Pashkova, P. Klein, et al., Chemistry of Materials, **24** (2012) 3231.
[79] R.M. Barrer, M.B. Makki, Canadian Journal of Chemistry, **42** (1964) 1481.
[80] T. Pang, X. Yang, C. Yuan, A.A. Elzatahry, et al., Chinese Chemical Letters, **32** (2021) 328.
[81] N. Wang, Y. Zhi, Y. Wei, W. Zhang, et al., Nat. Commun. , **11** (2020) 1079.
[82] Q. Lei, C. Wang, W. Dai, G. Wu, et al., Frontiers of Chemical Science and Engineering, **15** (2021) 1462.
[83] R. Millini, E. Previde Massara, G. Perego, G. Bellussi, Journal of Catalysis, **137** (1992) 497.
[84] X. Li, F. Rezaei, A.A. Rownaghi, Microporous and Mesoporous Materials, **276** (2019) 1.
[85] J. Ding, P. Chen, G. Zhao, Y. Liu, et al., Journal of Catalysis, **360** (2018) 40.
[86] L. Calabrese, Materials, **12** (2019) 59.
[87] H. Deng, H. Zhang, Microscopy Research and Technique, **78** (2015) 918.
[88] R. Cai, Y. Liu, S. Gu, Y. Yan, Journal of the American Chemical Society, **132** (2010) 12776.
[89] R.E. Morris, Chemical Communications, (2009) 2990.
[90] R.E. Morris, P.S. Wheatley, Angewandte Chemie International Edition, **47** (2008) 4966.
[91] I. Amghizar, L.A. Vandewalle, K.M. Van Geem, G.B. Marin, Engineering, **3** (2017) 171.
[92] M. Masih, I. Algahtani, L. De Mello, Energy Economics, **32** (2010) 1435.
[93] A. Farshi, F. Shaiyegh, S.H. Burogerdi, A. Dehgan, Petroleum Science and Technology, **29** (2011) 875.
[94] A. Masudi, N.W.C. Jusoh, O. Muraza, Catalysis Science & Technology, **10** (2020) 1582.
[95] M. Monai, M. Gambino, S. Wannakao, B. M. Weckhuysen, Chemical Society Reviews, **50** (2021) 11503.
[96] N. Rahimi, R. Karimzadeh, Applied Catalysis A: General, **398** (2011) 1.
[97] H. Cai, A. Krzywicki, M.C. Oballa, Chemical Engineering and Processing: Process Intensification, **41** (2002) 199.
[98] A. Yamaguchi, D. Jin, T. Ikeda, K. Sato, et al., Fuel Processing Technology, **126** (2014) 343.
[99] M. Stöcker, Microporous and Mesoporous Materials, **29** (1999) 3.
[100] C.D. Chang, A.J. Silvestri, Journal of Catalysis, **47** (1977) 249.
[101] J. Li, Y. Wei, G. Liu, Y. Qi, et al., Catalysis Today, **171** (2011) 221.
[102] L. Bing, A. Tian, F. Wang, K. Yi, et al., Chemistry – A European Journal, **24** (2018) 7428.
[103] J. Zhong, J. Han, Y. Wei, P. Tian, et al., Catalysis Science & Technology, **7** (2017) 4905.
[104] W. Dai, X. Wang, G. Wu, N. Guan, et al., ACS Catalysis, **1** (2011) 292.
[105] P. Tian, Y. Wei, M. Ye, Z. Liu, ACS Catalysis, **5** (2015) 1922.
[106] H. Koempel, W. Liebner, in: F. Bellot Noronha, M. Schmal, E. Falabella Sousa-Aguiar (Eds.) Studies in Surface Science and Catalysis, Elsevier2007, pp. 261.
[107] M. Bjørgen, S. Akyalcin, U. Olsbye, S. Benard, et al., Journal of Catalysis, **275** (2010) 170.
[108] M. Yang, D. Fan, Y. Wei, P. Tian, et al., Advanced Materials, **31** (2019) 1902181.
[109] S. Xu, Y. Zhi, J. Han, W. Zhang, et al., in: C. Song (Ed.) Advances in Catalysis, Academic Press2017, pp. 37.
[110] S. Wang, Y. Chen, Z. Qin, T.-S. Zhao, et al., Journal of Catalysis, **369** (2019) 382.
[111] I.M. Dahl, S. Kolboe, Catalysis Letters, **20** (1993) 329.
[112] D. Chen, A. Grønvold, K. Moljord, A. Holmen, Industrial & Engineering Chemistry Research, **46** (2007) 4116.
[113] M. Bjørgen, S. Svelle, F. Joensen, J. Nerlov, et al., Journal of Catalysis, **249** (2007) 195.
[114] S. Svelle, F. Joensen, J. Nerlov, U. Olsbye, et al., Journal of the American Chemical Society, **128** (2006) 14770.
[115] M. Wen, X. Wang, L. Han, J. Ding, et al., Microporous Mesoporous Mater., **206** (2015) 8.
[116] G. Qi, Z. Xie, W. Yang, S. Zhong, et al., Fuel Processing Technology, **88** (2007) 437.

[117] J.F. Haw, W. Song, D.M. Marcus, J.B. Nicholas, Accounts of chemical research, **36** (2003) 317.
[118] M. Guisnet, L. Costa, F.R. Ribeiro, Journal of Molecular Catalysis A: Chemical, **305** (2009) 69.
[119] X. Xian, M. He, Y. Gao, Y. Bi, et al., Applied Catalysis A: General, **623** (2021) 118278.
[120] M. Guisnet, P. Magnoux, Catalysis Today, **36** (1997) 477.
[121] M. Guisnet, P. Magnoux, Applied Catalysis A: General, **212** (2001) 83.
[122] K. Egeblad, C.H. Christensen, M. Kustova, C.H. Christensen, Chemistry of Materials, **20** (2008) 946.
[123] S. Standl, O. Hinrichsen, Catalysts, **8** (2018) 626.
[124] U. Olsbye, S. Svelle, M. Bjørgen, P. Beato, et al., Angewandte Chemie International Edition, **51** (2012) 5810.
[125] C.F. Holder, R.E. Schaak, ACS Publications, 2019, pp. 7359.
[126] A.A. Bunaciu, E.G. UdriŞTioiu, H.Y. Aboul-Enein, Critical reviews in analytical chemistry, **45** (2015) 289.
[127] C. Baerlocher, L.B. McCusker, D.H. Olson, Elsevier2007.
[128] M.F. De Lange, T.J. Vlugt, J. Gascon, F. Kapteijn, Microporous and Mesoporous Materials, **200** (2014) 199.
[129] S.A. Khan, S.B. Khan, L.U. Khan, A. Farooq, et al., Handbook of materials characterization, Springer2018, pp. 317.
[130] P. Dugkhuntod, C. Wattanakit, Catalysts, **10** (2020) 245.
[131] T. Wakihara, J. Tatami, Journal of the Japan Petroleum Institute, **56** (2013) 206.
[132] H. Wang, G. Du, J. Jia, S. Chen, et al., Frontiers of Chemical Science and Engineering, **15** (2021) 1444.
[133] M.M. Pereira, E.S. Gomes, A.V. Silva, A.B. Pinar, et al., Chemical science, **9** (2018) 6532.
[134] C. Pagis, A.R. Morgado Prates, D. Farrusseng, N. Bats, et al., Chemistry of Materials, **28** (2016) 5205.
[135] T. Weissenberger, A.G. Machoke, B. Reiprich, W. Schwieger, Advanced Materials Interfaces, **8** (2021) 2001653.
[136] S. Han, Z. Wang, L. Meng, N. Jiang, Materials Chemistry and Physics, **177** (2016) 112.
[137] Y. Tao, M. Endo, K. Kaneko, Journal of the American Chemical Society, **131** (2009) 904.
[138] Y.-Y. Chen, C.-J. Chang, H.V. Lee, J.C. Juan, et al., Industrial & Engineering Chemistry Research, **58** (2019) 7948.
[139] D.-C. Li, H. Jiang, Bioresource Technology, **246** (2017) 57.
[140] S.K. Das, G.K. Ghosh, R. Avasthe, K. Sinha, Journal of Hazardous Materials, **407** (2021) 124370.
[141] P. Liu, L.-N. Jin, C. Jin, J.-N. Zhang, et al., Microporous and Mesoporous Materials, **262** (2018) 217.
[142] M. Yabushita, R. Osuga, A. Muramatsu, CrystEngComm, **23** (2021) 6226.
[143] X. Jiang, X. Su, X. Bai, Y. Li, et al., Microporous and Mesoporous Materials, **263** (2018) 243.
[144] S. Zhang, B. Zhang, Z. Gao, Y. Han, Industrial & Engineering Chemistry Research, **49** (2010) 2103.
[145] H.-G. Jang, H.-K. Min, S.B. Hong, G. Seo, Journal of Catalysis, **299** (2013) 240.
[146] Z. Wan, G.K. Li, C. Wang, H. Yang, et al., Applied Catalysis A: General, **549** (2018) 141.
[147] Y. Yang, C. Sun, J. Du, Y. Yue, et al., Catalysis Communications, **24** (2012) 44.
[148] P. Losch, A.B. Pinar, M.G. Willinger, K. Soukup, et al., Journal of Catalysis, **345** (2017) 11.
[149] H. Schulz, K. Lau, M. Claeys, Applied Catalysis A: General, **132** (1995) 29.
[150] H. Khezri, A. Izadbakhsh, A.A. Izadpanah, Fuel Processing Technology, **199** (2020) 106253.
[151] J. Li, M. Liu, X. Guo, S. Xu, et al., ACS Applied Materials & Interfaces, **9** (2017) 26096.
[152] S. Standl, O. Hinrichsen, Catalysts, **8** (2018) 626.
[153] P. He, J. Ding, Z. Qin, L. Tang, et al., Inorganic Chemistry Frontiers, **7** (2020) 2080.
[154] S. Ivanova, B. Louis, B. Madani, J. Tessonnier, et al., The Journal of Physical Chemistry C, **111** (2007) 4368.
[155] S. Ivanova, E. Vanhaecke, L. Dreibine, B. Louis, et al., Applied Catalysis A: General, **359** (2009) 151.
[156] B. Louis, F. Ocampo, H.-S. Yun, J.-P. Tessonnier, et al., Chemical engineering journal, **161** (2010) 397.

[157] S.H. da Silva Filho, P. Vinaches, S.B. Pergher, Materials Letters, **227** (2018) 258.
[158] M. Kasai, Y. Kobayashi, M. Togo, A. Nakahira, Materials Today, **16** (2019) 232.
[159] P.F. Corregidor, P.M. Cuesta, D.E. Acosta, H.A. Destéfanis, Applied Catalysis A: General, **587** (2019) 117262.
[160] I. Lee, H.-K. Jeong, Microporous and mesoporous materials, **141** (2011) 175.
[161] Y. Xue, J. Li, P. Wang, X. Cui, et al., Applied Catalysis B: Environmental, **280** (2021) 119391.
[162] S. Tanaka, R. Fukui, A. Kosaka, N. Nishiyama, Materials Research Bulletin, **130** (2020) 110958.
[163] Z. Wan, W. Wu, G.K. Li, C. Wang, et al., Applied Catalysis A: General, **523** (2016) 312.
[164] S. Tanizume, S. Maehara, K. Ishii, T. Onoki, et al., Separation and Purification Technology, **254** (2021) 117647.
[165] M. Wen, X. Wang, L. Han, J. Ding, et al., Microporous and Mesoporous Materials, **206** (2015) 8.
[166] Y. Jiao, C. Jiang, Z. Yang, J. Zhang, Microporous and mesoporous materials, **162** (2012) 152.
[167] Z. Han, F. Zhou, J. Zhao, Y. Liu, et al., Microporous and Mesoporous Materials, **302** (2020) 110194.

Acknowledgements

I would like to thank to everyone who helped me during my research and writing of this thesis.

A special acknowledgement should be firstly given to Dr. Benoit Louis. Thank to him for all the care, encouragement and help during these three years. This is invaluable to me who is introverted and not confident enough. Because of his help, my PhD thesis can be successfully completed. I want to give him a warm hug.

Sincere gratitude should be also given to all of people working and studying in R4N1 at the present and in the past. Thank to them for letting me know the kindness and warmth from all over the world. This is extremely precious to my life.

Besides, my warm gratitude is also given to my friends, family, and dear Mr. Chen. Thank to them for giving me strength and courage when I encounter setbacks and challenges in my life.

Finally, I would like to express my gratitude to ICPEES (Institut de chimie et procédés pour l'énergie, l'environnement et la santé) in Université de Strasbourg and my motherland China. Thank to the China Scholarship Council (CSC) for the financial supporting during my PhD study.

ZHANG Yu

Environmental Friendless Approaches to Optimize ZSM-5 Zeolite for MTO Reaction

Résumé

Insérer votre résumé en français suivi des mots-clés

Les zéolithes ZSM-5 sont des candidats prometteurs pour la réaction MTO en raison de leurs propriétés uniques, telles que des sites acides forts et ajustables, une surface spécifique élevée et une sélectivité de forme épatante. Néanmoins, il convient toujours d'augmenter la durée de vie, de diminuer le coût ainsi qu'éviter la pollution pour la modification de la zéolithe ZSM-5 en catalyse hétérogène.

Sur la base de ces demandes, dans cette thèse, des zéolithes ZSM-5 modifiées ont été conçues par une méthode de synthèse hydrothermale in situ, en utilisant respectivement des biochars comme matrice dure et des perlites comme supports. Les deux matières premières (biochar et perlite) sont issues de la nature et contiennent de nombreux hétéroéléments. Les biochars en tant que matrice dure fournissent une surface externe élevée pour la zéolithe; La perlite peut non seulement être utilisée comme support mais également comme source d'Al pour la zéolite. De plus, les hétéroéléments présents dans les biochars et les perlites ont montré une capacité remarquable à ajuster l'acidité de la zéolithe ZSM-5.

En résumé, la surface externe élevée, l'acidité de Brønsted modérée du système biochar/zéolithe ZSM-5 et l'excellente efficacité de diffusion au sein de la perlite/zéolithe ZSM-5 lui confèrent des propriétés catalytiques remarquables.

Résumé en anglais

Insérer votre résumé en anglais suivi des mots-clés

ZSM-5 zeolites are promising candidates for the MTO reaction due to their unique properties, such as numerous and adjustable acid sites, high surface area, and excellent shape selectivity. Nevertheless, increase the lifetime, decrease the cost as well as avoid the pollution remain critical targets for the modification of ZSM-5 zeolite.

Based on these demands, in this Thesis, modified ZSM-5 zeolites were designed by in situ hydrothermal synthesis method, using biochars as hard template and perlites as supports, respectively. Both raw materials (biochar and perlite) come from nature, and contain abundant heteroelements. Biochars, as hard template, provide high external surface area for the zeolite; The perlite could not only be used as support material but also as Al source for the zeolite. In addition, the heteroelements present in biochars and perlites exhibited remarkable ability to adjust acidity for the preparation of ZSM-5 zeolite.

In summary, the high external surface area, moderate Brønsted acidity of biochar/ZSM-5 zeolite and excellent diffusion efficiency of perlite/ZSM-5 zeolite led to powerful catalytic properties.

Keywords: Zeolite, MTO, Biochars, Perlite